

CLASSIFICATIONS OF GROSS MORPHOLOGIC
AND MAGNETIC RESONANCE IMAGES OF
HUMAN INTERVERTEBRAL DISCS

By

J. PAUL THOMPSON

M.D., University of Western Ontario, 1981

A THESIS SUBMITTED IN PARTIAL FULFILLMENT OF
THE REQUIREMENTS FOR THE DEGREE OF
MASTER OF SCIENCE

in

THE FACULTY OF GRADUATE STUDIES
DEPARTMENT OF ANATOMY

We accept this thesis as conforming
to the required standard

THE UNIVERSITY OF BRITISH COLUMBIA

JUNE 1987

© J. Paul Thompson, 1987

In presenting this thesis in partial fulfilment of the requirements for an advanced degree at the University of British Columbia, I agree that the Library shall make it freely available for reference and study. I further agree that permission for extensive copying of this thesis for scholarly purposes may be granted by the head of my department or by his or her representatives. It is understood that copying or publication of this thesis for financial gain shall not be allowed without my written permission.

Department of ANATOMY

The University of British Columbia
1956 Main Mall
Vancouver, Canada
V6T 1Y3

Date 07 AUG 87

ABSTRACT

The pathogenesis of low back pain is complex but likely involves the intervertebral disc (Nachemson, 1976). Direct evidence for its importance is lacking because an accurate in vivo method of imaging the lumbar intervertebral disc has not been established. The objective of this research was to develop classifications of gross morphologic appearance and magnetic resonance image (MRI) of the disc that describe the changes associated with aging and degeneration, thereby permitting interpretation of the MRI in terms of gross morphology and allowing correlation of morphologic, chemical, mechanical, radiologic and epidemiologic data with a standard reference of disc aging and degeneration.

The classifications were developed on the basis of literature review, detailed examination of 55 discs and expert advice. Two sets of three observers, one for the morphologic classification and one for the MRI classification evaluated 68 life size randomized duplicates of discs making detailed observations about overall category and 17 regional morphologic parameters and 11 regional MRI parameters. The data was tested to demonstrate the validity of the classifications using established criteria (Tugwell & Bombardier, 1982; Guyatt & Kirschner, 1985; Feinstein, 1985). The consistency with which the classifications could be applied was evaluated by calculating weighted kappa, a statistical test of agreement that corrects for agreement by chance; the ability of the classifications to distinguish stages in the process of ageing and degeneration by stepwise discriminant analysis; their conformity with other measures by comparisons within and between classifications and,

comparisons with histologic and chemical data.

The degree of agreement for all six intra-observer pairs was 'almost perfect' (weighted kappa > 0.80); for 5 interobserver pairs 'substantial' (weighted kappa > 0.60) and for one MRI interobserver pair 'moderate' (weighted kappa > 0.50). This represented a satisfactory level of agreement and indicated the classifications could be applied consistently (Feinstein, 1981). The linear regression model developed by stepwise discriminant analysis clearly demonstrated the ability of the classifications to distinguish distinct stages in disc aging and degeneration. Wilk's lambda, a likelihood ratio statistic reflecting discriminatory function, approached zero in both the morphologic (0.0408) and MRI (0.0480) classifications. In both models, parameters pertaining to the nucleus pulposus of the disc accounted for the majority of the variance (morphologic partial R^2 0.8598 and MRI partial R^2 0.8841) suggesting nuclear parameters are the most important in distinguishing overall category. The correlation table generated by principal component analysis demonstrated that the categories assigned to regional parameters correlated significantly ($p > 0.0001$) with each other and with the overall category. From the linear combinations of parameters (principal components) generated the weighting of the nucleus pulposus behaved independently attesting to its importance. Comparisons of the morphologic and MRI classifications yielded high indices of trend (Pearson correlation coefficient of 0.84) and concordance (kappa of 0.62). Trends in the histologic and chemical data were consistent with the classifications but could not be evaluated statistically because only 15 specimens were studied.

This research suggests that the classifications are valid and will form a basis for the interpretation of MRI. Preliminary evidence suggested MRI is sensitive to early changes in extracellular matrix composition not apparent in gross morphology.

TABLE OF CONTENTS

	PAGE
Title Page	i
Abstract	ii
Table of Contents	v
List of Tables	vii
List of Figures	viii
List of Appendices	xi
Abbreviations	xii
Acknowledgements	xiii
Introduction	1
1.1 Objective	2
1.2 Definition: Low Back Pain	2
1.2.2 Definition: Disc Degeneration	3
1.3 Epidemiology	4
1.4 Intervertebral Disc Morphology	6
1.5 Intervertebral Disc Composition	15
1.6 Mechanical Properties of the Intervertebral Disc	18
1.7 Nerve Supply to the Intervertebral Disc	18
1.8 Intervertebral Disc Nutrition	19
1.9 Proposed Mechanisms of Intervertebral Disc Degeneration	20
1.10 Radiology of the Intervertebral Disc	21
1.11 Issues in Measurement	26
1.11.1 Content Validity	27
1.11.2 Face Validity	27
1.11.3 Criterion Validity	27
1.11.4 Discriminant Validity	30
1.11.5 Construct Validity	30
1.12 Aims of Thesis	31
Methods	33
2.1 Collection of Specimens	34
2.2 Magnetic Resonance Imaging of Specimens	34
2.3 Specimen Processing and Macrophotography	35
2.4 Development of the Classifications for Gross Morphology and Magnetic Resonance Images	38
2.5 Testing the Classifications	40
2.6 Chemical Analysis	46
2.7.1 Histologic Preparation: Fresh Specimens	51
2.7.2 Histologic Preparation: Frozen Specimens	52
2.7.3 Photomicrography	53

Results	54
3.1 Specimen Profile	55
3.2 Magnetic Resonance Imaging	55
3.3 Testing of the Classifications	55
3.4 Chemical Analysis	89
3.5 Histologic Analysis	121
Discussion	148
4.1 General	149
4.2 Method Limitations	149
4.2.1 Sample Characteristics	149
4.2.2 Imaging	151
4.2.3 Development and Testing of the Classification	152
4.2.4 Histology and Chemistry	153
4.3 Results	155
4.4 Summary	171
4.4.1 Conclusion	172
References	173

LIST OF TABLES

TABLE NO.	TITLE	PAGE
1	Publications Describing Intervertebral Disc Morphology	8
2	Publications Describing Magnetic Resonance Imaging of the Lumbar Spine	24
3	Demographic Data of the Donors	56
4	Evaluation of Intra-observer Agreement for Overall Morphologic Category	59
5	Evaluation of Intra-observer Agreement for Overall MRI Category	62
6	Evaluation of Interobserver Agreement for Overall Morphologic Category	65
7	Evaluation of Interobserver Agreement for Overall MRI Category	68
8	Stepwise Discriminant Analysis of the Morphologic Data	74
9	Stepwise Discriminant Analysis of the MRI Data	75
10	Principal Component Analysis of the Morphologic Data	77
11	Principal Component Analysis of the MRI Data	82
12	Evaluation of Agreement on Overall Category Between the Morphologic and MRI Data	88
13	Principal Component Analysis by MRI Observer	158
14	Evaluation of Agreement Between Nuclear Zone and Overall MRI Category	162
15	Interobserver Agreement for Overall MRI Category, Nuclear Zone and Regression Equation	164

LIST OF FIGURES

FIGURE NO.	TITLE	PAGE
1	Division of the Spines	36
2	Typical Photograph of Gross Morphology	37
3	Disc Zones	39
4	Morphologic and MRI Classification of Discs	41
5	Sites of Tissue Sampling for Chemical Analysis.....	47
6	Age Distribution of the Donors	57
7	Effect of Delay in Magnetic Resonance Imaging of the Disc	58
8	Distribution of Discs Selected for Chemical and Histologic Analysis by Morphologic and MRI Categories	90
9	Water Content by MRI Category	91
10	Water Content by Morphologic Category	96
11	Chondroitin Sulphate Content by MRI Category	99
12	Chondroitin Sulphate Content by Morphologic Category	102
13	Keratan Sulphate Content by MRI Category	106
14	Keratan Sulphate Content by Morphologic Category	109
15	Ratio of Keratan Sulphate to Chondroitin Sulphate by MRI Category	112
16	Collagen Content by MRI Category	115
17	Collagen Content by Morphologic Category	118
18	Comparison of Alcianophilic Structures with MRI of an MRI Category 1 Disc	122

19	Hematoxylin and Eosin Staining of the Anulus of an MRI Category 1 Disc	124
20	Hematoxylin and Eosin Staining of the Nucleus of an MRI Category 1 Disc	125
21	Hematoxylin and Eosin Staining of the Endplate of an MRI Category 1 Disc	128
22	Alcian Blue and Mallory Trichrome Staining of an MRI Category 2 Disc	129
23	Alcian Blue and Mallory Trichrome Staining of the Anulus of an MRI Category 2 Disc	130
24	MRI Scan of an MRI Category 2 Disc	131
25	Mallory Trichrome Staining of MRI Category 1 and 2 Nuclear Zones	133
26	Alcian Blue Staining of an MRI Category 2 Endplate	134
27	Hematoxylin and Eosin Staining of the Vertebral Body Margin of an MRI Category 3 Disc	136
28	Alcian Blue Staining of an MRI Category 3 Nucleus	137
29	Hematoxylin and Eosin Staining of an MRI Category 3 Endplate	138
30	Gross Morphology and MRI Scan of an MRI Category 4 Disc	139
31	Hematoxylin and Eosin Staining of a Cleft in an MRI Category 4 Disc	140
32	Alcian Blue Staining, Gross Morphology and MRI Scan of an MRI Category 5 Disc	142
33	Mallory Trichrome Staining of an MRI Category 5 Disc ..	145
34	Mallory Trichrome Staining of a Cleft in an MRI Category 5 Disc	146

35	Mallory Trichrome Staining of an MRI Category 5 Disc	147
36	Distribution of Discs According to Morphologic and MRI Category	150
37	Plots of Overall MRI Category and Nuclear Zone by Observer	165
38	Gross Morphology of an MRI Category 2 and Morphologic Category 1 Disc	168
39	Gross Morphology, MRI Scan and Alcian Blue Staining of a Category 5 Disc	170

LIST OF APPENDICES

APPENDIX NO.	TITLE	PAGE
1	Descriptions of Morphologic and MRI Grades	178
2	Parameters Assessed by Observers and Procedure for Recording Observations	182
3	Histochemical Methods	191

LIST OF COMMONLY USED ABBREVIATIONS

AZAI	Anular Zone Anterior Inferior
AZAS	Anular Zone Anterior Superior
AZPI	Anular Zone Posterior Inferior
AZPS	Anular Zone Posterior Superior
CIEP	Cartilaginous Inferior Endplate
CS	Chondroitin Sulphate
CSEP	Cartilaginous Superior Endplate
EPI	Endplate Inferior
KS	Keratan Sulphate
MI	Myocardial infarction
MRI	Magnetic Resonance Imaging
MVA	Motor Vehicle Accident
NZ	Nuclear Zone
SIEP	Subchondral Inferior Endplate
SSEP	Subchondral Superior Endplate
TIAIAZ	Tissue Integrity of the Anterior Inferior Anular Zone
TIASAZ	Tissue Integrity of the Anterior Superior Anular Zone
TINZ	Tissue Integrity of the Nuclear Zone
TIPIAZ	Tissue Integrity of the Posterior Inferior Anular Zone
TIPSAZ	Tissue Integrity of the Posterior Superior Anular Zone
TMAIAZ	Tissue Morphology of the Anterior Inferior Anular Zone
TMNZ	Tissue Morphology of the Nuclear Zone
TMPIAZ	Tissue Morphology of the Posterior Inferior Anular Zone
TMPSAZ	Tissue Morphology of the Posterior Superior Anular Zone
VBAI	Vertebral Body Anterior Inferior
VBAIAZ	Vertebral Body of the Anterior Inferior Anular Zone
VBASAZ	Vertebral Body of the Anterior Superior Anular Zone
VBPI	Vertebral Body Posterior Inferior
VBPSAZ	Vertebral Body of the Posterior Superior Anular Zone

ACKNOWLEDGEMENTS

I wish to recognize and thank the following people:

- Dr. R.H. Pearce, for providing me the opportunity, guidance and encouragement to pursue this research.
- Miss Bev Grimmer, Ms. Joyce Mathieson and Mr. Bernie Cox, for their patience in teaching the laboratory skills required to do this research.
- Dr. Paul Bishop, for his participation as an observer and provision of Faxitron images.
- Dr. Mark Adams, Dr. Ian Tsang, Dr. David Li and Dr. Boris Flak, for their participation as observers.
- Dr. Brian Ho, for his guidance with respect to Magnetic Resonance Imaging and participation as an observer.
- Dr. Martin Schechter, for his guidance and assistance in the statistical evaluation of this research.
- Dr. W.K. Ovalle, for his assistance in the histologic examination.
- Dr. C.E. Slonecker, for providing the time, facilities and encouragement to pursue this research.
- Arthritis Society for supporting this research.

CHAPTER 1

INTRODUCTION

1.1 OBJECTIVE

The central role of the intervertebral disc in the pathogenesis of low back pain has been cited by many investigators. However, direct evidence for its importance is lacking. Accurate in vivo imaging of the intervertebral disc could establish its clinical relevance by correlating the state of the tissue with clinical presentation. Magnetic resonance imaging (MRI) has demonstrated potential in this respect (Modic, 1984; Maravilla, 1985; Michael, 1985).

The objective of this research was to develop valid morphologic and MRI classifications of intervertebral disc aging and degeneration satisfying the criteria defined by Tugwell & Bombardier (1982), Kirshner & Guyatt (1985), and Feinstein (1985). Such classifications would permit formal testing of hypotheses, form a basis for accurate interpretation of magnetic resonance images and provide investigators with a standard method of recording the gross morphology and MRI appearances of the disc.

1.2 DEFINITION: LOW BACK PAIN

Low back pain is a common symptom causing considerable suffering and disability. The etiology is diverse, but has been classified under the following headings: viscerogenic, neurogenic, vascular, psychogenic, and spondylogenic. Spondylogenic low back pain is the most common and enigmatic type and is defined as pain arising from the spinal column and its associated structures. The pathogenesis of spondylogenic low back pain includes myofascial strain, osteoporosis with fracture, facet joint osteoarthritis, disc degeneration, disc herniation, spinal stenosis, fracture - dislocations and spondylolisthesis. The precise role of disc degeneration in spondylogenic back pain is not clear. The other mechanisms have clearly defined roles in the

induction of low back pain and can be managed by efficacious therapeutic interventions.

Clinically, low back pain is characterized by pain, muscle spasm and a restricted range of motion in the lumbosacral spine. Referred pain to the buttock and posterior thigh frequently accompanies low back pain. Sciatica and radicular pain are associated with low back pain when neural tissue is under compression or tension. Where the compression or tension is severe, neuropraxia with neurologic dysfunction occurs. Like the clinical findings, the spectrum of radiographic changes is broad and the changes are often non-specific, ranging from the poorly correlated plain x-ray findings of osteophyte formation, loss of disc space height and facet osteoarthritis to the well correlated CT scan finding of sequestered disc fragments.

Terms used synonymously with low back pain include: lumbago, low back syndrome, lumbar insufficiency, sciatica, lumbar spondylosis.

1.2.2 DEFINITION: DISC DEGENERATION

Disc degeneration is an abnormal process of unknown etiology predominantly affecting the lumbar spine but also the cervical and thoracic spines. The extent to which disc degeneration is a pathologic process or an inevitable consequence of aging is not clear. Although not precisely delineated, disc degeneration appears to be a disease process in which changes in the chemical composition of the disc result in alterations of its structural and biomechanical properties. As a consequence, the disc is prone to derangement by mechanical stresses. Pathologically, this process is characterized by a sequence of changes in the nucleus pulposus, anulus fibrosus, vertebral body and endplate culminating in tissue loss and disorganization, cartilage

proliferation and osteophyte formation. Radiographically, the process is identified by loss of disc space height, end plate sclerosis, the vacuum phenomenon and osteophytes. Clinically, the role of disc degeneration in idiopathic low back pain and in the established causes of low back pain such as herniation, facet syndrome and spinal stenosis is not clear.

1.3 EPIDEMIOLOGY

Disorders of the lumbar spine producing low back pain are common in western countries. 80% of people will have an episode of significant low back pain at some time during their lives (Nachemson, 1976). Impairments of the back and spine are the most frequent cause of activity limitation in persons under 45 years (Kelsey, 1980). Among industrial workers, the yearly incidence of low back disorders is approximately 50 per 1,000 workers (White, 1969).

The economic costs brought about by low back pain are considerable. In British Columbia, for the fiscal year 1981-82 hospital costs for low back pain were approximately \$16 million (Hospital Services Commission, 1983). These figures do not reflect outpatient costs, physician visits or drug costs. The annual cost of low back pain in the U.S.A., not including loss of productivity, is estimated to be \$14 billion (Kelsey, 1980). A study conducted at Kodak estimated that productivity decrease averaged 4 hours per person per week (Rowe, 1971). The chronic nature of the problem increases its economic significance. In the State of Washington, of individuals off work for greater than 6 months, only 50% return to work (McGill, 1968). In addition to the economic costs of low back pain, there is unaccountable morbidity, disability and activity limitation. Low back pain has been shown to be the most expensive

ailment in the 30-60 year age group (Nachemson, 1980). Males and females are equally affected by low back pain and white collar workers as often as blue collar workers. Individuals who drive most of their working day, such as truck drivers, have three times the risk of developing low back pain as compared to the general population. Psychosocial stresses influencing low back incapacity include disturbed personality (MMPI), alcoholism, divorce, education and job dissatisfaction. Mechanical stresses contributing to low back incapacity include repeated lifting of heavy loads, a forward stooping position, sudden maximal physical effort, long lasting unchanging position and vibrational stress. Back morbidity rates are stable with age but the proportion of individuals severely disabled by back pain increases with age. Tall and/or heavy individuals appear to be likely to develop low back pain (Kelsey, 1980).

The prevalence of disc degeneration increases markedly with age. Early changes associated with disc degeneration begin in the third decade of life (Lawrence, 1969). By the age of 55, 50-70% males and females will have radiographic evidence of advanced degeneration as indicated by narrowing of the disc space and osteophytosis (Kellgren & Lawrence, 1958). Although a common finding, the clinical significance and consequences of disc degeneration are, at present, difficult to assess.

Although practically all anatomic structures in the lumbar spine motion segments have their proponents in etiologic hypotheses, the intervertebral disc is the most likely source. Support for this includes:

- 1) Disc herniation is usually preceded by low back pain (Hirsch, 1966)
- 2) Intradiscal injection of hypertonic saline or contrast media reproduces symptoms (Holt, 1968)

- 3) Irritation of the outer anulus and nerve root reproduces symptoms (Smyth, 1958)
- 4) Radiating ruptures of the posterior anulus extend into regions with a rich nerve supply (Bogduk, 1983)
- 5) Only the disc shows anatomic changes at the early age that low back pain develops.

However, the precise role of the intervertebral disc in low back pain is not clear. Research has been unable to differentiate physiologic (aging) and pathologic (degenerative) changes in the disc by studies of the natural history and clinical relevance of disc changes. The lack of an accurate in vivo method of imaging disc morphology and the lack of a standard method of recording disc morphology have hampered investigations into the natural history and clinical relevance of lumbar intervertebral disc aging and degeneration.

1.4 INTERVERTEBRAL DISC MORPHOLOGY

During the fourth week of development, the cells of the sclerotomes migrate medially to surround the spinal cord and notochord. The sclerotomic blocks are separated by less dense areas containing the intersegmental arteries. The vertebral bodies form by fusion of the caudal and cephalic portions of adjacent sclerotomes. Cells from the cephalic part fill the space between two precartilaginous vertebrae and form the anulus fibrosus. The notochord persists in the region of the intervertebral disc and forms the nucleus pulposus. Hyaline cartilage anlagen of the vertebra form and develop primary ossification centres by the eighth to tenth week. The vertical cylindrical surface of the body becomes covered with compact bone, but the cancellous upper and lower surfaces remain covered with a layer of hyaline

cartilage to form the endplate. Ring apophyses, appearing after puberty, complete the vertebral body formation and fuse with the body early in the third decade (Last, 1966; Langman, 1975).

After its embryologic formation, the intervertebral disc undergoes a dramatic sequence of changes unlike any other tissue in the body. The changes begin at the start of the third decade and progress at a rate differing markedly between individuals. The following account outlining the sequence of changes in aging and degeneration of the disc is based on the work of the experienced observers listed in Table 1. One must exercise a certain amount of caution in interpreting their data for the following reasons:

- 1) Observations are empiric and not evaluated statistically
- 2) Observations are based on post-mortem specimens
- 3) No standardized terminology exists to permit comparison between investigators.

The intervertebral discs contribute 33% of the length of the lumbar spine. They are the main structures uniting the vertebral bodies. Their structure and composition provide mobility, load bearing and shock absorption for the spine. The principal components of an intervertebral disc are the anulus fibrosus, nucleus pulposus, endplate and adjacent vertebral body. The morphology of each of these components will be considered separately.

Anulus Fibrosus. On gross inspection, the anulus is composed of discrete fibrous lamellae. The breadth and thickness of the lamellae are greater anteriorly than posteriorly. The number of lamellae average fifteen to twenty. The anulus is clearly demarcated from the nucleus. The outer portions of the anulus are contiguous with the anterior and posterior longitudinal ligaments (Coventry, 1945).

TABLE 1: PUBLICATIONS DESCRIBING INTERVERTEBRAL DISC MORPHOLOGY

Section 1.4.1 is a summary of these publications. The observations and conclusions of each author were based on the number of specimens shown. These observations and conclusions were not evaluated by objective analysis.

<u>Date of Publication</u>	<u>Author</u>	<u>Number of Specimens</u>
1932	Schmorl & Junghanns	Life work, not specified
1949	Hirsch & Friberg	100
1945	Coventry	85
1953	Hirsch & Schajowicz	120
1954	Harris & McNab	123
1964	Lewin	104
1970	Fahrni & Ritchie	59
1977	Pritzker	50
1977	Vernon-Roberts	100
1980	Buckwalter	Review Article
1982	Milgram	1,000

Microscopically, cell density averages $9,000/\text{mm}^3$ (Buckwalter, 1980). The outer and inner lamellae have distinctive cell types and extracellular matrix compositions. The outer one-third is tendon-like and consists of fibrocytic cells and highly organized collagenous fascicles. The inner two-thirds is more fibrocartilaginous and consists of chondrocytic cells and less well organized collagenous fascicles embedded in a more abundant and metachromatic interstitial matrix (Pritzker, 1977). The outer lamellae are oriented vertically and insert directly into the vertebral bodies by Sharpey's fibers. The inner lamellae are oriented obliquely (nearly horizontal centrally) and insert into the cartilaginous endplate (Buckwalter, 1980).

Ultrastructurally, the collagenous fascicles of one lamella are oriented at approximately 60° to those in the adjacent lamella (Harris, 1954). The cells of the outer lamellae resemble those of tendon and ligament. These elongate fibrocytic cells have oval nuclei and cytoplasmic organelles including Golgi apparatus, rough endoplasmic reticulum, glycogen granules and mitochondria. Collagen packing is dense, forming tight concentric lamellae. The cells of the inner lamellae more closely resemble chondrocytes with an eccentric round nucleus, abundant rough endoplasmic reticulum, Golgi apparatus and mitochondria. A distinct territorial matrix consisting of fine extracellular filaments, matrix granules and elastic fibers surrounds these cells. Elastic fibers are present in small numbers and are oriented parallel to the adjacent collagenous fibers (Buckwalter, 1980).

With aging and degeneration, the following changes are observed. Macroscopically, the anulus increases in breadth due to appositional growth provided by the perichondrium and apparent growth due to loss of demarcation between the anulus and nucleus. Circumferential and then radial disruptions

become evident, particularly posteriorly (Hirsch, 1953; Vernon-Roberts, 1977). The lamellar organization is lost and replaced by a consolidated tissue identical to that seen in the aging nucleus. Tissue loss and propagation of the tissue disruptions results in macroscopic clefts and gross disorganization of disc morphology. Blood vessels and connective tissue emanating from the endplate and periphery line the macroscopic clefts (Schmorl, 1932; Vernon-Roberts, 1977).

Microscopic examination demonstrates an increase in the amount of interstitial matrix relative to collagen. This interstitial matrix is amorphous and stains with alcian blue. It tends to be deposited in basophilic foci initially between lamellae located centrally and posteriorly in the anulus and then between lamellae in the anterior anulus. The cells involved in this cartilaginous metaplasia are chondrocytic. Those cells near the innermost anular fibers appear identical to the chondrocytic cells (giant chondrons) seen in the nucleus (Pritzker, 1977). This cartilaginous metaplasia, evident as stacks of cartilaginous plates, results in separation of the existing anular fibers and a net change in fiber direction from vertical to horizontal. Microscopic circumferential and radial disruptions develop in areas heavily infiltrated by these basophilic cartilaginous foci (Pritzker, 1977; Vernon-Roberts, 1977). Disruptions adjacent to the periphery of the anulus and to the vertebral body are invaded by capillaries and connective tissue. Continued mechanical stresses may propagate the microscopic disruptions resulting in gross disruptions (Vernon-Roberts, 1977). The cartilaginous tissue, a poorly organized fibrocartilage, is indistinguishable from that seen in the nucleus and is composed of chondrocytic cells ("giant chondrons") and extracellular matrix with poorly organized collagenous fibers in varying amounts of

interstitial matrix.

At the ultrastructural level, early changes include an increase in collagen fibre size and variability. The number of fibrils enveloped by a dense granular material, possibly a glycoprotein or proteoglycan, increases. Fraying and splitting of the inner anular fibers precedes radial tearing. The fibers assume an increasingly horizontal orientation, particularly, the more central fibers. Elastic fibers increase in density and increase their central amorphous component. The cellular territorial matrix density increases with age. Cells accumulate an increasing number of intermediate filaments and ultimately undergo necrosis in situ (Buckwalter, 1980).

Nucleus Pulposus. The nucleus appears as a bulging, gel-like mass situated eccentrically in the middle to posterior third of the disc. It is bounded superiorly and inferiorly by the hyaline endplates. The nucleus accounts for 50% or more of the disc volume. The transition from nucleus to anulus is clear (Coventry, 1945).

Light microscopic examination reveals a tissue rich in extracellular matrix with an average cell density of $4,000/\text{mm}^3$ (Buckwalter, 1980). Notochordal cells are present at birth but gradually decrease with age and are not found after the first decade. Thereafter, the cells usually present are elongated fibrocytes which increase in number with age (Pritzker, 1977; Buckwalter, 1980). Sparse randomly oriented collagenous fibrils are embedded in a basophilic, intensely alcianophilic extracellular matrix (Pritzker, 1977).

Electron microscopic examination of notochordal cells within the nucleus shows relatively few organelles but large bundles of microfilaments, many vacuoles and frequent glycogen granules in the cytoplasm. Adjacent cells interdigitate to form gap junctions, tight junctions and desmosomes. Cell

processes extend around large areas of extracellular matrix and possess microvilli-like processes. Collagenous fibrils form a loose unorganized network. Granular material coats some of the fibrils and obscures their cross banding. Elastic fibers in small numbers are present and without discernible orientation (Buckwalter, 1980).

The earliest changes in disc morphology occur in the nucleus. With aging and degeneration, the nucleus becomes smaller, more fibrous and indistinguishable from the annulus. Focal disruptions appear in the nucleus and form clefts that are initially parallel to the endplate and confined to the nucleus. The clefts become contiguous with disruptions in annulus and are lined by a vascular connective tissue. Mechanical stress may propagate the clefting and result in gross disruption (Vernon-Roberts, 1977).

Microscopically, changes in the cell types and extracellular matrix composition are seen beginning in the third decade. The nucleus becomes populated by two new cell types which resemble chondrocytes. First, large cells occurring singly or in groups, called "giant chondrons", similar to those of the inner annulus, appear in increasing numbers and elaborate a distinct alcian blue territorial matrix. Second, groups of small cells, called "mini chondrons", similar to those seen where endplate fracture callus has formed, appear in smaller numbers near the endplate and also elaborate an alcian blue-staining territorial matrix (Pritzker, 1977; Buckwalter, 1980). The extracellular matrix of the nucleus begins to stain less intensely with alcian blue and progressive centripetal encroachment of collagen from the annulus occurs. Accompanying the fibrocartilaginous metaplasia is the formation of tissue disruptions which give rise to macroscopic clefts (Vernon-Roberts, 1977). These clefts, which become contiguous with annular clefts, are lined by

a vascular connective tissue that has been variously described as granulation tissue, synovial tissue and fibrous tissue with vascular rami (Schmorl, 1932; Gardner, 1968; Vernon-Roberts, 1977).

Electron microscopy confirms the chondrocytic character of the cells. These cells accumulate increasing numbers of intermediate filaments in their cytoplasm that may be characteristic of aging and degeneration. The territorial matrix increases in density with aging and consists of fine collagenous fibers, matrix granules and elastic fibers. The chondrocytic cells undergo necrosis in situ. Examination of the extracellular matrix demonstrates an increase in density and diameter of collagenous fibers with age. The frequency of collagen sheaths increases with age. Elastic fibers increase in density and increase their central amorphous component (Buckwalter, 1980).

Endplate. The endplate consists of subchondral bone and an overlying cartilaginous lamina. The subchondral bone is divided into three regions:

- 1) A central region with numerous small perforations that connect with the marrow cavities of the vertebral body.
- 2) A peripheral region, to which the anulus attaches, with fewer larger perforations.
- 3) An epiphyseal ring composed of dense compact bone.

The cartilaginous plate is hyaline in appearance, like articular cartilage, approximately 1mm in thickness and covers the perforated regions of the endplate adjacent to the nucleus and inner anulus (Coventry, 1945).

Microscopically, the subchondral bone is trabecular in the central regions and compact peripherally. The trabecular pattern is similar to that in the marrow cavity of the vertebral body. Where perforations are present, the blood vessels of the marrow contact the cartilaginous plate (Pritzker, 1977). The

cartilaginous plate is composed of hyaline cartilage with chondrocytes, numbering 15,000/mm³, oriented horizontally. Where the anulus inserts, there is a gradual transition from fibrocartilage to hyaline cartilage (Buckwalter, 1980).

Aging and degeneration results in thinning of the cartilaginous plate followed by the appearance of focal defects and gradual loss of thickness with replacement by reactive cartilage resembling fracture callus. The subchondral bone becomes irregular and subsequently develops a second subchondral plate ("doubles"), and becomes sclerotic (Vernon-Roberts, 1977). Microscopic changes in the cartilage endplate may precede changes in other components of the disc (Pritzker, 1977). In the third decade, cell death and loss of metachromasia in the superficial layers, chondrocyte cloning and disorganization can be seen. These findings suggest decreased function and attempted regeneration resembling early osteoarthritic articular cartilage (Pritzker, 1977; Buckwalter, 1980). Subsequently, fibrillation and fissuring in the superficial layers coincide with calcification and replacement of the deeper layers by endochondral ossification. Further loss of cartilage is evident and microfractures occur resulting in the formation of reactive cartilage, similar to fracture callus, and new bone (Vernon-Roberts, 1977; Milgram, 1982).

Periphery of the Vertebral Body. The periphery of the vertebral body adjacent to the disc space is formed by the ring apophysis. It is composed of the outer compact bone and forms a slightly raised and rounded border (Coventry, 1945). Lamellae of the anulus and the anterior and posterior longitudinal ligaments insert directly into bone via Sharpey's fibers (Buckwalter, 1980). In the presence of advanced aging or degenerative changes in other disc components, traction spurs or osteophytes form (Vernon-Roberts,

1977). Metaplastic cartilage of the anulus becomes calcified and subsequently undergoes endochondral ossification.

1.5 INTERVERTEBRAL DISC COMPOSITION

The main chemical constituents of the disc are water, collagen and proteoglycan. Noncollagenous protein, elastin and lipids are also found. This section presents a synopsis of the works detailing the composition of the disc. Studies examining disc composition must be evaluated carefully for a number of reasons. Observations are often based on small numbers. Specimens typically come from postmortems, animal models or surgical pathology. No standard means of evaluating disc degeneration exists to permit comparisons.

Water. Water is the main constituent of the disc, comprising 900 mg/g of fresh tissue weight at birth, 800 mg/g at age 20 and 700 mg/g at age 80 (Puschel, 1930; Gower & Pedrini, 1969). The water content expressed as a ratio of mg water to mg dry tissue increases centripetally with values of 1-2 for the outer anulus, 2-3 for the inner anulus and 3-4 for the nucleus (Urban, 1977).

Collagen. Both the concentration and type of collagen differ in various regions of the disc. Collagen accounts for approximately 500 mg/g dry weight of the disc with 600-700 mg/g in the anulus and 200-300 mg/g in the nucleus (Pedrini, 1973).

The collagen concentration in the anulus increases progressively caudad in the lumbar spine and increases from the inner to the outer anulus (Adams, 1977). Types I and II collagen coexist in the anulus and account for 40 and 60 per cent of the total respectively (Eyre and Muir, 1977). The collagen types are distributed unevenly, the peripheral anulus containing chiefly type I with sections approaching the nucleus containing a steadily higher proportion of

type II relative to type I until essentially only type II is found adjacent to the nucleus (Eyre & Muir, 1976). Type II is the predominant collagen of the nucleus (Eyre & Muir, 1977). With aging there is an increase in collagen concentration particularly in the nucleus (Pedrini, 1973). The ratio of type II to type I collagen in the anulus may increase with age (Eyre & Muir, 1977).

Proteoglycan. Proteoglycans are the third most abundant component of the young vertebral disc, accounting for approximately 50% of the dry weight of the nucleus and diminishing toward the periphery of the anulus to approximately 10% of the dry weight (Hardingham & Muir, 1976). Five distinct proteoglycans have been demonstrated in both nucleus and anulus (Di Fabio *et al.*, 1987). Chondroitin 6-sulphate (CS) and keratan sulphate (KS) are the principal glycosaminoglycans of the mature disc. These are linked to a peptide core with a CS-rich region consisting of clusters containing on average four CS chains and some KS chains, and a KS-rich region, which contains no CS chains (Stevens *et al.*, 1979). The average molecular weight of chondroitin sulphate is 20,000 and that of keratan sulphate, 10,000 (Pearce & Grimmer, 1976). The proportion of proteoglycan existing as aggregate is 20-30 per cent in the nucleus and 60 per cent in the anulus (Pedrini & Pedrini-Mille, 1979). Evidence suggests that the lack of a hyaluronate binding region rather than insufficient hyaluronate acid is responsible for the low proportion of aggregated proteoglycan (Stevens, 1979). The proportions and molecular weights of glycosaminoglycans and the proportion of proteoglycan aggregated distinguishes the disc from hyaline cartilage.

Proteoglycan content falls before morphologic aging and degeneration are apparent (Pearce, Grimmer & Adams, *in press*). Proteoglycan molecules in older degenerate discs, relative to young discs, are less readily extracted (Adams &

Muir, 1976). They are also smaller, richer in protein and keratan sulphate (Gower & Pedrini, 1969), less aggregated and contain an higher ratio of glucosamine to galactosamine (Adams & Muir, 1976). Hyaluronate increases five-fold with age (Hardingham & Adams, 1976). The changing quality and quantity of proteoglycans could be due to an altered cellular biosynthetic product, to altered relative rates of removal from the extracellular matrix (Eyre, 1979) or to changes in the proportion of proteoglycan species.

Protein. In common with other connective tissues, the intervertebral disc contains a significant amount of non-collagenous protein. Sources of non-collagenous protein, much of it containing carbohydrate, include core proteins of proteoglycan molecules, link protein, excess free hyaluronate binding region, lysozyme, and protein bound to collagenous fibers (Sorce *et al.*, 1984).

With aging and degeneration, non-collagenous protein increases from 20 to 45 per cent of the dry weight of the nucleus and from 5 to 25 per cent of the anulus (Dickson *et al.*, 1967). Much of this accumulation has been attributed to a small chondroitin sulphate-rich proteoglycan. This hypothesis accounts for the decrease in average size of proteoglycan (Adams & Muir, 1976), the increase in protein content and in the ratio of keratan sulphate to chondroitin sulphate (Gower & Pedrini, 1969).

Elastin. Sparse elastic fibers present in the anulus and nucleus have been noted with electron microscopy (Buckwalter, 1980). A trace of elastin was recovered from porcine nucleus (Keith *et al.*, 1977). The source of these elastic fibers and any changes they may undergo with aging and degeneration have not been investigated.

Lipids. Using classical lipid solvents, 0.5 to 2 per cent of nucleus and

endplate cartilage tissue were estimated to be lipid (Franklin & Hull, 1966). With aging and degeneration, the extracellular deposition of lipid and of the derived pigment lipofuchsin has been reported (Copius Peereboom, 1970, 1973).

1.6 MECHANICAL PROPERTIES OF THE INTERVERTEBRAL DISC

The hydrostatic pressures within the nucleus in vivo have been measured using a needle attached to a manometer (Nachemson, 1975). Proteoglycans, due to their high fixed charge density, exhibit a high swelling pressure which is balanced by the compressive load on the spine (Urban, 1979). As a consequence of its viscoelastic properties, the nucleus transmits forces evenly to the endplates and converts axial compression to tensile forces exerted on the annulus.

The annulus functions much like a fibre-reinforced incompressible elastic solid (Wu & Yao, 1976). The high tensile strength of collagenous fibrils and their unique arrangement allow the annulus to withstand high tensile, compressive and rotational forces. Evidence suggests that the annulus is least effective in resisting shear and torsional forces compared with other forces acting on the disc (Farfan, 1977).

1.7 NERVE SUPPLY TO THE INTERVERTEBRAL DISC

Unencapsulated plexiform and free unmyelinated nerve endings originating from the sinuvertebral nerve, ventral rami and the gray rami committantes are present in the outer layers of the annulus (Jackson, 1966; Bogduk, 1983). The nerves terminate as free nerve fibre endings and complex unencapsulated endings. Although the inner annulus and nucleus of the fetal and neonatal disc contain unmyelinated nerves, these nerves disappear with growth and are not

present in mature discs (Wyke, 1980). The cartilage plates have perivascular nerves, but no other types of nerve endings (Jackson, 1966).

With aging and degeneration, nerves accompanying the ingrowth of blood vessels and connective tissue in macroscopic clefts (Vernon-Roberts, 1985).

1.8 INTERVERTEBRAL DISC NUTRITION

In the adult, blood vessels do not penetrate the disc further than the outer lamellae of the anulus (Buckwater, 1980). The blood vessels penetrating from the endplate and lateral borders in fetal and neonatal discs are not seen after the first decade (Hassler, 1970). Thus, in the adult, nutrients must diffuse from capillary beds at the disc margins and then be transported through the extracellular matrix by molecular diffusion and fluid transport stimulated by movement of the spine. The importance of capillary beds in the peripheral anulus and the central one-third endplate for the provision of nutrients to the disc has been documented with experiments utilizing hydrogen washout (Ogata & Whiteside, 1981) and dye injection (Brodin, 1955; Nachemson, 1976) studies. The relative importance of these two capillary beds depends on the solute characteristics: uncharged solutes such as oxygen enter equally by both routes; negatively charged solutes such as sulphate enter principally through the anulus; positively charged solutes, such as calcium, principally through the endplate (Urban *et al.*, 1977). A study of the relative importance of diffusion and fluid flow suggested that diffusion is the more important process, particularly for small solutes (Urban *et al.*, 1977). An *in vivo* study using a canine model has suggested that physiologic levels of exercise are important in maintaining disc nutrition (Nachemson, 1985).

With aging and degeneration, a significant proportion of adult discs show

a reduction in endplate permeability. A strong correlation exists between closure of endplate foramina and disc degeneration (Nachemson et al., 1970).

1.9 PROPOSED MECHANISMS OF INTERVERTEBRAL DISC DEGENERATION

The etiology of disc degeneration is complex and poorly understood. Various investigators have collected evidence to support hypotheses ranging from autoimmune disease to abnormal physical stresses. High biomechanical stresses are imposed on the lumbar spine by bipedal orthograde stance (Nachemson, 1970). In response to mechanical stresses, biosynthesis may alter the quality or concentration of proteoglycan and/or collagen and result in the changes in composition and morphology with age and degeneration (Eyre, 1979). Furthermore, as the nucleus becomes more rigid with age, it is thought to be possibly less efficient in distributing loads on the spine; the resulting focal stress may disrupt the tissue. Experimental studies with animal models indicate that stresses imposed by bipedal stance may be important in the pathogenesis of degeneration. Rats forced to assume a bipedal stance developed the morphologic features of human disc degeneration not normally found in rats (Higuchi, 1983). That disc degeneration may be an autoimmune disease has also been proposed. Immunologic studies have suggested that auto-antibodies may develop against components of the nucleus; these components are normally sequestered from the circulation and the reticuloendothelial system (Naylor et al., 1975). Evidence has accumulated to suggest that impaired disc nutrition may be responsible for the alterations in tissue composition seen with aging and degeneration. The decreased permeability of the endplates (Nachemson, 1970; Brown & Tsaltas, 1976) could be expected to lead to nutritional deficiencies and the accumulation of metabolic products. Pritzker (1977)

further emphasized the importance of the endplates by proposing that the chondrocytes of the endplate were responsible for synthesizing the extracellular matrix of the nucleus. He suggested that degeneration was attributable to a diminished capacity of these cells to synthesize extracellular matrix. The various possible etiologies of disc degeneration summarized here are not mutually exclusive. Indeed, the possibility that disc degeneration may be a multifactorial disease has been proposed (Rothman, 1982).

1.10 RADIOLOGY OF THE INTERVERTEBRAL DISC

Radiologic approaches currently available for the evaluation of the intervertebral disc include plain film radiography, contrast discography and computed tomography and magnetic resonance imaging (Park, 1980; Resnick, 1981; Price, 1983; Michael, 1985).

Plain film radiography will only demonstrate osseous, juxta-osseous or para-articular abnormalities. Consequently, the radiographic criteria for aging and degeneration (disc space narrowing, endplate sclerosis, osteophyte formation and vacuum phenomena) represent more advanced stages of degeneration; early changes are not seen. In addition to its inability to detect soft tissue changes in the disc, standard lumbar radiographs have a poor predictive value in separating normal individuals from individuals complaining of low back pain (Lawrence, 1969; Nachemson, 1976).

Studies performed on cadavers (Erlacher, 1952; Adams *et al.*, 1986) using contrast discography have demonstrated soft tissue of intervertebral disc accurately. However, the interpretation is influenced by the injection pressure and the volume of the contrast medium. In addition, the procedure is invasive and frequently causes pain, the significance of which is difficult

to interpret. For these reasons, discography is rarely used except in pre-operative cases where the clinical signs are inconclusive. In this capacity, discography is a reliable indicator of the disc space giving rise to symptoms (Simmons & Segil, 1975).

Myelography was the definitive investigation for lumbar disc herniation and sequestration. Its role in disc imaging has diminished. CT scan has proven to be more reliable and sensitive. The contrast material only provides information about the contour of the posterior disc and extruded fragments. It does not provide any information about the state of disc aging and degeneration.

Computed tomography (CT) provides more precise information about osseous morphology than plain film radiography. CT allows direct evaluation of soft tissue planes, particularly when loose areolar connective tissue separates these planes, allowing CT to delineate disc margins accurately. As a consequence, CT has become the accepted diagnostic technique for the investigation of disc herniation and spinal stenosis. It is more sensitive than plain film radiography in detecting soft tissue calcification, gas or changes in soft tissue density (Park, 1980). Unfortunately, CT is unable to demonstrate subtle changes in soft tissue density such as would be seen in the earlier stages of disc aging and degeneration.

Nuclear magnetic resonance (NMR) imaging or magnetic resonance imaging (MRI) is a powerful new imaging modality which produces cross-sectional images in all three anatomic planes. As with CT, MRI is composed of picture elements (pixels) generated by a computer. The numerical value of each pixel reflects the intensity of the NMR signal coming from that voxel (element of volume) of tissue. The intensity of the signal is determined by the density of resonating

nuclei (protons). The signal is generated by the interaction of protons and radiofrequency radiation in the presence of a strong magnetic field. The magnetic relaxation times T_1 (longitudinal or spin lattice) and T_2 (transverse or spin-spin) reflect two types of proton interactions, those which disperse the excess energy to the lattice and those which cause loss of coherence, respectively. The computer generates an image by using a logarithmic equation that relates signal intensity, relaxation times and proton density. The form of the equation varies with the pulse sequence used.

Since MRI has become available, a number of reports have been published discussing the usefulness of MRI in imaging the intervertebral disc. Table 2 summarizes these reports and indicates the data base for the observations. In general, the following limitations apply:

- 1) The 'gold standard' for interpretation has been CT, myelographic or surgical findings, rather than actual morphology,
- 2) The focus has been on disc herniation rather than disc degeneration,
- 3) The correlation with gross morphology, histology and chemical composition has been very limited,
- 4) The selection of patients has not been controlled, and the number of patients examined has been relatively small,
- 5) The technical data concerning field strength and pulse sequences vary,
- 6) No standardized terminology has been followed in the description of the discs, and
- 7) Observations have not been tested for reliability or accuracy.

TABLE 2 PUBLICATIONS DESCRIBING MAGNETIC RESONANCE IMAGING
OF THE LUMBAR SPINE

Summary of articles and number of patients on which observations
and conclusions concerning MRI scans of discs were made.

<u>Date of Publication</u>	<u>Author</u>	<u>Number of Patients</u>
1983	Han et al.	41 patients (5 with disc herniation)
1983	Chafetz et al.	14 patients with disc herniation
1984	Modic et al.	65 patients (35 with disc degeneration)
1985	Agulla et al.	40 patients, 3 cadaver spines
1985	Maravilla et al.	18 patients
1985	Pech et al.	10 cadaver spines
1985	Mikhael et al.	75 patients

Compared with plain film radiography, CT and myelography, MRI appears to be the most sensitive technique for the detection of disc degeneration (Modic, 1984; Maravilla, 1985; Michael, 1985). Degeneration appears to decrease signal intensities arising from the nucleus pulposus in T₂-weighted spin echo image sequences. As a result, the demarcation between nucleus and anulus is less distinct in degenerate discs than in normal. T₂ weighted spin echo images show the nucleus as a uniform region of high signal intensity and the anulus as a well demarcated region of lesser signal intensity. Hypotheses have been forwarded regarding the source of the bright and dark signal intensities. On the basis of T₂ weighted spin echo image sequences, it has been suggested that bright and dark signals reflect high and low water content regions of the disc respectively. These suggestions make intuitive sense since T₂ correlates closely with water content (Newton & Potts, 1983). This hypothesis has not been tested experimentally and other evidence collected suggests it may be an oversimplification. For example, a review of disc images before and after chymopapain injection suggests the decrease in signal intensity which may represent either a loss of proteoglycan or of water or of both (Chafetz, 1983; Michael, 1985). Chemical shift artifact, as may occur at the disc-endplate interface (Pech, 1985), could complicate further this simple interpretation of signal intensity. Attempts to correlate the MRI with morphology in disc degeneration have been made. Aguila (1985) imaged three cadaver spines and then examined their histology in order to evaluate the intranuclear cleft or axial dark line commonly seen in MRI images and concluded that the cleft represented tissue similar to that of the anulus. On the basis of experience with 40 patients, he concluded that the intranuclear cleft was normal after age 30. This conclusion was not documented and no further analysis was undertaken.

Pech (1985) examined corresponding gross morphologic and MRI sections of 10 cadaver spines and suggested that MRI differentiated two components of the disc: one corresponding to the collagenous fibers in the periphery of the disc; the other, a combination of nucleus and anulus. However, their morphologic technique is less sensitive than others available. The axial dark line or intranuclear cleft did not have a recognizable correlate in the anatomic sections. Furthermore, sampling technique, imaging protocol and methods of tissue evaluation limit the usefulness of their observations.

While these studies suggest that MRI has potential for imaging disc degeneration, they do not provide unequivocal objective support. Further studies involving correlation of MRI with morphology and composition of the disc with adequate numbers and testing of hypotheses were required.

1.11 ISSUES IN MEASUREMENT

Fundamental to the quality of any research is the acquisition of data. The use of an arbitrary ordinal scale, such as a classification, to express data describing pathologic processes or clinical phenomena is common practice among researchers and clinicians. Ordinal scales permit a continuum of descriptive data to be expressed in an explicit, quantifiable manner, thus summarizing information, facilitating communication of observations and permitting formal testing of hypotheses. To achieve these goals in an objective manner, specific criteria for selecting endpoints in an ordinal scale must be met. The criteria for a valid classification can be summarized in five categories (Tugwell & Bombardier, 1982; Kirschner & Guyatt, 1985; Feinstein, 1985).

1.11.1 CONTENT VALIDITY

Does the classification include all plausible items appropriate to its purpose? Is the classification comprehensive? For example, if one were to classify the palatability of oranges, items such as colour, texture and seeds would be appropriate items to use in classifying oranges into different categories. However, it would not be appropriate to use an item such as protein content. The approach for selecting items can be either judgmental, when no previous standards exist, or statistical, when previous standards have identified items for possible inclusion.

1.11.2 FACE VALIDITY

Does the classification appear rational? The method chosen to classify oranges should appear sensible. This implies that one will accept the observer's opinions concerning colour and texture. It also implies that the manner in which the items are quantified is meaningful and will allow one to apply the results.

1.11.3 CRITERION VALIDITY

Does the classification consistently reflect the best available estimate of the truth? The assessment of accuracy or criterion validity, is done by measuring and minimizing the sources of random error and bias. For a classification, assessment requires measuring agreement, the proportion of observations on an orange that are the same, and minimizing observer disagreement. The importance of assessing observer agreement is emphasized by the fact that physicians frequently disagree (Koran, 1975). Before testing a classification or process evaluation for observer agreement, Feinstein (1985) suggested minimizing sources of error in each component of a process evaluation (classification). The input spectrum, for example a bag of oranges, to test

the classification should provide an adequate and unbiased challenge spectrum ensuring that each category or grade of the classification is appropriately represented. Performance of the procedure, that is, applying the classification, should be clearly defined, simple and objective. The output formation or recording of results should include observational procedures, recording the parameters (i.e. colour, texture, etc.) that define the categories, and conversion procedures, that is, recording the actual designated category. Such detailed recording requires that observers make careful observations and judgments, and allows the identification of specific areas of disagreement.

To measure observer agreement with respect to categorial observations, most authors have suggested that weighted kappa is the statistic of choice (Fleiss & Cohen, 1968; Cicchetti, 1976; Kramer & Feinstein, 1981). Although Berk (1979) has suggested that the intraclass correlation-generalizability theory approach offers a number of advantages including the ability to identify bias and to make comparisons involving more than two observers, he recognized that weighted kappa provides precise estimates of the magnitude of measurement error for categorial observations.

Weighted kappa was developed by Cohen (1968) as a measure of agreement between two observers on a categorial (nominal or ordinal) scale. This statistic of concordance corrects for the agreement expected by chance and offers these advantages: (1) distribution free, (2) allows credit for partial observer agreement, (3) makes use of individual items in the rating scale, (4) corrects for differences in rater mean scores.

Weighted kappa is defined by:

$$K_w = \frac{P_o - P_c}{1 - P_c}$$

where P_o and P_c refer to the observed agreement and the agreement expected chance, respectively. For a continuous-ordinal scale, a linear system of weights defined by

$$W_{ij} = \frac{1 - |i - j|}{(k - 1)}$$

where k = number of categories, and P_o and P_c defined by

$$P_o = \sum_{i=1}^K \sum_{j=1}^K W_{ij} P_{ij}$$

$$P_c = \sum_{i=1}^K \sum_{j=1}^K W_{ij} (P_i - P_j)$$

has been suggested where i and j represent the category assigned by observer A and B respectively (Cicchetti, 1976, 1977). The minimum suggested sample size for stochastic significance of weighted kappa is defined by:

$$n = 2k^2$$

where k represents the number of categories for ordinal scales with three to seven categories (Cicchetti, 1976, 1977).

To interpret the strength of agreement inferred by weighted kappa, the guidelines established by Landis and Koch (1974) are generally applied. To be considered an acceptable degree of agreement, K_w should exceed +0.5 to +0.6 (Kramer & Feinstein, 1981).

When no 'gold standard' or arbitrarily designated standard for a classification exists, comparisons with the "truth" cannot be made. As a result, only intra- and interobserver agreement or consistency, but not accuracy or conformity, can be assessed. In the situation in which no

definitive standard for evaluating accuracy or conformity exists, the demonstration of content, face and construct validities are important for establishing the accuracy of a classification.

1.11.4 DISCRIMINANT VALIDITY

Does the classification demonstrate detectable or significant changes along the spectrum of a clinical phenomena or pathologic process? That is, the items chosen to classify oranges should represent changes that are sensitive to the smallest significant change in palatability. Indirectly, the strength of intra- and interobserver agreement can reflect a classification's responsiveness to change. Stepwise discriminant analysis provides a more direct measure of discriminatory function (Klecka, 1980). The descriptive parameters that contribute most to the discriminatory power of the model defining category or grade in the classification, are selected on the basis of Wilks' lambda. The partial correlation coefficient, F statistic and probability levels for each model, measure the discriminatory function based on a subset of variables. Wilks' lambda indicates which descriptive parameters contribute most to the discrimination of overall category (SAS Institute Inc., 1985).

1.11.5 CONSTRUCT VALIDITY

Does the classification produce results that conform to other methods of assessment? For example, the orange classification should conform with measures of water content, glucose content and pH. This question is important when there is no good direct method for measuring the true value, as is the case when no 'gold standard' or 'truth' for classifying clinical phenomena or pathologic processes exists. Demonstrating convergence, or how well independent measures of the same categories agree, is another approach. A strong correlation between colour and texture items in the same category should

exist. For example, in the separate morphologic and radiologic classifications of disc degeneration to be described, the relation of the designated categories could be examined by following procedures:

- (a) The correlation between the categories assigned to individual descriptive parameters and the overall designated category. To investigate this, principal component analysis, a multivariate technique for examining relationships among such semi-quantitative variables, was used. Principal component analysis examines all dimensions of all variables and provides a measure of these correlations. In addition, the principal components for overall category are calculated as a function of corresponding categories of descriptive parameters in descending order of eigenvalue (SAS Institute Inc., 1985). It serves as an exploratory technique defining groupings of items best fitting a linear equation. Each principal component identifies a significant variable and what other variables follow.
- (b) The correlation and concordance of designated categories between the morphologic and the radiologic classifications can be calculated.
- (c) The correlation of overall designated categories of the morphologic and MRI classifications with the histologic and chemical data is an appropriate comparison with other measures.

1.12 AIMS OF THESIS

The intervertebral disc is believed to have a central role in the pathogenesis of low back pain (Nachemson, 1976). The overall purpose of this work is to provide a firm morphologic basis for interpretation of magnetic resonance imaging (MRI), an important new method of imaging the disc in vivo. The specific aims are: 1) to develop corresponding morphologic and MRI

classifications of the disc describing the changes seen in aging and degeneration; 2) to evaluate these classifications by determining their consistency, their ability to distinguish stages in the process of aging and degeneration, and their consistency within and between classifications and their conformity with two other measures of disc status, the histology and chemical composition.

CHAPTER 2

METHODS

2.0 METHODS

2.1 COLLECTION OF SPECIMENS

To provide an adequate sample for statistical testing, the anterior and middle columns of 15 human lumbar spines were collected from the morgues of the Vancouver General Hospital and the U.B.C. Health Sciences Centre Acute Care Unit before 1200 hours. Permission for autopsy had been granted by the next of kin and clearance for studies involving human material obtained. The specimens were selected on the basis of the following criteria:

- 1) Approximately equal representation of each decade of life from the second to the eighth.
- 2) Less than 24 hours from the time of death.
- 3) No pathologic process involving the retroperitoneum or dorsolumbar spine (e.g. neoplasm, trauma).

Any specimen not meeting these criteria was excluded.

The specimens were removed from each cadaver by transection of the origins of the psoas muscle and lumbar spinal nerves and subsequent transection of the pedicles of vertebrae L1 to S1 with an oscillating saw. Division of the vertebral bodies of L1 and S1 permitted removal of the specimen without damage to the disc spaces L1-L2 to L5-S1. The specimens were cleaned of any extraneous tissue, placed in an occlusive wrap and kept at room temperature for magnetic resonance imaging.

2.2 MAGNETIC RESONANCE IMAGING OF SPECIMENS

The specimens were transported promptly to the Magnetic Resonance Imaging Unit at the U.B.C. Health Sciences Centre Hospital. A 10 mm thick image in

the median sagittal plane was obtained using a small parts (wrist) receiver coil in a Picker Cryogenic Magnetic Resonance Imaging Unit operating at a field strength of 0.15 T. One hour was required to produce images with the following sequences:

<u>Image Description</u>	<u>Time To Echo (TE)</u>	<u>Repeat Time (TR)</u>
1) Scout	40 ms	400 ms
2) Spin Echo 40	40 ms	2000 ms
3) Spin Echo 80	80 ms	2000 ms
	<u>Time Interval (TI)</u>	
4) Inversion Recovery 400	400 ms	2000 ms

Because T1 and T2 relaxation times are sensitive to temperature, imaging was carried out at room temperature (18°C). Images produced had an in-plane resolution of 1mm. Duplicate life-size images of each spine were obtained.

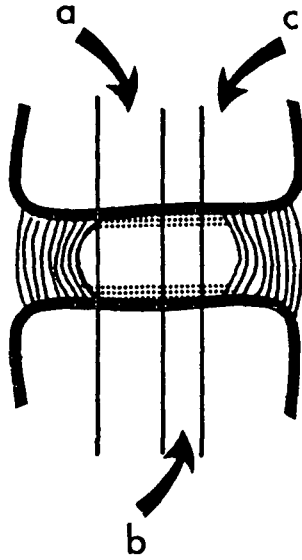
To assess the influence of the interval between death and imaging, three specimens were imaged a second time 24 hours after the first. Qualitative direct comparisons of the images were made.

2.3 SPECIMEN PROCESSING AND MACROPHOTOGRAPHY

Upon completion of the imaging, specimens were split sagittally in the median plane as shown in Figure 1. From one half of the spine, a 10mm sagittal slice was taken for biochemical assay. This specimen was placed in impermeable plastic (Saran wrap) and aluminum foil and kept at -80° C. From the other half of the spine, a 5mm sagittal slice was taken for histological study. This specimen was placed in 10% formalin (v/v) [47% (w/v) formaldehyde containing 27

FIGURE 1: DIVISION OF THE SPINES

Diagram of a coronal section of disc indicating how each spine was sagittally split with a band saw to provide slices for chemical analysis (a), histologic processing (b), and macro photography (c).



(w/v) calcium acetate] at room temperature for a minimum period of three weeks. The remainder of the latter half of the spine was gently washed and brushed with a soft toothbrush under a stream of cool tap water, then blotted; a colour photograph was taken to record the gross morphology (Kodak, Ektachrome ASA 100). An internegative was made from the 35 mm slide to allow production of life-sized duplicate colour photographs (Figure 2). This sequence was completed on the day of specimen collection with the exception of three specimens. Because a band saw was unavailable initially, these three specimens were frozen immediately after imaging. When the band saw was available, the specimens were split while frozen and processed as indicated above with the exception that the 5mm specimens for histological study were placed in a 1% solution of picric acid in absolute ethanol at -80°C for fixation by freeze substitution (see section 2.7.2).

2.2.4 DEVELOPMENT OF THE CLASSIFICATIONS FOR GROSS MORPHOLOGY AND MAGNETIC RESONANCE IMAGES

The literature concerned with the morphology and the magnetic resonance images of intervertebral discs was reviewed to provide a thorough understanding of the sequence of changes seen with aging and degeneration. Prior to the development of these classifications, 55 discs, representing a spectrum of age groups had been imaged and photographed. Each photograph and image was reviewed in detail recording observations about descriptive parameters pertaining to the anulus fibrosus, nucleus pulposus, endplate and vertebral body in seven zones (Figure 3). The observations recorded for the corresponding photographs and images were compared. On the basis of the literature review and this detailed personal observation, corresponding

THE QUALITY OF THIS MICROFICHE IS HEAVILY DEPENDENT UPON THE QUALITY OF THE THESIS SUBMITTED FOR MICROFILMING.

UNFORTUNATELY THE COLOURED ILLUSTRATIONS OF THIS THESIS CAN ONLY YIELD DIFFERENT TONES OF GREY.

LA QUALITE DE CETTE MICROFICHE DEPEND GRANDEMENT DE LA QUALITE DE LA THESE SOUMISE AU MICROFILMAGE.

MALHEUREUSEMENT, LES DIFFERENTES ILLUSTRATIONS EN COULEURS DE CETTE THESE NE PEUVENT DONNER QUE DES TEINTES DE GRIS.

FIGURE 2: TYPICAL PHOTOGRAPH OF GROSS MORPHOLOGY

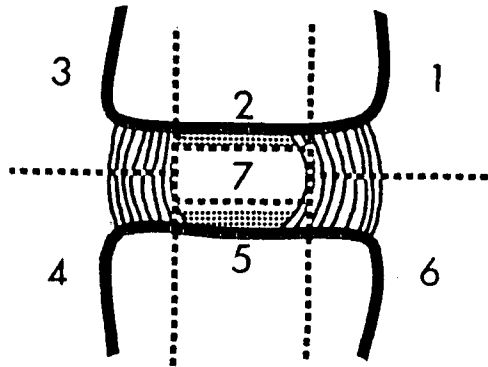
Color photograph of a sagittally split specimen from an 89 year old female (magnification 0.85x). Disc spaces L1,2 through L5,S1 are shown and represent categories (grades) 3 to 5.



FIGURE 3: DISC ZONES

Diagram demonstrating the seven zones examined in the morphologic and MRI assessment of each disc. The zones are described as follows:

(1) anterior superior anular zone (ASAZ), (2) superior endplate (SEP), (3) posterior superior anular zone (PSAZ), (4) posterior inferior anular zone (PIAZ), (5) inferior endplate (IEP), (6) anterior inferior anular zone (AIAZ), (7) nuclear zone (NZ).



tentative classifications, each containing five categories, for gross morphology and magnetic resonance images of intervertebral discs were proposed. Each category of the classifications was defined by a representative photograph or image and an accompanying detailed description containing all plausible parameters pertaining to the anulus fibrosus, nucleus pulposus, endplate and vertebral body margin. Experienced observers, including Prof. B. Vernon-Roberts of the Department of Pathology, University of Adelaide, Australia and Dr. K.P.H. Pritzker of the Department of Pathology, University of Toronto reviewed the classifications critically. The draft classifications were revised four times before establishing the final descriptions defining each category (Figure 4, Appendix 1).

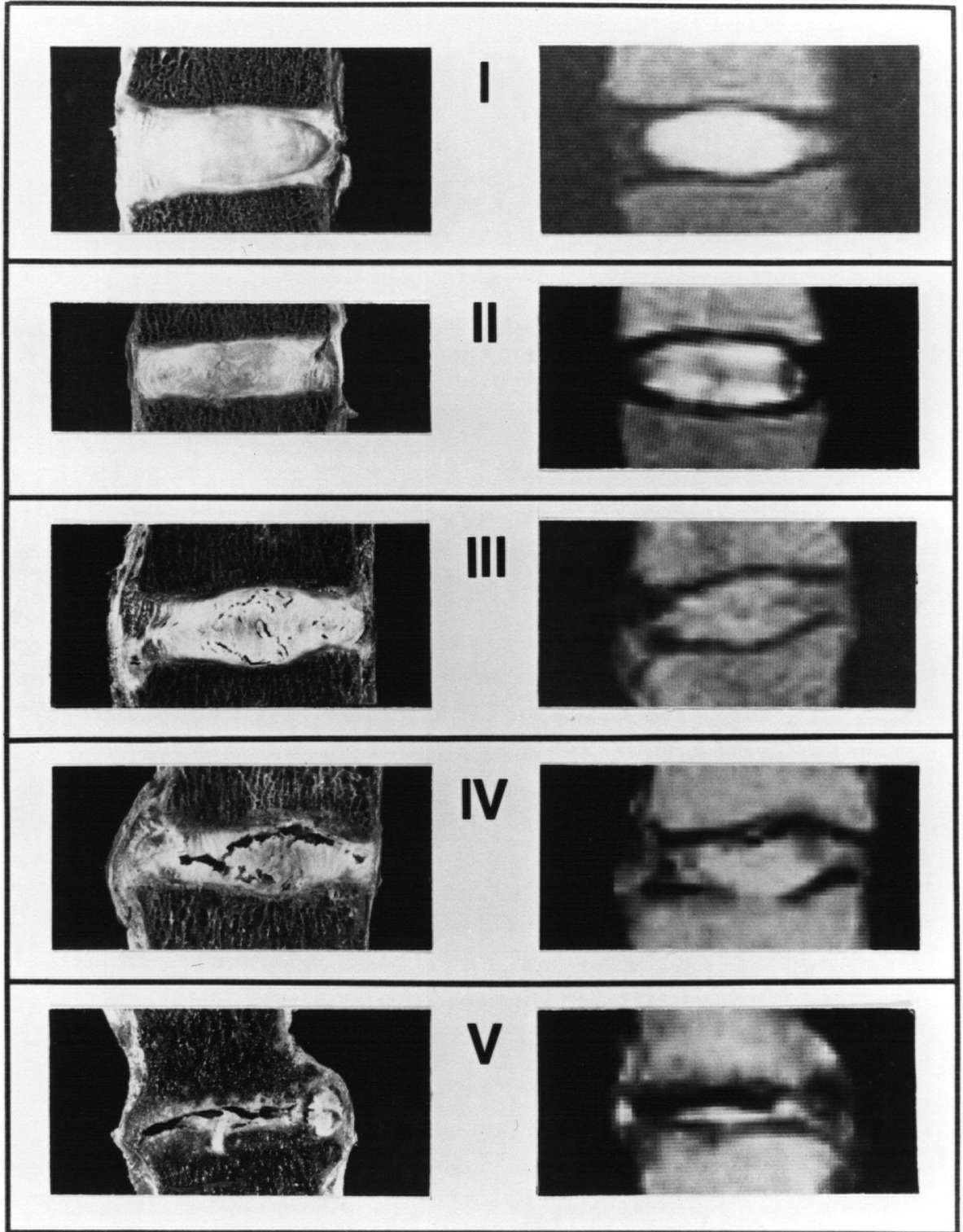
2.5 TESTING THE CLASSIFICATIONS

The corresponding five-category gross morphologic and MRI classifications were tested using established criteria for the selection of endpoints (Tugwell, 1982; Kirshner, 1985; Feinstein, 1985). The criteria for validity were examined using the following categories:

- 1) Content Validity. Extensive literature review and personal observation of 55 discs were used to ensure that the descriptions included all plausible items defining the different stages of disc degeneration. Each category or grade was defined by a representative photograph or image and an accompanying description.
- 2) Face Validity. Literature review and personal experience suggested the classifications were credible and sensible. Critical review of the classifications by experienced observers, Prof. B. Vernon-Roberts and

FIGURE 4: MORPHOLOGIC AND MRI CLASSIFICATIONS

Representative examples of morphologic and MRI grades (categories).
The detailed description of each category is given in Appendix 1.
Macro photographs appear on the left and the corresponding MRI images
are seen on the right. The category or grade for each pair is
designated by the Roman numeral between them.



Dr. K.P.H. Pritzker, confirmed this. Changes made on their recommendation consisted of adopting more precise anatomic and pathologic terminology.

3) Criterion Validity. Efforts were made to reduce observer variability by attention to these components of a process evaluation (Feinstein, 1985):

- 1) Input Spectrum. Fifteen lumbar spines were selected on the basis of age to ensure each category was appropriately represented, thus providing observers with an unbiased challenge spectrum. Furthermore, the fifteen spines provided a sufficient number of discs for statistical analysis including kappa calculations.
- ii) Performance of Procedure. As a compromise between sensitivity and complexity, the ordinal scale was restricted to five categories. To maintain objectivity, randomized duplicate life-sized photographs and MRI images of 68 discs were mounted separately without identifying marks and subsequently evaluated, blindly, by each observer. Observers with an interest in low back pain and morphology were recruited to review the gross appearance of the discs. Morphologic observer 1 was a doctoral candidate in the Department of Pathology, U.B.C. As a practising chiropractor, this observer had a keen interest in clinical and pathologic conditions of the lumbar spine. Observer 2 was a clinical professor in the Division of Rheumatology, Faculty of Medicine, U.B.C. This observer's clinical and research interests involved the U.B.C. Back Pain Clinic. Observer 3 was an associate professor in the Division of Rheumatology with an active interest in connective tissue research. Observers with an interest in magnetic resonance imaging of the spine evaluated the

MRI images of the discs. MRI Observers 2 and 3 were clinical associate professors in the Department of Radiology. Both were active in research projects involving the U.B.C. MRI Unit. Observer 1 was a clinical associate professor in the Department of Radiology. Before using the classifications, observers were familiarized with the terminology used in the description of each category and each parameter. The process for evaluation of each disc and the form for recording data were clearly defined (Appendix 2). Each observer completed a pilot trial of ten discs to allow for the identification and clarification of problems.

- iii) Output formation. Observers performed a seven zone analysis on each disc recording descriptive parameters on the form provided (observational procedure). Eleven parameters were noted for the MRI classification and 17 for the morphologic classification. An overall category was assigned to each disc according to examples in Figure 4 (conversion procedure). The descriptive parameters described features of the annulus, nucleus, endplate and vertebral body that change with aging and degeneration. Each of the descriptive parameters were subdivided into five categories, each category corresponding to the finding in the overall category of the disc. For a particular zone, observers selected the parameter that best described what they observed in the disc under examination.

The data compiled by each of the six observers - three for the morphologic and three for the MRI - were analyzed statistically using the SAS Statistical Package (SAS Institute Inc., 1985). To measure

intra- and interobserver agreement, weighted kappa was calculated using a program kindly provided by Dr. Martin Schechter of the Department of Health Care and Epidemiology, U.B.C. This program calculated both unweighted and weighted kappa, the latter using a system of linear weights. Before constructing the interobserver agreement matrices, one of the replicates was selected randomly to avoid any bias that might have arisen by summing replicates and rounding up or down their average. The strength of agreement was evaluated using the guidelines established by Landis & Koch (1974).

- 4) Discriminant Validity. To quantitate the ability of the classifications to differentiate categories along the spectrum of intervertebral disc aging and degeneration, discriminant analysis was done. A stepwise discriminant analysis technique was used to demonstrate sensitivity of the classifications to change and indicate which parameters were most important in distinguishing categories.
- 5) Construct Validity. To demonstrate convergence, the following comparisons were made looking for correlation and concordance:
 - (a) The correlation of individual descriptive parameters with overall category and other descriptive parameters using principal component analysis.
 - (b) The correlation and concordance between the MRI and morphologic classifications, with respect to category, using correlation coefficients and weighted kappa.
 - (c) The trends seen when the histologic and chemical data for fifteen discs were compared with their MRI and morphologic category (grade).

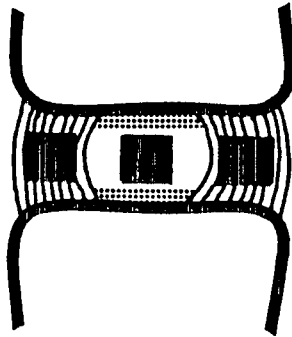
2.6 CHEMICAL ANALYSIS

The 10 mm slice reserved for chemical analysis was kept tightly wrapped in impermeable plastic film and aluminum foil and stored at -80°C until the analysis could be undertaken, at which time the specimen was thawed overnight at 4°C . Specimens were selected to provide two adjacent discs from the cadaver spines of three young individuals and to provide three adjacent discs, two typical for the age and one severely degenerate (category 5), from the spines of three older individuals. Blocks of tissue, weighing approximately 300 mg each, were dissected from the anterior anulus, the nucleus and the posterior anulus (Figure 5). The tissue blocks were minced with a scalpel and then placed in separate, tightly stopped, labelled glass vials. The samples were transferred to a teflon C capsule and frozen in liquid nitrogen at -70°C . After ten to fifteen minutes, the capsules were removed from the liquid nitrogen and mounted on a Mikro Dismembrator (B Braun Instruments) which was operated for one minute. On average, three cycles of freezing and homogenization were required for each sample. When homogenization was complete, samples were warmed to room temperature without opening the capsule. Duplicate samples of approximately 100 mg were weighed into previously labelled, tared 13mm x 100mm culture tubes. These duplicate samples were subsequently analyzed for water, chondroitin sulphate, keratan sulphate and collagen.

Water. The weighed samples were spread as a thin film on the walls of the tube, the tube was stoppered and the contents frozen by immersion in dry ice-methanol for 10-15 minutes. A 900ml freeze-drying flask was cooled by immersion in dry ice-methanol in a Dewar vacuum flask. The freeze-drying flask was positioned to permit rapid attachment to the freeze-drying apparatus. When the samples and flask were thoroughly chilled, each sample in turn was wiped,

FIGURE 5: SITES OF TISSUE SAMPLING FOR CHEMICAL ANALYSIS

The regions from which blocks of tissue (black squares) were harvested from the anterior annulus, nucleus and posterior annulus. The dissection was attempted to avoid transition zones and to remain strictly in annulus or nucleus.



the stopper was removed and the tube was transferred to the flask. The flask was sealed, attached to the freeze-dryer, and the valve opened to evacuate the flask. When the vacuum had fallen to 0.01 mm Hg, the freeze-drying flask was placed in an ice-salt mixture. Drying required 24-48 hours, at which time the vacuum was released and the samples were transferred to a vacuum desiccator for drying over phosphorus pentoxide. After 16 to 24 hours, the samples were quickly weighed on an analytical balance. The vacuum desiccation was repeated until 2 weighings agreed within 0.2 mg. The tissue water content calculated as follows:

$$\frac{\text{Loss in Weight (mg)}}{\text{Sample Weight (g)}} = \text{water (mg/g fresh wt.) (Sweeny et al., 1963)}$$

Digestion with papain. To permit the assays for chondroitin sulphate, keratan sulphate and collagen, the tissue was dissolved by papain digestion (Pearce & Mathieson, 1967). One ml of 0.2 M sodium acetate buffer pH 5.5 containing 5mM Na₂ EDTA was added to the dried sample and the mixture was allowed to soak overnight at 4° C. The sample was placed in a water bath at 55° C and a second 1 ml of buffer added. When required, a glass stirring rod was used to assure that all tissue was suspended in the buffer. Twenty µl of freshly prepared 0.5 M L-cysteine.HCl was added to each sample and then mixed with a vortex mixer. Twenty µl of activated papain, prepared by mixing 1.0 ml buffer, 125 µl of 0.5 M L-cysteine.HCl, 100 µl papain (32 mg/ml Millipore Corp.), and heating at 55°C for 30 minutes, was added to each sample avoiding agitation; digestion was continued overnight at 55°C. If digestion was incomplete, a second 20 µl of freshly prepared activated papain was added and the digestion continued 24 hours. When necessary, the digest was centrifuged and the supernatant fluid was decanted into a clean, labelled stoppered test tube.

Chondroitin Sulphate. A micro adaptation of the colorimetric assay for hexuronate described by Bitter and Muir (1962) was used to estimate the chondroitin sulphate content of the tissue.

Duplicate 10 μ l samples of the supernatant fluid and Na glucuronate (Corn Products) standards containing 0, 20, 40 or 60 nmoles were pipetted into duplicate labelled 13 x 100 mm test tubes. The volume was diluted to 200 μ l with distilled water and chilled in an ice bath; 1.2 ml of cold (4°C) boro-sulphuric acid (0.025 M $\text{Na}_2\text{B}_4\text{O}_7 \cdot 10\text{H}_2\text{O}$ in 18 M (conc.) H_2SO_4) were added to each tube and mixed immediately with a vortex mixer. The tubes were kept chilled until all additions were complete and then transferred to a boiling water bath for 10 min. Upon completion of heating, the tubes were replaced in the ice bath before the addition of 50 μ l of carbazole reagent [125 mg of carbazole in 100 ml abs. ethanol (Eastman)] to each tube and mixing. The tubes were then placed in the boiling water bath for 15 min. and then chilled in the ice bath before reading absorbance at 530 nm. The concentration of hexuronate, in μ mole per ml sample, was calculated using a linear regression equation. Using the factor 0.503 mg chondroitin sulphate per μ mole hexuronate derived from the weight of the repeating unit, results were expressed as mg chondroitin sulphate per g fresh tissue.

Keratan Sulphate. A micro adaptation of a colorimetric assay for hexose (Scott & Melvin, 1953) was used to assay the keratan sulphate of the tissue. Duplicate 25 μ l portions of the supernatant fluid and of standards containing 0, 20, 40 or 80 nmole galactose (Calbiochem) were diluted to 500 μ l with distilled water and placed in an ice bath. One ml of chilled anthrone reagent [200 mg anthrone in 100 ml 18 M (conc.) H_2SO_4 (Fisher)] was added into each tube and immediately mixed with a vortex mixer. The tubes were heated in a

and bath at $90^{\circ} \text{C} \pm 1^{\circ} \text{C}$ for 10 min., then cooled in an ice bath before reading absorbance at 620 nm. The HP97 programmable calculator was used to calculate the μmole galactose per g fresh wt. for each sample. The factor 0.495 mg keratan sulphate per μmole galactose, corresponding to the weight of the repeating unit, was used to obtain the mg keratan sulphate per g fresh tissue.

Collagen. A micro adaptation of the colorimetric assay for hydroxyproline as described by Woessner (1961) was used to estimate collagen.

Samples containing 20-100 nmoles hydroxyproline, approximately 25 μl of anulus digest and 50 μl of nucleus digest, were hydrolyzed in 1.0 ml of 6M HCl at 120°C for 16 hours. The contents of the tubes were transferred with three 1 ml rinses of distilled water into a 50 ml beaker and dried in vacuo over flake NaOH. The dried hydrolysates were dissolved in 5.00 ml of distilled water. Duplicate 500 μl portions of the standards containing 0, 5, 10, 15 or 20 nmoles each of hydroxyproline (Calbiochem) and of hydrolysates were pipetted into labelled 13 x 100 mm test tubes. Reagents were added and mixed immediately in the following sequence:

- 1) 250 μl freshly prepared 0.05M chloramine T (Eastman) [0.28 g chloramine T in 4 ml dist. water, 5 ml methyl cellosolve and 10 ml Na citrate-acetate buffer pH 6.0]. After exactly 20 min. at room temp.,
- 2) 250 μl 3.15 M HClO_4 was added and mixed; after at least 5 min. at room temp.
- 3) 250 μl 20% (w/v) p-dimethylaminobenzoic acid in methyl cellosolve were added and mixed.

The tubes were heated at 60°C for 20 min., cooled in tap water for 5 min. and the absorbance at 557 nm read. The HP97 programmable calculator was used

to calculate μ moles hydroxyproline per g fresh wt. and the factor 0.952 mg collagen per μ moles hydroxyproline, derived from amino acid analysis, used to obtain mg collagen per g fresh weight.

2.7.1 HISTOLOGIC PREPARATION: FRESH SPECIMENS

The 5 mm sagittal slice for histological study was fixed in 10% formalin for a minimum of 21 days. Decalcification with EDTA, although slow, was chosen to minimize tissue injury; 500ml of dist. water containing 50g of disodium ethylenediamine tetraacetate adjusted to pH 6 was used. The solution was prepared fresh and changed every fourth day. The endpoint, usually after four changes, was verified by Faxitron examination of the specimen.

The specimens, 10 discs at a time, were embedded in paraffin. After decalcification, specimens were washed overnight in tap water and then placed in 70% (v/v) ethanol for a minimum of 24 hours. The specimens were trimmed of excess bone and marked for identification and orientation with a no. 22 scalpel. The individual discs were placed in separate tissue cassettes with appropriate labels and sequentially washed in 750 ml solutions of 95% (v/v) ethanol, absolute ethanol and chloroform for 90 min. Solutions were mixed using a magnetic stirrer. The tissue cassettes were passed through three paraffin baths for 30 min. each, at 60°C. Paper boats, with dimensions 10 cm x 3 cm x 3 cm, were filled with paraffin at 60°C, two discs were placed in the bottom of each boat at a slight obliquity. To decrease paraffin granule size and increase hardness, the boats were cooled quickly by immersion in cold water. The blocks were allowed to harden overnight before trimming excess paraffin around the discs and attachment to a mounting block. Each tissue block was appropriately labelled and the presenting surface for the microtome bevelled.

The blocks were trimmed by sectioning at a thickness of 10 μm . The final sections were cut at a thickness of 7 μm and strung across the surface of a 46°C water bath. An adhesive, containing equal volumes of egg white and glycerin, was spread thinly on 25 x 75 mm glass slides. A heated knife was used to separate sections on the water bath; individual sections were mounted on the slides and then baked for a minimum of 1 hour at 60° C. Four sections of each disc were cut and mounted on separate slides.

Three of the sections were stained with hematoxylin and eosin as a standard, alcian blue to identify proteoglycan, and Mallory's trichrome to identify collagen, respectively, using the methods outlined in Appendix 3.

Cover slips were mounted and allowed to dry for 48 hours.

Sections were examined with a binocular dissecting microscope with zoom objective (Bausch and Lomb) and a binocular optical microscope with 4x, 10x and 40x objectives (Swift).

2.7.2 HISTOLOGIC PREPARATIONS: FROZEN SPECIMENS

The three specimens preserved at -80°C were split when the band saw became available. The 5 mm specimen required for histology was fixed by freeze-substitution (Feder & Sidman, 1958; Thompson, 1966; Pearse, 1968) in an effort to minimize tissue distortion by ice-crystals. To ensure thorough fixation before decalcification, the following adaptation of the method described by Feder & Sidman (1958) was used: the frozen specimen was placed in 250ml of 1% (w/v) picric acid in abs. ethanol at -80° C for a minimum of 14 days, then transferred to a 1% (w/v) solution of picric acid in 80% (v/v) ethanol at -4° C. After 72 hours, the specimen was placed in 10% (v/v) formalin at -4° C, then after 72 hours allowed to warm to room temperature. Formalin fixation was allowed to proceed over 14 days, when the specimen was

decalcified, embedded, sectioned, stained and mounted as described for the fresh specimens.

2.7.3 PHOTOMICROGRAPHY

A Leitz (Wild Leitz, Ottawa) orthoplan photomicroscope utilizing bright field objectives of 4, 10 and 40x was used in conjunction with Kodachrome 35 mm colour slide film (Kodak, Kodachrome ASA 25). Inter- negatives from these slides were used to produce colour prints.

CHAPTER 3

RESULTS

3.1 PROFILE OF THE SPECIMENS

Fifteen lumbar spines from five female and ten male donors (Table 3) with an equitable age distribution (Figure 6) formed the sample population from which 68 discs were selected to form the input spectrum for testing the classifications. Three L5-S1 discs were excluded because of damage during specimen collection, two L5-S1 discs because of pelvic trauma involving S1 and two discs because the photographs were of poor quality.

3.2 THE EFFECT OF DELAY IN IMAGING

Images obtained immediately after specimen collection were compared with those at 24 hours. No differences were apparent for either the spin echo or inversion recovery sequences in any of three specimens (Figure 7).

3.3 TESTING OF THE CLASSIFICATIONS

Content and Face Validity. On the basis of literature review, personal observation and critical review by experienced observers, the classifications fulfilled the criteria for content and face validity.

The observational data, or descriptive parameters, and the overall designated category, or grade, of each disc for each observer was entered into a computer disc file. Data was entered according to spine, disc and observer under column headings for each parameter recorded (Appendix 2).

Criterion Validity - Intra-Observer Agreement. The frequency matrices, observed agreement, expected (chance) agreement and kappa statistics for intra-observer agreement are shown in Tables 4 and 5.

TABLE 3: DEMOGRAPHIC DATA OF THE DONORS

Age, sex and cause of death of the donors

	SPECIMEN	AGE	SEX	CAUSE OF DEATH
1	G18	16	M	MVA
2	G19	51	F	FALL
3	G20	75	F	MI
4	G21	21	M	MVA
5	G22	63	M	MI
6	G23	36	F	Leukemia
7	C1	21	M	MVA
8	C2	39	M	MVA
9	C3	16	M	MVA
10	C4	73	M	MI
11	C5	57	M	MI
12	C6	33	M	MVA
13	U32	85	F	Pneumonia
14	U34	89	F	MI
15	U35	44	M	Hepatic Failure

FIGURE 6: AGE DISTRIBUTION OF DONORS

The specimens obtained provided an even representation of each decade.

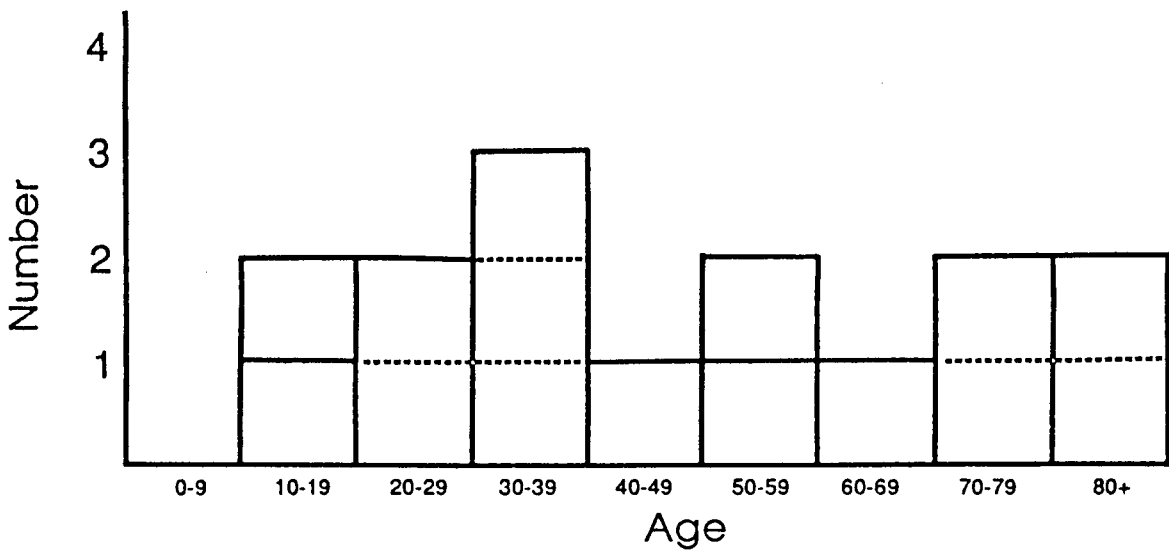
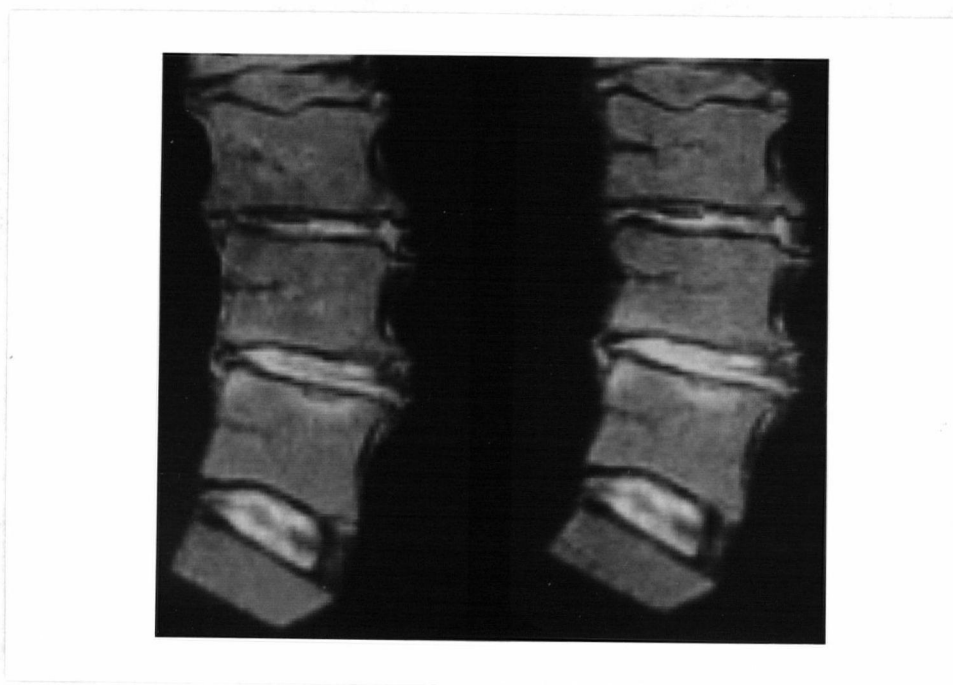


FIGURE 7: THE EFFECT OF DELAY IN MAGNETIC RESONANCE IMAGING OF THE DISC

MRI images of discs L2,3 to L5,S1 of specimen C4 at time of collection (a) and 24 hours later (b). The lack of apparent change suggests that time delay and ex vivo imaging are not important.



a

b

TABLES 4a-c: EVALUATION OF INTRA-OBSERVER AGREEMENT FOR
OVERALL MORPHOLOGIC CATEGORY

The frequency matrices comparing the overall morphologic category assigned to duplicates of each disc by observers 1 (a), 2 (b) and 3 (c). The diagonal indicates perfect agreement.

4(a) OBSERVER 1

Replicate 2

Replicate 1

	1	2	3	4	5	
1	11	0	0	0	0	11
2	2	16	0	0	0	18
3	0	4	11	2	0	17
4	0	0	0	14	0	14
5	0	0	0	1	7	8
	13	20	11	17	7	68

OBSERVED AGREEMENT 0.9670
 EXPECTED AGREEMENT 0.6417
 KAPPA STATISTIC 0.9077

4 (b) OBSERVER 2

Replicate 2

Replicate 1

	1	2	3	4	5	
1	5	3	0	0	0	8
2	0	29	1	0	0	30
3	0	3	9	1	0	13
4	0	0	0	14	1	15
5	0	0	0	1	1	2
	5	35	10	16	2	68

OBSERVED AGREEMENT	0.9632
EXPECTED AGREEMENT	0.7243
KAPPA STATISTIC	0.8667

4 (c) OBSERVER 3

Replicate 2

Replicate 1

	1	2	3	4	5	
1	10	0	0	0	0	10
2	3	17	1	0	0	21
3	0	2	12	3	0	17
4	0	0	0	13	0	13
5	0	0	0	0	7	7
	13	19	13	16	7	68

OBSERVED AGREEMENT 0.9670

EXPECTED AGREEMENT 0.6506

KAPPA STATISTIC 0.9053

TERMINOLOGY. Observed Agreement is the simple frequency with which two observers agree. Expected Agreement is the frequency with which two observers would agree on the basis of chance alone. Kappa is the statistic which more accurately reflects agreement within or between observers by correcting for chance.

TABLES 5a-c: EVALUATION OF INTRA-OBSERVER AGREEMENT FOR OVERALL MRI CATEGORY

The frequency matrices comparing the overall MRI category assigned to duplicates of each disc by observers 1 (a), 2 (b) and 3 (c). The diagonal represents perfect agreement.

5 (a). OBSERVER 1

		Replicate 2					
		1	2	3	4	5	
Replicate 1	1	0	0	0	0	0	0
	2	1	16	4	0	0	21
	3	0	5	22	2	0	29
	4	0	0	2	7	0	9
	5	0	0	0	0	9	9
		1	21	28	9	9	68

OBSERVED AGREEMENT 0.9490

EXPECTED AGREEMENT 0.7335

KAPPA STATISTIC 0.8070

5(b). OBSERVER 2

Replicate 2

Replicate 1

	1	2	3	4	5	
1	6	2	0	0	0	8
2	0	27	7	0	0	34
3	0	1	10	1	0	12
4	0	0	2	7	0	9
5	0	0	0	1	4	5
	6	30	19	9	4	68

OBSERVED AGREEMENT	0.9490
EXPECTED AGREEMENT	0.7200
KAPPA STATISTIC	0.8162

5(c). OBSERVER 3

Replicate 2

Replicate 1

	1	2	3	4	5	
1	3	0	0	0	0	3
2	0	26	2	0	0	28
3	0	2	22	0	0	24
4	0	0	1	7	0	8
5	0	0	0	1	4	5
	3	28	25	8	4	68

OBSERVED AGREEMENT 0.9780
EXPECTED AGREEMENT 0.7490
KAPPA STATISTIC 0.9121

TABLES 6a-c: EVALUATION OF INTEROBSERVER AGREEMENT
FOR OVERALL MORPHOLOGIC CATEGORY

Tables 6a-c. The frequency matrices of overall morphologic category assigned by observers 1 vs 2 (a), 2 vs 3 (b) and 3 vs 1 (c). The diagonal represents perfect agreement. The cross hatched regions indicate the systematic differences of observer 2 with respect to observers 1 and 3.

6(a) OBSERVERS 1 AND 2

		Observer 2					
		1	2	3	4	5	
Observer 1	1	7	4	0	0	0	11
	2	1	17	0	0	0	18
	3	0	9	7	1	0	17
	4	0	0	6	8	0	14
	5	0	0	0	6	2	8
		8	30	13	15	2	68

OBSERVED AGREEMENT 0.9007
 EXPECTED AGREEMENT 0.6745
 KAPPA STATISTIC 0.6950

6(b) OBSERVERS 2 AND 3

Observer 3

		1	2	3	4	5	
Observer 2	1	7	1	0	0	0	8
	2	3	19	8	0	0	30
	3	0	1	8	9	0	13
	4	0	0	1	9	5	15
	5	0	0	0	0	2	2
		10	21	17	13	7	68

OBSERVED AGREEMENT 0.9154

EXPECTED AGREEMENT 0.6853

KAPPA STATISTIC 0.7313

6(c). OBSERVERS 3 AND 1

		Observer 1					
		1	2	3	4	5	
Observer 3	1	10	0	0	0	0	10
	2	1	18	2	0	0	21
	3	0	0	15	2	0	17
	4	0	0	0	12	1	13
	5	0	0	0	0	7	7
		11	18	17	14	8	68

OBSERVED AGREEMENT	0.9780
EXPECTED AGREEMENT	0.6554
KAPPA STATISTIC	0.9360

TABLES 7a-c: EVALUATION OF INTEROBSERVER AGREEMENT FOR OVERALL MRI CATEGORY

The frequency matrices of overall MRI category assigned by observers 1 vs 2 (a), 2 vs 3 (b) and 3 vs 1 (c). The diagonal represents perfect agreement. The crosshatched areas indicate the systematic differences of observer 1 with respect to observers 2 and 3.

7(a) OBSERVERS 1 AND 2

		Observer 2					
		1	2	3	4	5	
Observer 1	1	0	0	0	0	0	0
	2	7	14	0	0	0	21
	3	1	18	8	2	0	29
	4	0	2	3	4	0	9
	5	0	0	1	3	5	9
		8	34	12	9	5	68

OBSERVED AGREEMENT 0.8493
 EXPECTED AGREEMENT 0.6973
 KAPPA STATISTIC 0.5020

7(b) OBSERVERS 2 AND 3

		Observer 3					
		1	2	3	4	5	
Observer 2	1	3	5	0	0	0	8
	2	0	22	12	0	0	34
	3	0	1	9	2	0	12
	4	0	0	3	6	0	9
	5	0	0	0	0	5	5
		3	28	24	8	5	68

OBSERVED AGREEMENT	0.9154
EXPECTED AGREEMENT	0.7209
KAPPA STATISTIC	0.6970

7(c). OBSERVERS 3 AND 1

Observer 1

Observer 3

	1	2	3	4	5	
1	0	2	1	0	0	3
2	0	17	10	1	0	28
3	0	2	17	5	0	24
4	0	0	1	3	4	8
5	0	0	0	0	5	5
	0	21	29	9	9	68

OBSERVED AGREEMENT 0.8971

EXPECTED AGREEMENT 0.7330

KAPPA STATISTIC 0.6146

The clustering of observations along the diagonals of the frequency matrices and the high kappa values indicated that the observers were consistent in the application of their interpretation of the classification. Intra-observer disagreements, or deviations from the diagonal, were no more than one category. The strength of agreement within observers was "almost perfect" for all six according to the criteria of Landis & Koch (1974). Agreement tended to be greater for the morphologic observers than the MRI observers. The frequency distribution of overall grade differed between observers, particularly for the MRI observers. This indicated that although individual observers were assigning categories consistently, differences in interpretation and application of the classifications occurred between observers. These differences were more striking between the MRI observers. In addition, the distribution of overall grade differed between the morphologic and MRI classifications. The MRI classification identified fewer discs with overall category I and V than the morphologic classification (Figure 36).

Criterion Validity - Interobserver Agreement. The frequency matrices, observed agreement, expected (chance) agreement and kappa statistics for interobserver agreement on overall category are shown in Tables 6 and 7. Observations by observer pairs tended to cluster along the diagonals. As the differing frequency distributions of the intra-observer totals for overall category indicated, the clustering along the diagonal and kappa values for interobserver pairs were less than those for intra-observer pairs. Nonetheless, differences between observers were no more than 1 category for morphology and no more than 2 for MRI. The strength of agreement was substantial in all morphologic interobserver pairs and two MRI interobserver pairs and "moderate" in one MRI interobserver pair (Landis & Koch, 1974). This degree of agreement

is considered acceptable for observations with respect to categorical data (Kramer & Feinstein, 1981).

The strength of interobserver agreement was greater for morphologic observer pairs than the MRI. This result was predictable if the differences in observer tasks are considered. The MRI observers had to form their observations from computer images with less resolution (1 mm) than the colour photograph of the actual physical specimen. Furthermore, MRI is a relatively new technology and experience with interpreting images of discs is limited. As a consequence, a greater likelihood of differences in observations occurring would be expected.

In both classifications, one of the observers - Observer 2 in the gross morphology and Observer 1 in the MRI - frequently disagreed with the other two observers who agreed "substantially". The systematic differences between these observers and the others reflected their inexperience in examination and interpretation of morphologic and MRI specimens. Morphologic Observer 2 was involved in clinical research primarily and consequently had had little opportunity to carefully evaluate pathologic materials. MRI Observer 1, although an experienced radiologist, had had limited exposure to MRI image interpretation. The differences between these observers and the others were systematic as shown by the cross-hatched areas of the frequency matrices. Morphologic observer 2 consistently underestimated overall category and MRI observer 1 consistently overestimated overall category. Better preparation and more experience would likely have resulted in better interobserver agreement between these two observers and the other more experienced observers.

Discriminant Validity. The results of the kappa statistic suggested that the classifications were responsive to change. As confirmation, discriminant

analysis developed a highly significant linear model for overall category (grade) that used most of the descriptive parameters (variable) for both the MRI and morphologic classifications (Tables 8 and 9).

The stepwise selection of variables (descriptive parameters) for the morphologic model predicting overall grade (category) continued until all but three parameters were used. This indicated that observers used all information except that concerning the cartilaginous inferior end plate (CIEP) and the anterior and posterior inferior vertebral bodies (VBAIAZ, VBPIAZ) in distinguishing the overall category to which a particular disc belonged. Wilks' lambda, a likelihood ratio statistic for testing the hypothesis that the means of the categories on the selected variables are equal, approached zero suggesting the categories were well separated. This measure of discriminatory function quickly approached zero (0.1402) with the initial model using tissue morphology of the nuclear zone (TMNZ). Further additions to the model resulted in less impressive decreases in Wilks' lambda, suggesting that tissue morphology of the nuclear zone was the most important parameter in distinguishing one grade from another. The high partial correlation coefficient for this variable (0.8598) also attests to its relative importance in decisions about overall grade.

TABLE 8: STEPWISE DISCRIMINANT ANALYSIS OF THE MORPHOLOGIC DATA

The summary of stepwise discriminant analysis of the morphologic data for the model with overall category as the dependent variable. The independent variables were added and deleted according to the F value (the ratio of the regression mean square to the error mean square). The only variables not added to model were CIEP, VBIAZ and VBPIAZ. The partial R^2 represents the square of the multiple correlation coefficient of each variable. The tissue morphology of the nuclear zone (TMNZ) accounted for the greatest portion of the variance for the model (0.8598). Wilk's lambda, a likelihood ratio statistic, approached zero indicating the variables in the model were able to distinguish and therefore characterize accurately overall grade.

STEP	VARIABLE ENTERED	PARTIAL R * * 2	F STATISTIC	PROB > F	WILKS LAMBDA
1	TMNZ	0.8598	617.989	0.0001	0.1402
2	TIASAZ	0.2511	33.694	0.0001	0.1050
3	SIEP	0.1699	20.517	0.0001	0.0871
4	TMASAZ	0.1408	16.386	0.0001	0.0749
5	TINZ	0.1326	15.254	0.0001	0.0649
6	TIPSAZ	0.0804	8.698	0.0001	0.0597
7	TMPSAZ	0.0788	8.490	0.0001	0.0550
8	CSEP	0.0669	7.103	0.0001	0.0513
9	VBASAZ	0.0437	4.512	0.0014	0.0491
10	SSEP	0.0408	4.195	0.0024	0.0471
11	TMPIAZ	0.0354	3.601	0.0067	0.0454
12	TIPIAZ	0.0406	4.143	0.0027	0.0436
13	VBPSAZ	0.0285	2.865	0.0232	0.0423
14	TIAIAZ	0.0187	1.860	0.1168	0.0415
15	TMAIAZ	0.0178	1.758	0.1165	0.0408

TABLE 9: STEPWISE DISCRIMINANT ANALYSIS OF THE MRI DATA

Summary of stepwise discriminant analysis of the MRI data for the model with overall category as the dependent variable. The independent variables were added and deleted according to the F value (the ratio of the regression mean square to the error mean square). The partial R^2 represents the square of the multiple correlation coefficient of each variable, that is, the fraction of the total variance attributable to the variable. The nuclear zone (NZ) accounted for a much greater portion of the variance of the model for grade than any other variable. Wilks' lambda, a likelihood ratio statistic, approached zero indicating the variables in the model were good at discriminating between overall categories.

STEP	VARIABLE ENTERED	PARTIAL R * * 2	F STATISTIC	PROB > F	WILKS LAMBDA
1	NZ	0.8841	768.738	0.0001	0.1159
2	VBPI	0.3013	43.331	0.0001	0.0810
3	AZAI	0.2265	29.347	0.0001	0.0626
4	VBAI	0.0620	6.611	0.0001	0.0587
5	AZPI	0.0566	5.985	0.0001	0.0554
6	EPI	0.0504	5.282	0.0004	0.0526
7	AZAS	0.0379	3.911	0.0040	0.0506
8	VBPS	0.0310	3.172	0.0139	0.0491
9	VBAS	0.0208	2.096	0.0807	0.0480

In the MRI model for predicting overall grade, only the superior end plate (SIEP) and posterior superior anular zone (AZPS) did not contribute significantly. Although the model derived from the data suggested observers used most of the parameters to distinguish grade, nuclear zone provided most of the discriminatory function as reflected by Wilks' lambda (0.1159) and the partial correlation coefficient (0.8841) for the model consisting of nuclear zone (NZ) alone. The other parameters provided further refinement.

In both the morphologic and MRI analyses, the importance of the nuclear zone in distinguishing grades was striking. The other parameters tended to fine tune the discrimination of one grade from another.

Construct Validity. Principal component analysis of the morphologic and MRI data was done to investigate the relationships of each variable with overall grade and with other variables and develop linear models relating the variables. As an exploratory technique investigating relationships between variables, principal component analysis performs two main functions. First, it generates a table of correlations among all the variables to indicate how strongly, for example, a grade 4 nucleus is related to a grade 4 anulus. Second, it develops linear combinations of variables (models) in which it finds grouping of variables which behave similarly. These models (principal components) develop axes based on factor loadings. The models derived tend to provide a reflection of the decision process used by observers to establish grade (Table 10 and 11). That is to say, the weightings assigned to each disc parameter in the principal components indicate the relative importance the observer ascribes to that parameter in deciding the overall category of the disc.

TABLE 10: MORPHOLOGIC PRINCIPAL COMPONENT ANALYSIS

The principal component analysis (SAS Institute Inc., 1985) included a table of correlations (a), principal components (b) and eigenvalues for each principal component (c).

10(a.) CORRELATIONS

	GRADE	TIASAZ	TIAIAZ	TIPSAZ	TIPIAZ	TMASAZ	TMAIAZ	TMPSAZ	TMPIAZ	VBASAZ
GRADE	1.0000									
TIASAZ	0.7308	1.0000								
TIAIAZ	0.7140	0.8078	1.0000							
TIPSAZ	0.8046	0.6975	0.7361	1.0000						
TIPIAZ	0.7628	0.6464	0.6715	0.8485	1.0000					
TMASAZ	0.8069	0.8905	0.8115	0.7428	0.6796	1.0000				
TMAIAZ	0.7507	0.7590	0.9040	0.7397	0.6843	0.8438	1.0000			
TMPSAZ	0.8270	0.6798	0.7399	0.9319	0.8217	0.7779	0.7958	1.0000		
TMPIAZ	0.7982	0.6569	0.6790	0.8362	0.9218	0.7287	0.7437	0.8663	1.0000	
VBASAZ	0.6383	0.5917	0.6251	0.6105	0.5459	0.6044	0.6531	0.6242	0.6012	1.0000
VBAIAZ	0.5960	0.5761	0.5798	0.5484	0.5152	0.6101	0.6012	0.5636	0.5291	0.7155
VBPSAZ	0.5416	0.4880	0.5070	0.4758	0.4760	0.5230	0.5163	0.5022	0.4753	0.5314
VPBIAZ	0.4833	0.4469	0.4753	0.4505	0.4618	0.4823	0.5067	0.4734	0.4810	0.5255
CSEP	0.7138	0.4745	0.4997	0.5775	0.5544	0.5378	0.5371	0.6043	0.4794	0.3955
CIEP	0.6215	0.4005	0.4029	0.4838	0.4589	0.4796	0.4702	0.5182	0.4784	0.3666
SSEP	0.6799	0.4845	0.5084	0.5286	0.4609	0.5676	0.5706	0.6019	0.5206	0.4724
SIEP	0.6411	0.4026	0.4395	0.4883	0.4504	0.5041	0.5054	0.5529	0.5133	0.4294
TINZ	0.9000	0.7147	0.7100	0.8379	0.8183	0.7681	0.7447	0.8531	0.8407	0.6468
TMNZ	0.9239	0.6992	0.7062	0.8058	0.7897	0.7721	0.7428	0.8352	0.8364	0.6178

10(a). CORRELATIONS (cont.)

	VBAIAZ	VBPSAZ	VBPIAZ	CESP	CIEP	SSEP	SIEP	TINZ	TMNZ
GRADE									
TIASAZ									
TIAIAZ									
TIPSAZ									
TIP1AZ									
TMASAZ									
TMPSAZ									
TMP1AZ									
VBASAZ									
VBA1AZ	1.0000								
VBPSAZ	0.5704	1.0000							
VBPIAZ	0.5599	0.6180	1.0000						
CSEP	0.3610	0.4213	0.3116	1.0000					
CIEP	0.3511	0.4289	0.3540	0.7746	1.0000				
SSEP	0.4420	0.4325	0.3439	0.7119	0.5807	1.0000			
SIEP	0.4330	0.3734	0.3985	0.6522	0.7180	0.7071	1.0000		
TINZ	0.6112	0.5548	0.4946	0.6427	0.5379	0.6080	0.5523	1.0000	
TMNZ	0.5755	0.5572	0.4911	0.6709	0.5764	0.6368	0.5969	0.9225	1.0000

10(b). PRINCIPAL COMPONENTS

	PRIN1	PRIN2	PRIN3	PRIN4	PRIN5	PRIN6	PRIN7	PRIN8	PRIN9	PRIN10
GRADE	0.265252	0.080709	-.087277	0.019567	-.048711	-.155708	-.030958	-.298656	-.171317	-.158284
TIASAZ	0.231998	-.207105	-.057468	-.390487	0.218153	-.077749	0.124928	-.350816	-.065785	0.036862
TIAIAZ	0.238923	-.205160	-.048282	-.362867	0.175360	0.134701	0.005730	0.332720	0.022333	0.019045
TIPSAZ	0.252079	-.092162	-.237796	0.176427	-.050750	0.050999	0.019327	0.172839	0.119987	0.051124
TIPIAZ	0.241020	-.099534	-.254121	0.360445	0.032912	0.071915	0.067299	0.057675	0.143353	0.205542
TMASAZ	0.250560	-.136034	-.058286	-.334534	0.172770	0.005227	0.022942	-.282960	0.070256	-.038024
TMAIAZ	0.249067	-.145279	-.033102	-.299998	0.101156	0.205244	-.039336	0.344803	0.037756	-.040597
TMPSAZ	0.259689	-.047600	-.199116	0.135896	-.071377	0.092431	-.101184	0.194405	0.153461	-.029620
TMPIAZ	0.250750	-.073582	-.233208	0.297596	-.041575	0.125016	-.018485	0.044317	0.060346	0.037218
VBASAZ	0.210781	-.186934	0.268273	-.033805	-.525298	-.075467	0.212957	0.305124	-.441032	-.363236
VBAIAZ	0.200976	-.193115	0.386194	-.037002	-.442692	-.111628	0.256155	-.195394	0.365267	0.518544
VBPSAZ	0.185065	-.072807	0.466571	0.213145	0.401013	-.520126	-.149792	0.214199	0.339089	-.242621
VBPIAZ	0.172609	-.143711	0.503163	0.302503	0.290919	0.522653	-.181556	-.160149	-.378275	0.173369
CSEP	0.206612	0.438972	-.046968	-.024139	0.133702	-.216485	0.143191	0.186909	-.334349	0.441801
CIEP	0.185238	0.482466	0.110370	0.015071	0.212820	0.063791	0.581694	0.074736	0.016521	-.082575
SSEP	0.203063	0.355691	0.089003	-.234660	-.211531	-.115445	-.651949	0.097980	-.051495	0.231273
SIEP	0.191286	0.436734	0.153608	-.079256	-.192697	0.433562	-.063302	-.160651	0.401150	-.346490
TINZ	0.262800	-.021666	-.124715	0.162885	-.076045	-.186153	-.052006	-.227103	-.122852	-.107128
TMNZ	0.262435	0.037789	-.116886	0.131664	-.023094	-.169479	-.094113	-.273504	-.143507	-.215014

	PRIN11	PRIN12	PRIN13	PRIN14	PRIN15	PRIN16	PRIN17	PRIN18	PRIN19
GRADE	-.220459	-.053911	0.035090	-.023781	-.629202	-.214603	-.461032	-.188879	0.021709
TIASAZ	0.469898	0.025125	0.217807	0.130952	0.224103	0.225387	-.362468	.0131184	-.117739
TIAIAZ	-.285214	0.124039	0.386552	0.287614	-.121185	0.129086	0.224608	-.437790	0.063195
TIPSAZ	0.167110	-.558113	0.267128	0.069582	-.116912	-.048555	0.065101	0.332973	0.491025
TIPIAZ	0.234716	0.409240	0.073828	0.250507	-.211319	-.320160	0.165444	0.187750	-.400054
TMASAZ	0.170851	-.076537	-.361671	-.363368	-.134654	-.259541	0.534555	-.101721	0.084103
TMAIAZ	-.364250	0.130125	-.317555	-.116082	0.111431	-.172621	-.312850	0.489741	-.017950
TMPSAZ	0.029520	-.477089	-.141878	-.210143	0.124277	0.196654	-.123012	-.313490	-.570776
TMPIAZ	0.150488	0.417125	-.275742	-.186607	0.092108	0.338159	-.186786	-.290345	0.463196
VBASAZ	0.279517	0.079822	0.009177	-.054842	-.021962	-.037356	0.094305	0.012703	-.049540
VBAIAZ	-.216862	-.028867	-.036704	0.007415	-.013122	0.082926	-.026697	-.005343	0.014339
VBPSAZ	0.084573	0.055025	0.053020	-.089530	-.009819	-.012184	-.043341	0.004289	0.025961
VBPIAZ	-.010377	-.121161	0.007680	0.015317	-.003551	-.003544	0.010449	-.009155	-.003822
CSEP	-.037618	0.079732	0.287108	-.483729	0.076473	-.006315	0.040209	0.040401	-.036532
CIEP	0.033675	-.137208	-.355144	0.406968	0.005464	0.053055	0.009925	-.066244	0.032496
SSEP	0.224798	-.004005	-.232203	0.340714	-.027407	0.011406	0.028970	-.006316	0.046866
SIEP	0.048684	0.152106	0.06290	-.201161	0.073385	-.050816	0.005606	0.050368	-.015309
TINZ	-.259867	-.31495	0.068478	0.184767	0.642107	-.451384	0.019365	-.184349	0.096629
TMNZ	-.354174	0.058924	-.010556	0.076527	-.036281	0.560082	0.346549	0.365636	-.123639

10(c). EIGEN VALUES

	EIGEN VALUE	DIFFERENCE	PROPORTION	CUMULATIVE
PRIN. 1	12.2033	10.6795	0.642280	0.64228
PRIN. 2	1.5328	0.3725	0.080201	0.72248
PRIN. 3	1.1513	0.3941	0.060594	0.78308
PRIN. 4	0.7572	0.1942	0.039851	0.82293
PRIN. 5	0.5630	0.1181	0.029631	0.85256
PRIN. 6	0.4449	0.0487	0.023416	0.87597
PRIN. 7	0.3961	0.0465	0.020850	0.89682
PRIN. 8	0.3496	0.0587	0.018402	0.91522
PRIN. 9	0.2909	0.0246	0.015311	0.93054
PRIN. 10	0.2663	0.0339	0.014013	0.94455
PRIN. 11	0.2323	0.0094	0.012227	0.95678
PRIN. 12	0.2229	0.0616	0.011731	0.96851
PRIN. 13	0.1613	0.0291	0.008487	0.97699
PRIN. 14	0.1322	0.0463	0.006957	0.98395
PRIN. 15	0.0859	0.0145	0.004521	0.98847
PRIN. 16	0.0714	0.0141	0.003760	0.99223
PRIN. 17	0.0573	0.0069	0.003016	0.99525
PRIN. 18	0.0504	0.0105	0.002652	0.99790
PRIN. 19	0.0399		0.002100	1.00000

TABLE 11: MRI PRINCIPAL COMPONENT ANALYSIS

Principal component analysis of the MRI data showing correlations (a), principal components (b) and eigenvalues (c).

11(a). CORRELATIONS

	GRADE	EPS	EPI	NZ	AZAS	AZAI	AZPS	ASPI	VBAS	VBAI	VBPS	VBPI
GRADE	1.0000											
EPS	0.6740	1.0000										
EPI	0.5687	0.6962	1.0000									
NZ	0.9396	0.6470	0.5431	1.0000								
AZAS	0.6828	0.5567	0.4528	0.6131	1.0000							
AZAI	0.7485	0.5998	0.5010	0.6785	0.7936	1.0000						
AZPS	0.6468	0.5730	0.5294	0.6032	0.5933	0.6322	1.0000					
AZPI	0.6624	0.5561	0.5117	0.6143	0.5928	0.6623	0.9040	1.0000				
VBAS	0.5675	0.4721	0.3699	0.5198	0.4929	0.4921	0.4086	0.4561	1.0000			
VBAI	0.5564	0.4902	0.3780	0.4803	0.5019	0.5444	0.4263	0.4879	0.6584	1.0000		
VBPS	0.5794	0.4197	0.4100	0.5876	0.4935	0.4921	0.4199	0.4488	0.5223	0.4614	1.0000	
VBPI	0.5292	0.4330	0.3850	0.5096	0.4939	0.4462	0.4169	0.3961	0.4662	0.4187	0.7002	1.0000

11(b). PRINCIPAL COMPONENTS

	PRIN1	PRIN2	PRIN3	PRIN4	PRIN5	PRIN6
GRADE	0.338344	-.042419	0.051862	0.022582	-.337171	-.393307
EPS	0.289221	-.213830	0.300471	0.399678	-.000265	0.115660
EPI	0.258674	-.238788	0.419987	0.459761	0.265088	0.234182
NZ	0.320859	-.032684	0.151031	0.004631	-.351086	-.542719
AZAS	0.299934	-.039406	-.161901	-.176980	-.386441	0.542152
AZAI	0.314871	-.121796	-.184067	-.100942	-.376480	0.303694
AZPS	0.295781	-.368762	-.139163	-.317936	0.395729	-.080471
AZPI	0.301409	-.324845	-.226664	-.288551	0.381212	-.126881
VBAS	0.259546	0.380154	-.329246	0.352822	0.161558	-.133089
VBAI	0.255617	0.301098	-.500234	0.320079	0.160228	0.061625
VBPS	0.264148	0.449591	0.287981	-.270077	0.124802	-.069946
VBPI	0.249189	0.446300	0.367997	-.320334	0.180097	0.217739

	PRIN7	PRIN8	PRIN9	PRIN10	PRIN11	PRIN12
GRADE	0.085375	-.118737	0.136483	0.014139	-.001478	-.756262
EPS	-.378580	-.241558	-.633316	0.061619	-.025503	-.004010
EPI	0.335016	0.246132	0.434868	-.026877	-.021388	0.008871
NZ	0.079531	-.078765	0.124469	0.128517	-.008616	0.640884
AZAS	-.134060	0.116690	0.156660	0.588105	-.073642	0.016302
AZAI	0.101101	0.123454	-.094911	-.744249	0.095110	0.102774
AZPS	-.088212	-.056914	0.033813	0.092760	0.687175	0.004866
AZPI	-.016168	0.048544	-.050521	-.045874	-.707281	0.006896
VBAS	-.592553	0.266053	0.272066	-.119736	0.028845	0.018077
VBAI	0.543063	-.319855	-.200073	0.142007	0.046848	0.047222
VBPS	0.190535	0.579493	-.406514	0.085969	0.062119	-.055973
VBPI	-.110687	-.563391	0.243171	-.162447	-.070747	0.025535

11(c). EIGEN VALUES

	EIGEN VALUE	DIFFERENCE	PROPORTION	CUMULATIVE
PRIN. 1	7.06647	5.98079	0.588872	0.58887
PRIN. 2	1.08568	0.28947	0.090473	0.67935
PRIN. 3	0.79621	0.09121	0.066351	0.74570
PRIN. 4	0.70500	0.08529	0.058750	0.80445
PRIN. 5	0.61971	0.12595	0.051642	0.85609
PRIN. 6	0.49375	0.13623	0.041146	0.89723
PRIN. 7	0.35752	0.05198	0.029793	0.92703
PRIN. 8	0.30554	0.06043	0.025462	0.95249
PRIN. 9	0.24511	0.05748	0.020426	0.97292
PRIN. 10	0.18763	0.09964	0.015636	0.98855
PRIN. 11	0.08799	0.03859	0.007332	0.99588
PRIN. 12	0.04940		0.004117	1.00000

For a 1% two-tailed significance level, correlation coefficients must exceed 0.325 for 68 specimens (Snedecor & Cochran, 1980). Correlations were significant for every comparison in the MRI and morphologic analyses. This suggested that changes in one variable would be reflected by a similar change in other variables. For example, in a disc designated as overall category 5, the anular, nuclear, endplate and vertebral body parameters would also be category 5 with significant consistency. This suggests that with aging and degeneration, components of the disc change in concert rather than in isolation.

In both principal component analyses, the nuclear zone parameters (TMNZ, NZ) had the highest correlations with grade and with other parameters. Unlike the other parameters, the weighting of the nuclear zone in each of the principal components changed independent of the other variables. This suggested the nuclear zone parameter is important in determining overall category on its own and not wholly dependent on other variables. High correlations were also noted between the superior and inferior anular zones. The large partial R^2 of the nuclear parameters in stepwise discrimination and the independence of the nuclear zone parameter relative to other parameters in each principal component suggests two things. First, the nuclear zone parameter is the most important in establishing grade and second, changes in the nucleus are more consistent and may precede changes in other parameters.

The first principal component in both analyses had relatively even factor loadings. Subsequent principal components had uneven factor loadings that changed in an almost systematic fashion with each principal component. For example, in the morphologic and MRI analysis, the loadings changed in this fashion:

- MORPHOLOGIC PRINCIPAL COMPONENT 1 Evenly weighted, no particular axis
- MORPHOLOGIC PRINCIPAL COMPONENT 2 Endplate (CSEP, CIEP, SSEP, SIEP) weighted axis
- MORPHOLOGIC PRINCIPAL COMPONENT 3 Vertebral body (VBASAZ, VBAIAZ, VBPSAZ, VBPIAZ) weighted axis
- MORPHOLOGIC PRINCIPAL COMPONENT 4 Posterior vertebral body (VBPASAZ, VBPIAZ) and tissue integrity of the posterior anulus (TIPSAZ, TIPIAZ) weighted axis
- MORPHOLOGIC PRINCIPAL COMPONENT 5 Tissue integrity of the anterior anulus (TIASAZ, TIPIAZ) and posterior vertebral body (VBPSAZ, VBPIAZ) weighted axis
-
- MRI PRINCIPAL COMPONENT 1 Evenly weighted for all variables
- MRI PRINCIPAL COMPONENT 2 Vertebral body (VBAS, VBAI, VBPS, VBPI) weighted axis
- MRI PRINCIPAL COMPONENT 3 End plate (EPS, EPI) and posterior vertebral body (VBPS, VBPI) weighted axis
- MRI PRINCIPAL COMPONENT 4 End plate (EPS, EPI) and anterior vertebral body (VBAS, VBAI) weighted axis
- MRI PRINCIPAL COMPONENT 5 Posterior anular zone (AZPS, AZPI) weighted axis
- MRI PRINCIPAL COMPONENT 6 Anterior anular zone (AZAS, AZAI) weighted axis, and so on.

After morphologic principal component 5 and MRI principal component 6, the axes become less clearly defined in terms of even loadings on groups of variables, indicating that individual parameters become more important in completing the linear models for defining category.

The changes in parameter weights with each principal component suggests observers look at other parameters in addition to the nuclear zone parameter to arrive at a decision. Although the eigenvalue of the first principal component accounts for the largest variance of any linear combination of all the variables, the variance accounted for by the 'stepwise discrimination' model with nuclear zone as the only variable was greater (Table 8 and 9). These observations suggest the parameters other than the nuclear zone parameters may have a cluttering effect that obscures assigning overall grade to a disc. The high correlation of grade and nuclear zone support this.

The 5 x 5 matrix for agreement between the MRI and morphologic classifications is shown in Table 12. The clustering of comparisons along the diagonal suggested the classifications agreed with one another well. Furthermore, most disagreements were within one category. The pattern of disagreement was noteworthy. MRI appeared to consistently overestimate category at the lower end of the scale and underestimate at the higher end when compared with the morphologic grade. As a result, MRI had a greater proportion of categories 2,3 and 4 with fewer of categories 1 and 5. The index of trend (Pearson's correlation coefficient) between the of MRI and morphologic classifications was strong (0.8372) and was highly significant ($p < 0.0001$). The kappa statistic, indicating concordance between the classifications, was "substantial" (0.6172). Simple percentage or observed agreement approached

TABLE 12: EVALUATION OF AGREEMENT ON OVERALL CATEGORY
BETWEEN MORPHOLOGIC AND MRI DATA

Frequency matrix, kappa value and Pearson correlation coefficient for the comparison of morphologic and MRI category. The shaded area represents perfect agreement. The cross hatched area highlights the tendency for MRI to over and underestimate category.

		MORPHOLOGIC CATEGORY					
		1	2	3	4	5	
MRI CATEGORY	1	2	0	0	0	0	2
	2	9	16	3	0	0	28
	3	0	7	8	9	0	24
	4	0	0	2	5	2	9
	5	0	0	0	0	5	5
		11	23	13	14	7	68

OBSERVED AGREEMENT 0.8824

EXPECTED AGREEMENT 0.6924

KAPPA STATISTIC 0.6176

PEARSON CORRELATION COEFFICIENT

0.8372 P < 0.0001

90 per cent. These observations indicated that the morphologic and MRI classifications were comparable and thus provided MRI with a morphologic basis for interpretation.

As described below, when the histologic and chemical data were analyzed in relation to MRI and morphologic grade, the trends observed were consistent with published reports describing changes with aging and degeneration. This suggested the results of the classification agree with independent measures of aging and degeneration. A detailed account of the chemical and histologic data follows.

In summary, the results indicated that the classifications satisfy the criteria for validity.

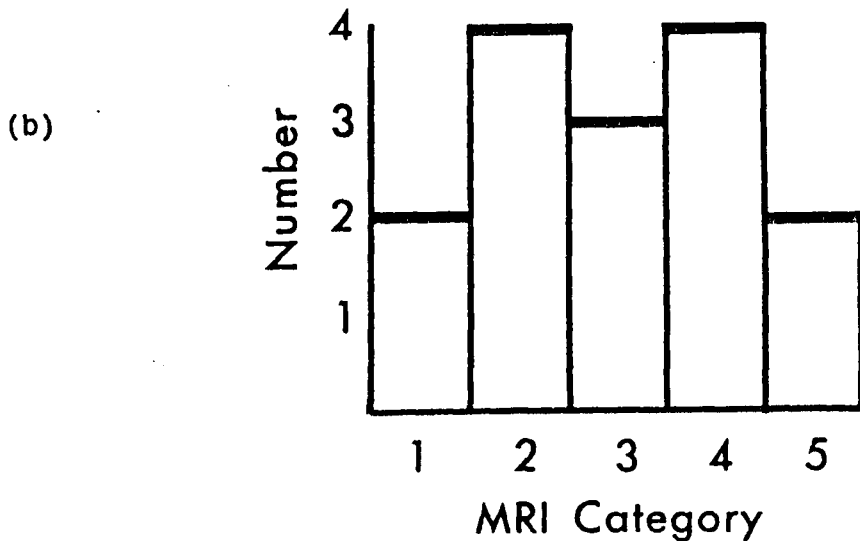
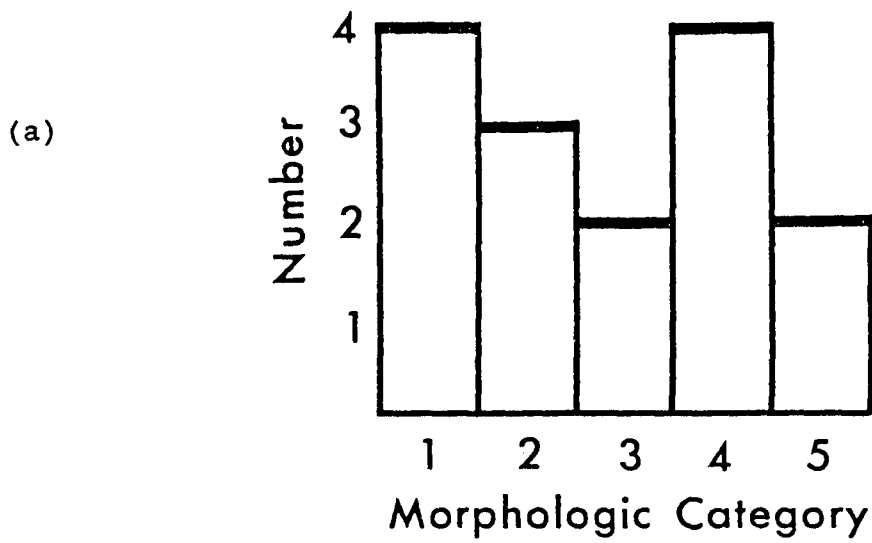
3.4 CHEMICAL ANALYSES

Serendipitously, the discs selected from the young and old spines were nearly evenly distributed by morphologic and MRI category (Figure 8). Differences in the distribution between the morphologic and MRI categories were consistent with those observed in Table 12 where there was a preponderance of MRI category 2, 3, and 4 discs.

Water. Stable weights were usually obtained after two to three weighings. The coefficient of variation of duplicate analyses was 1.27 percent. Water content ranged from 857 mg/g fresh weight for the nucleus of a "young" disc to 619 mg/g fresh weight for the anulus of a "severely degenerate" disc. When plotted as a function of MRI grade, water content of the nucleus fell, the greatest change occurring between MRI categories 2 and 3 (Figure 9a). A tendency for water content to rise slightly in MRI grade 5 was noted. In the anterior and posterior anulus, initial water content was less and an increase

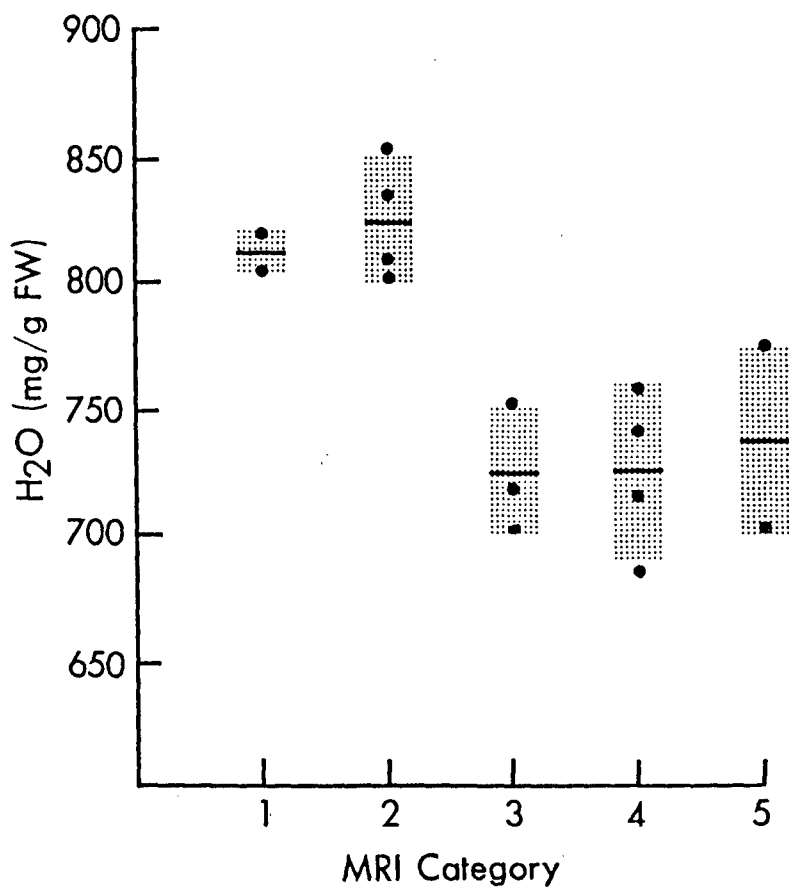
FIGURE 8: DISTRIBUTION OF DISCS SELECTED FOR CHEMICAL AND HISTOLOGIC ANALYSIS BY MORPHOLOGIC AND MRI CATEGORY

The number of discs by morphologic (a) and MRI (b) category



FIGURES 9a-c: WATER CONTENT BY MRI CATEGORY

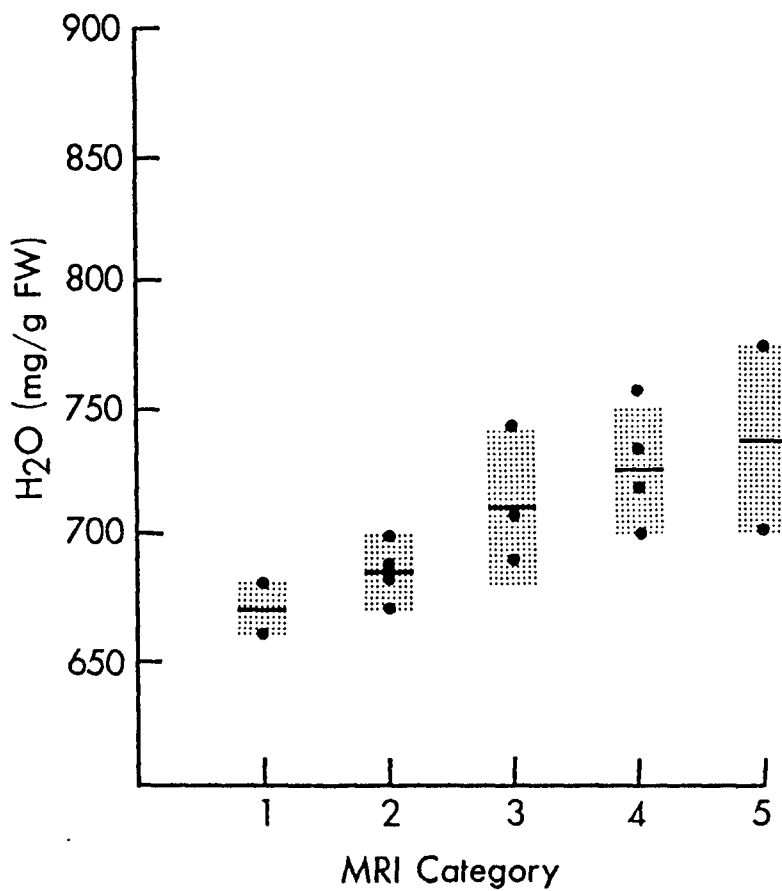
9(a). Water content of the nucleus. The change in water content with increasing category occurred abruptly between categories 2 and 3.



KEY: The horizontal bars represent the mean of the values (dots) for each category. The shaded area indicates the standard deviation.

WATER CONTENT BY MRI CATEGORY (cont'd)

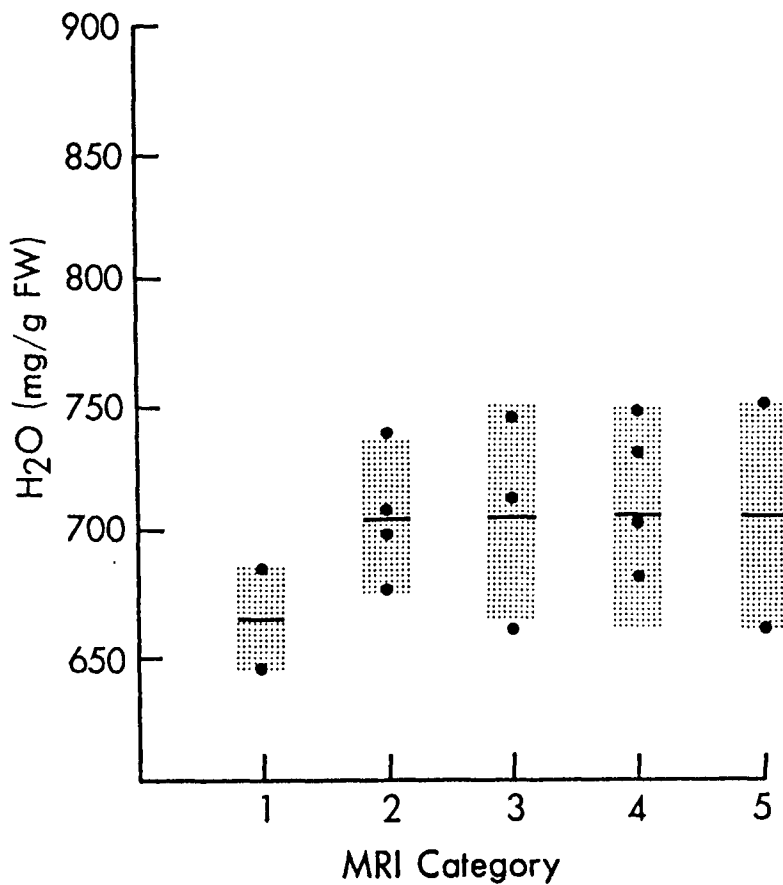
9(b). Water content of the anterior annulus. The increase in water content was gradual between categories 1 and 5.



WATER CONTENT BY MRI CATEGORY (cont'd)

9(c).

Water content of the posterior anulus. The increase in water content was subtle and appeared to occur between categories 1 and 2. The magnitude of change and scatter of data make firm observations difficult.



in water content, negligible after category 2 in the posterior annulus, occurred with increasing MRI category (Figure 9b and c). With increasing MRI category, the range of values for each category increased. This suggested either MRI was less reliable in distinguishing different water content with higher grades or that water content becomes more variable with increasing grade.

When plotted as a function of morphologic grade, trends similar to those in the MRI plots were seen in the anterior and posterior annulus (Figure 10b and c). However, the water content of the nucleus did not show a clear change with grade and demonstrated much greater variability (Figure 10a). This would suggest that gross morphology may be less reliable in determining the nuclear grade and, therefore, the overall grade if one assumes differences in water content are important distinctions between grades. Alternatively, and less likely, it may suggest water content is not specific for grade and the consistent results for water content as a function of MRI grade were fortuitous.

Despite repeated digestion of the old and severely degenerate discs, small amounts of residue remained. Separation of the supernatant and residue was accomplished by centrifugation at 25,000 rpm for 15 minutes.

Chondroitin Sulfate. The coefficient of variation of duplicate samples was less than 1.17%. The values for chondroitin sulphate ranged from 69.4 mg/g fresh weight in the nucleus of a young (grade 1) disc to 10.2 mg/g fresh weight in the nucleus of an old (grade 5) disc. The plot of chondroitin sulphate and MRI grade for the nucleus showed a fall in chondroitin sulphate with increasing MRI grade (Figure 11a). Unlike the plot for water content (Figure 9a), a decrease between MRI grades 1 and 2 was apparent. This decrease was not

apparent in a plot of chondroitin sulphate content and morphologic grade (Figure 12a). Furthermore, the wide variation in data for morphologic grade 2 discs made differences between grades 1 and 2 and grades 2 and 3 less distinct.

FIGURES 10a-c: WATER CONTENT BY MORPHOLOGIC CATEGORY

10(a).

Water content of the nucleus. A distinct change in water content occurs between categories 1 and 3. The wide range of values for category 2 discs suggests that some discs might be more appropriately classified as category 1 and 3 discs. The MRI classification (Figure 9a) appeared to conform more closely with water content changes.

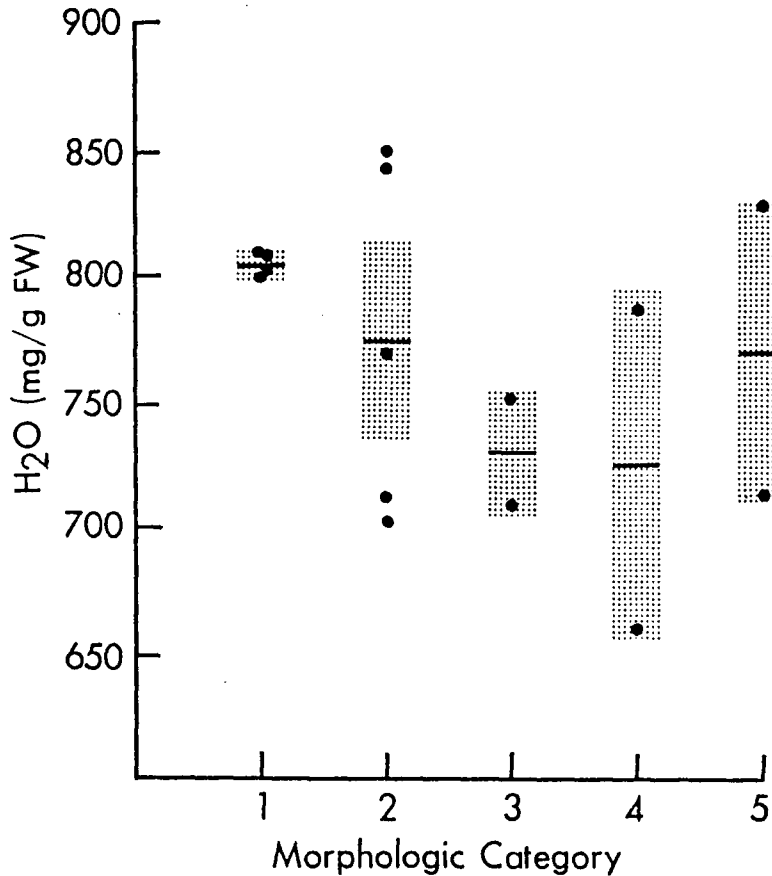


FIGURE 10b: WATER CONTENT BY MORPHOLOGIC CATEGORY (cont'd)

10(b). Water content of the anterior annulus. A trend to increasing water content was seen.

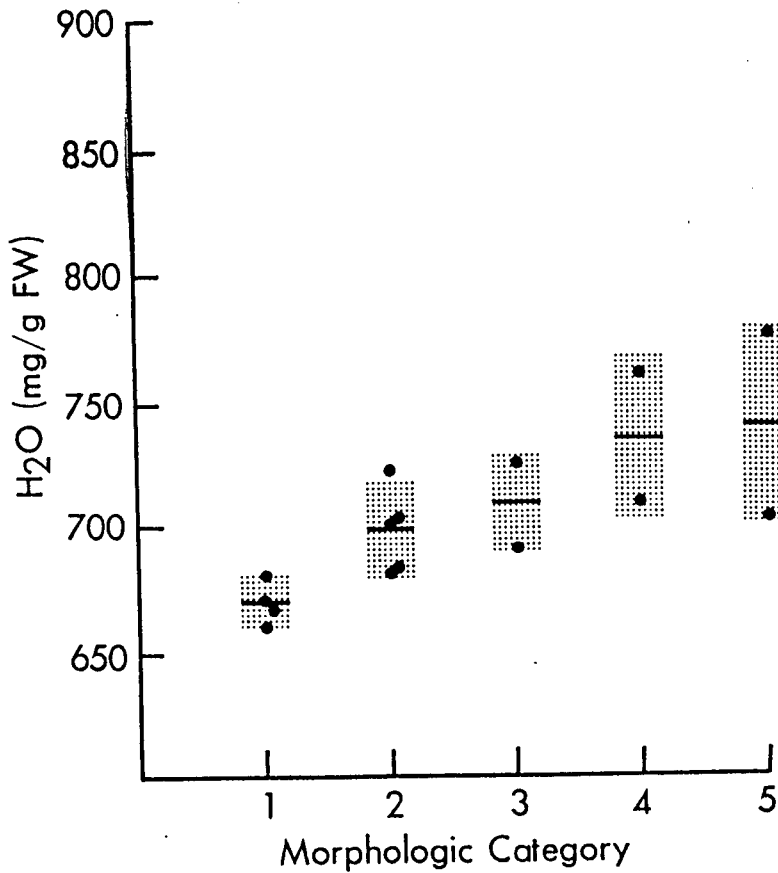
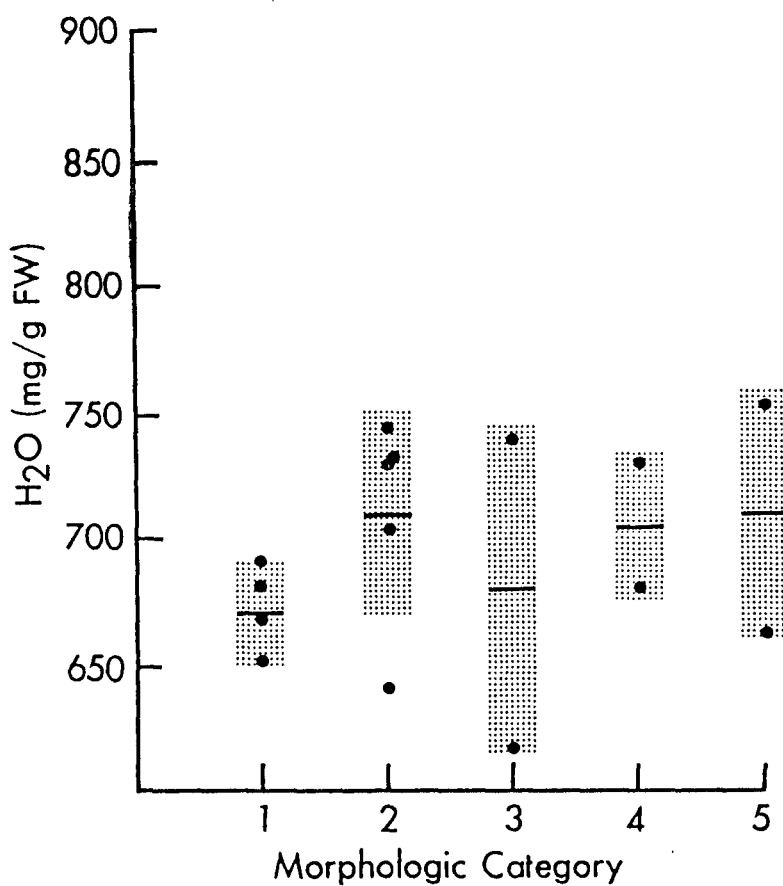


FIGURE 10c: WATER CONTENT BY MORPHOLOGIC CATEGORY (cont'd)

10(c). Water content of the posterior anulus. No clear trend could be seen.



FIGURES 11a-c: CHONDROITIN SULPHATE CONTENT BY MRI CATEGORY

11(a).

Chondroitin sulphate content of the nucleus. The apparent drop in CS content between category 1 and 2 discs precedes the change in water content. Like the water content, the largest drop in CS content occurs between category 2 and 3 discs. CS content remains stable for higher category discs.

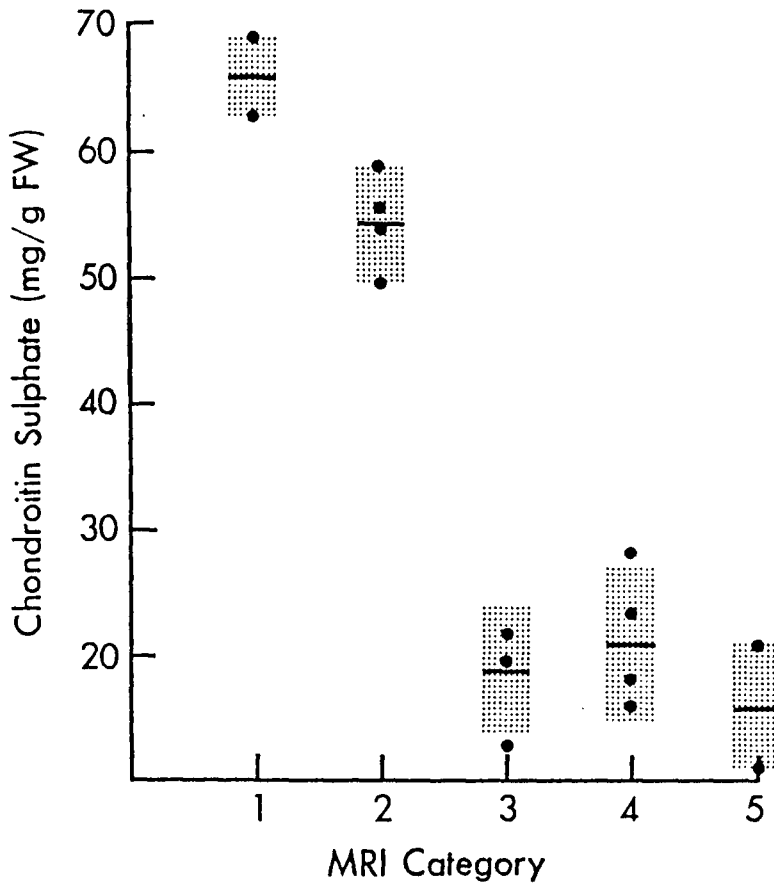


FIGURE 11b: CHONDROITIN SULPHATE CONTENT BY MRI CATEGORY (cont'd)

11(b). Chondroitin sulphate content of the anterior annulus. The trend in CS content appears to be a decrease in content with increasing category.

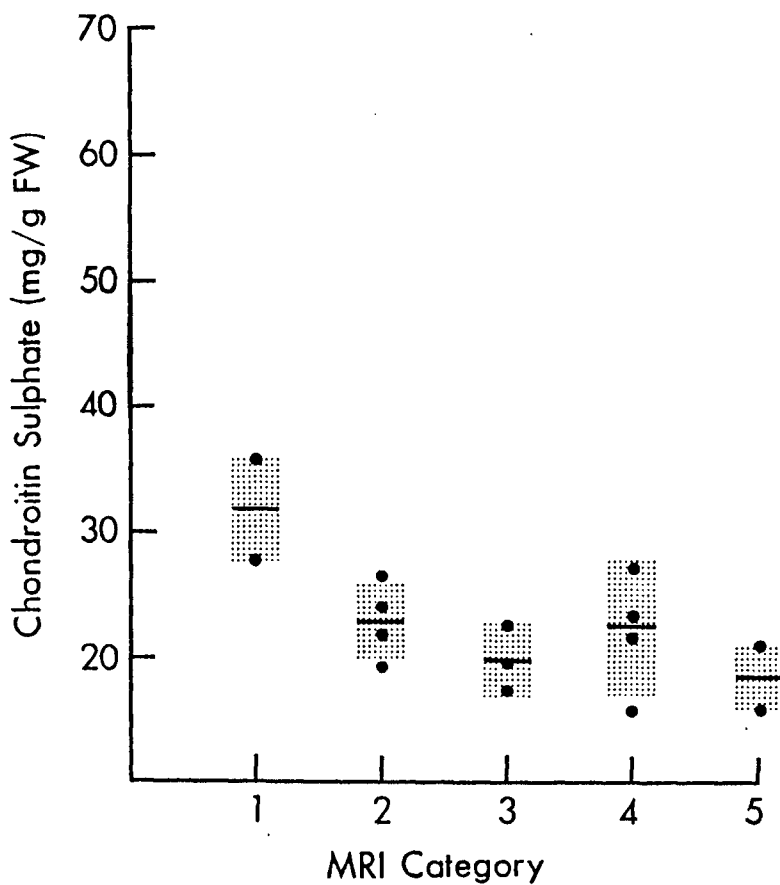
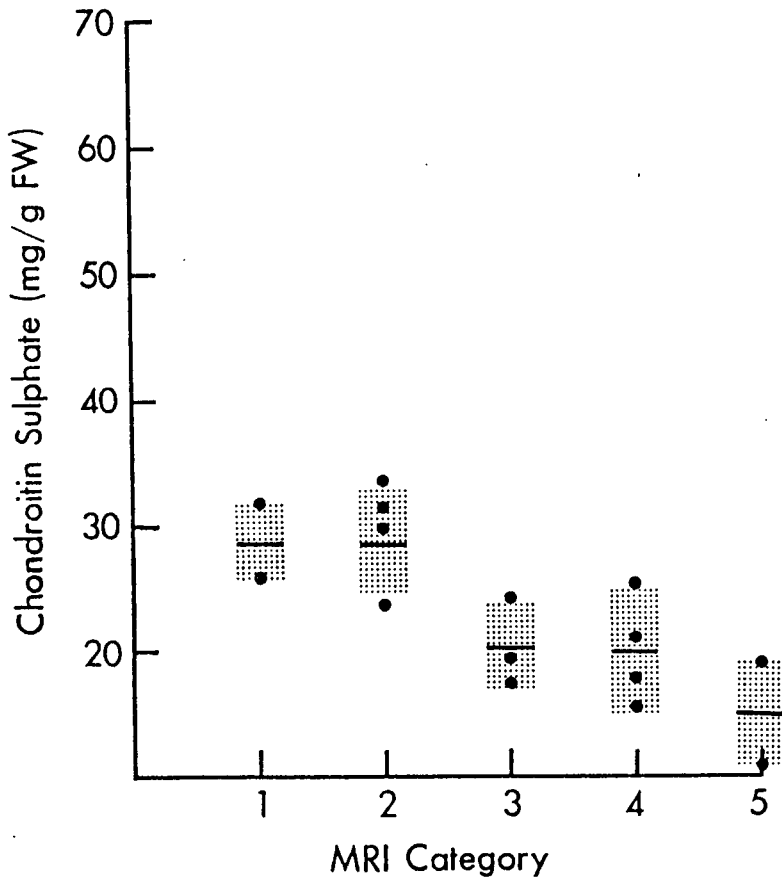


FIGURE 11c: CHONDROITIN SULPHATE CONTENT BY MRI CATEGORY (cont'd)

11(c). Chondroitin sulphate content of the posterior annulus. The trend is similar to that of the anterior annulus.



FIGURES 12a-c: CHONDROITIN SULPHATE CONTENT BY MORPHOLOGIC CATEGORY

12(a). Chondroitin sulphate content of the nucleus. In contrast to the plot of CS content and MRI category (Figure 11a), category 2 does not serve as a transition between the high CS content of category 1 discs and low CS content of category 3 discs. Like the data for water content (Figure 10a), there is a wide variation in values for morphologic category 2 discs, suggesting some inaccuracy in the definition of gross morphologic category 2 discs with respect to category 1 and 3 discs.

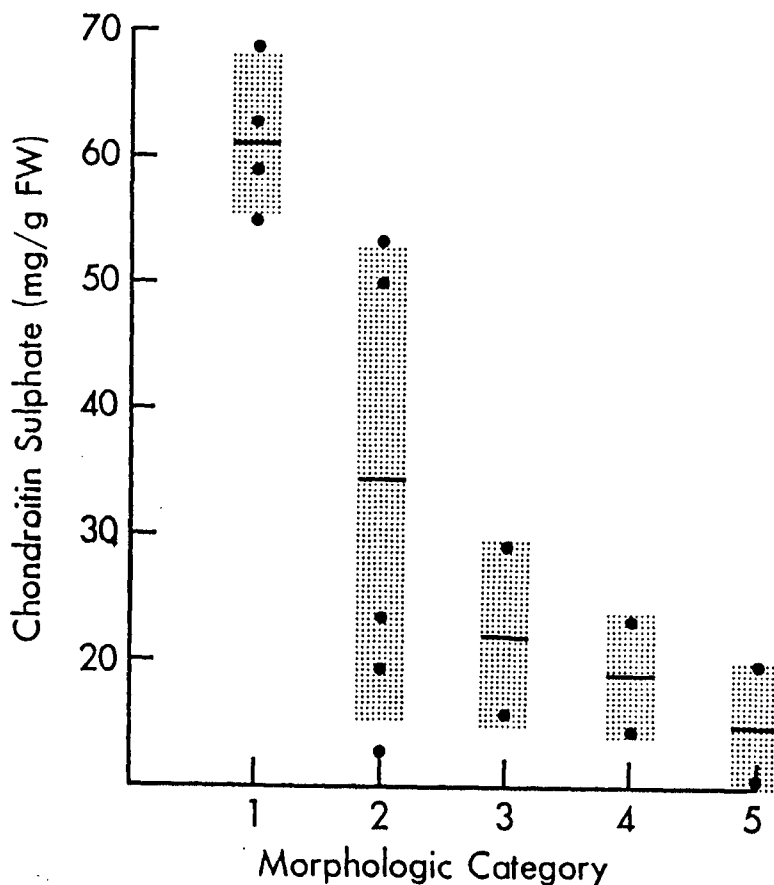


FIGURE 12b: CHONDROITIN SULPHATE CONTENT BY MORPHOLOGIC CATEGORY (cont'd)

12(b). Chondroitin sulphate content of the anterior annulus. The trend was for CS content to decrease with increasing grade.

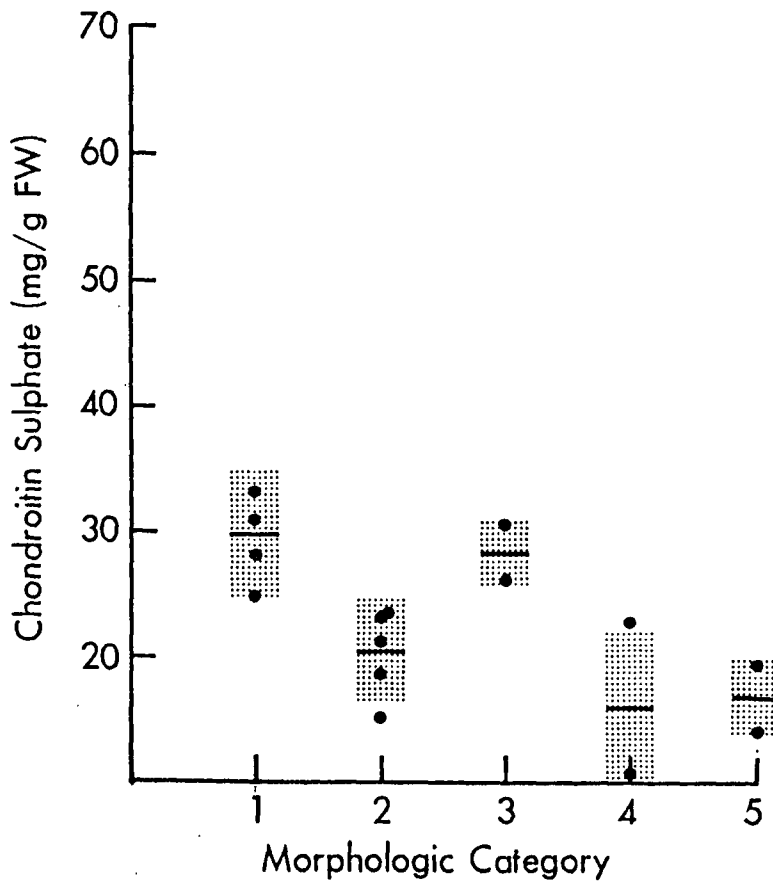
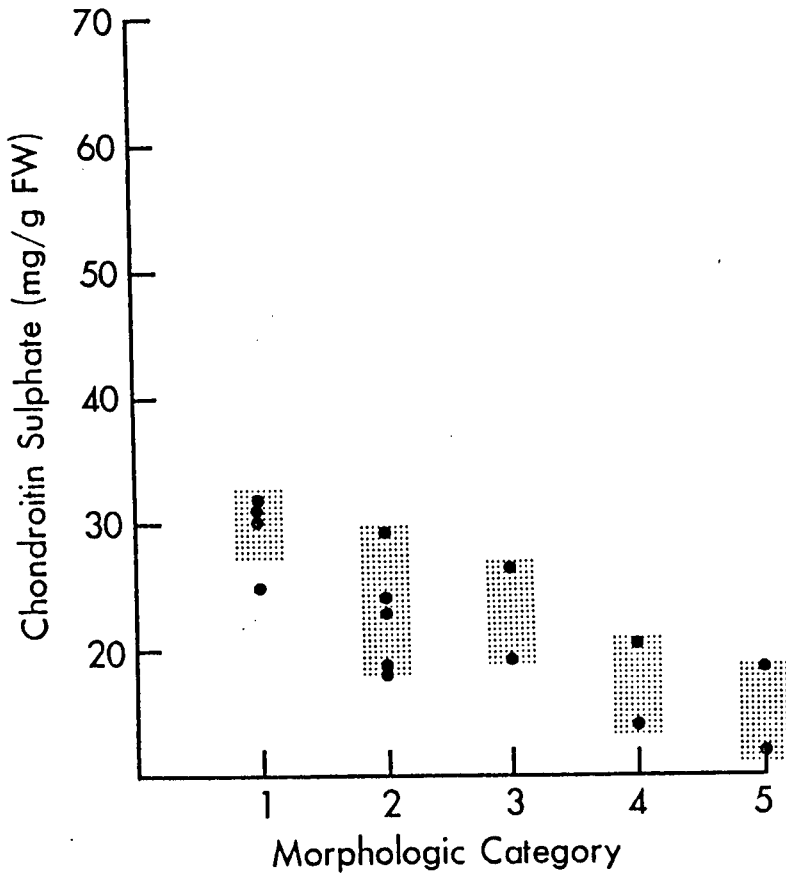


FIGURE 12c: CHONDROITIN SULPHATE CONTENT BY MORPHOLOGIC CATEGORY (cont'd)

12(c). Chondroitin sulphate content of the posterior anulus. A trend similar to that in the anterior anulus is apparent.



Although a change between MRI grades 1 and 2 was apparent, the decrease in chondroitin sulphate content, like that observed for water content, was most dramatic between MRI grades 2 and 3. In plots for the anterior and posterior annulus, the initial chondroitin sulphate contents were approximately one-half those of the nucleus and decreased less with increasing MRI and morphologic grade (Figures 11b,c, and 12b,c). Overall, the variation in the data for each category was less than that for water.

The data collected suggests the following observations. The consistency of the MRI data, particularly for grades 1, 2 and 3, suggests MRI more reliably distinguishes grade. The change seen between MRI grade 1 and 2 indicates that an early event in aging or degeneration of a disc may be a fall in chondroitin sulphate content. Change in water content, which occurs between grades 2 and 3, may be a consequence of this change in proteoglycan content.

Keratan Sulphate. The coefficient of variation of duplicate samples was less than 1.4 per cent. Keratan sulphate ranged from 64.7 mg/g fresh weight in the nucleus of a young disc (grade 1) to 16.2 mg/g fresh weight in the nucleus of an old disc (grade 5). In comparison with chondroitin sulphate, the plot of nuclear keratan sulphate vs. MRI and morphologic grade indicated a lower initial concentration and a less pronounced decrease with increasing MRI and morphologic grade (Figure 13a and 14a). In addition to the less distinct changes between grades 1 and 2 and 2 and 3, there was greater variation in the data for each grade. Subsequent work has shown there was a flaw in the method used for determining keratan sulphate. It was assumed that the hexose content of the whole tissue would reflect its keratan sulphate content as is the case when proteoglycan are assayed. Chromatographic profiles of alcohol precipitated preparations have demonstrated that oligosaccharides are a major fraction

FIGURES 13a-c: KERATAN SULPHATE CONTENT BY MRI CATEGORY

13(a).

Keratan sulphate content of the nucleus. With increasing MRI category, there is a drop in KS content. Compared with the CS data (Figure 11a-c), the changes are less clear because of the lesser magnitude of changes and greater variability in values for each category.

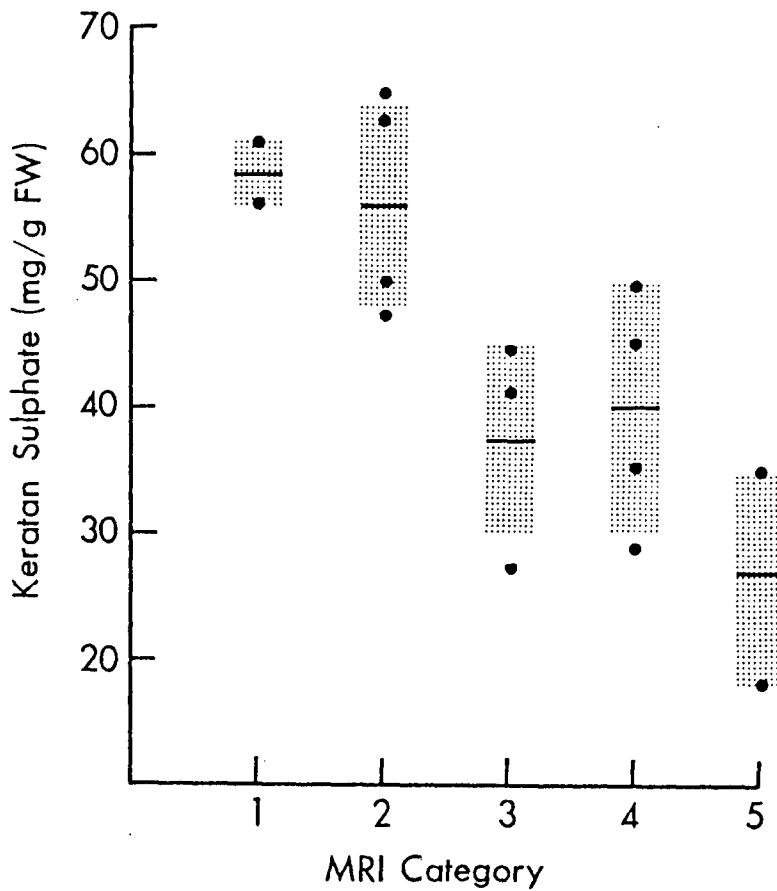


FIGURE 13b: KERATAN SULPHATE CONTENT BY MRI CATEGORY (cont'd)

13(b). Keratan sulphate content of the anterior annulus. A trend of decreasing KS content with increasing category was apparent. This was similar to the changes observed in CSS content (Figure 11b).

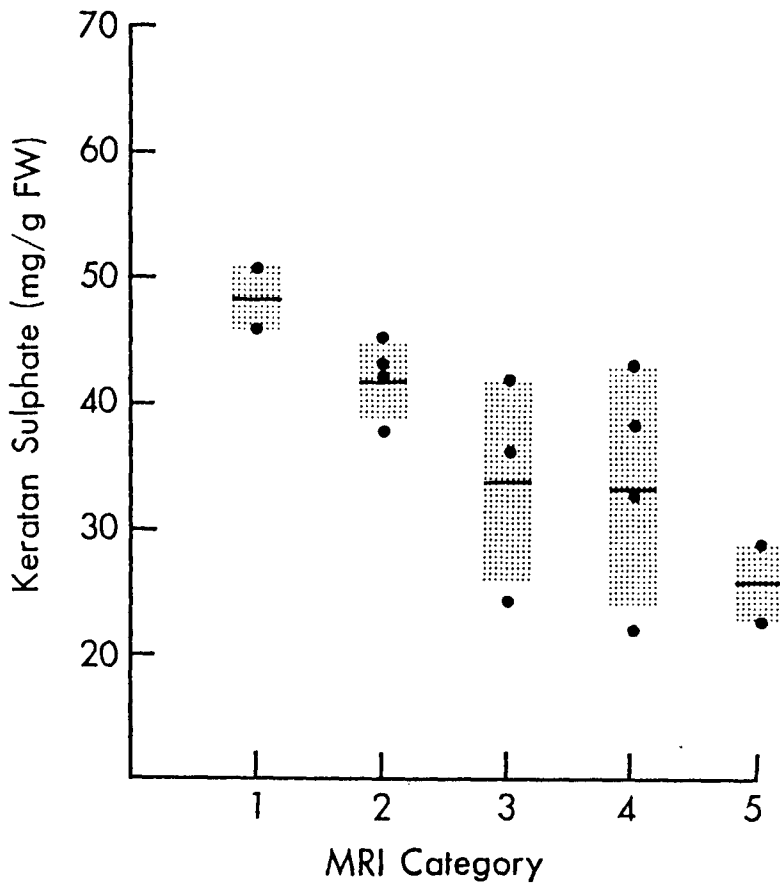


FIGURE 13c: KERATAN SULPHATE CONTENT BY MRI CATEGORY (cont'd)

13(c). Keratan sulphate content of the posterior anulus. The trend observed was similar to the anterior anulus (Figure 13b) and that observed for CS content (Figure 11c).

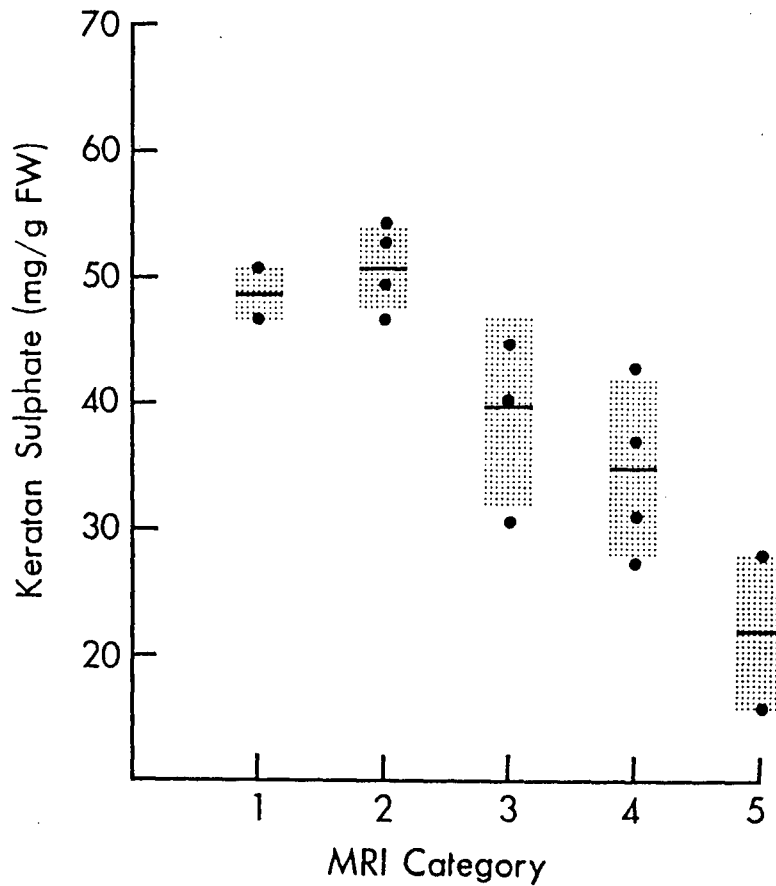


FIGURE 14a-c: KERATAN SULPHATE CONTENT BY MORPHOLOGIC CATEGORY

14(a).

Keratan sulphate content of the nucleus. As in the MRI data (Figure 13a), there was a trend for KS content to decrease. However, the morphologic category 2 disc interrupted the orderly trend from category 1 to 5 which again suggested difficulty in assigning category 2 discs morphologically.

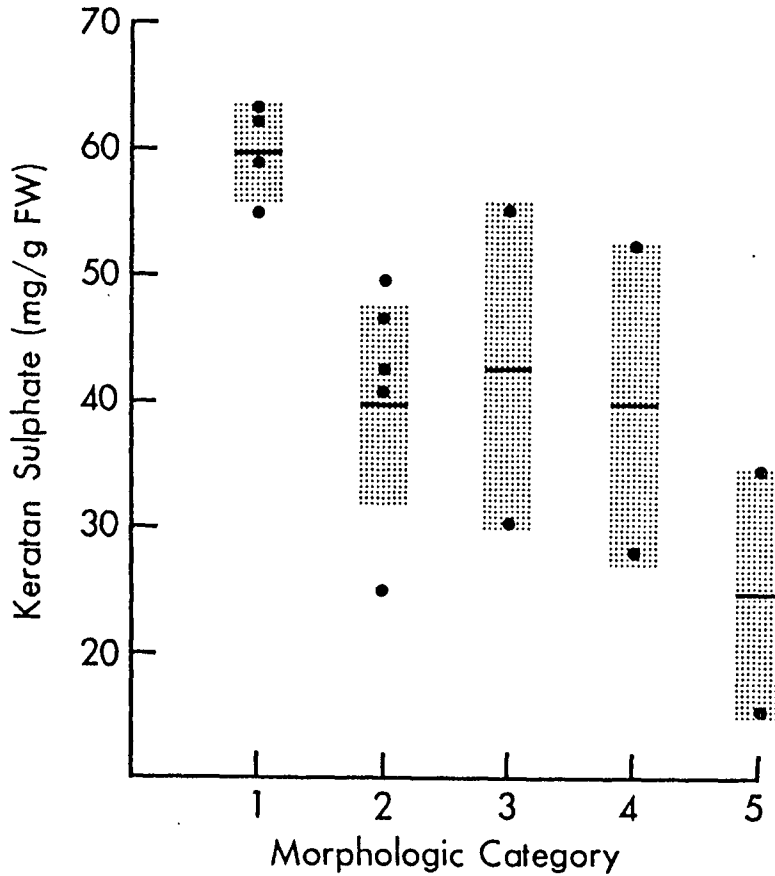


FIGURE 14b: KERATAN SULPHATE CONTENT BY MORPHOLOGIC CATEGORY (cont'd)

14(b). Keratan sulphate content of the anterior annulus. Although the trend was for KS content to decrease, the progression was not orderly and variation in values existed.

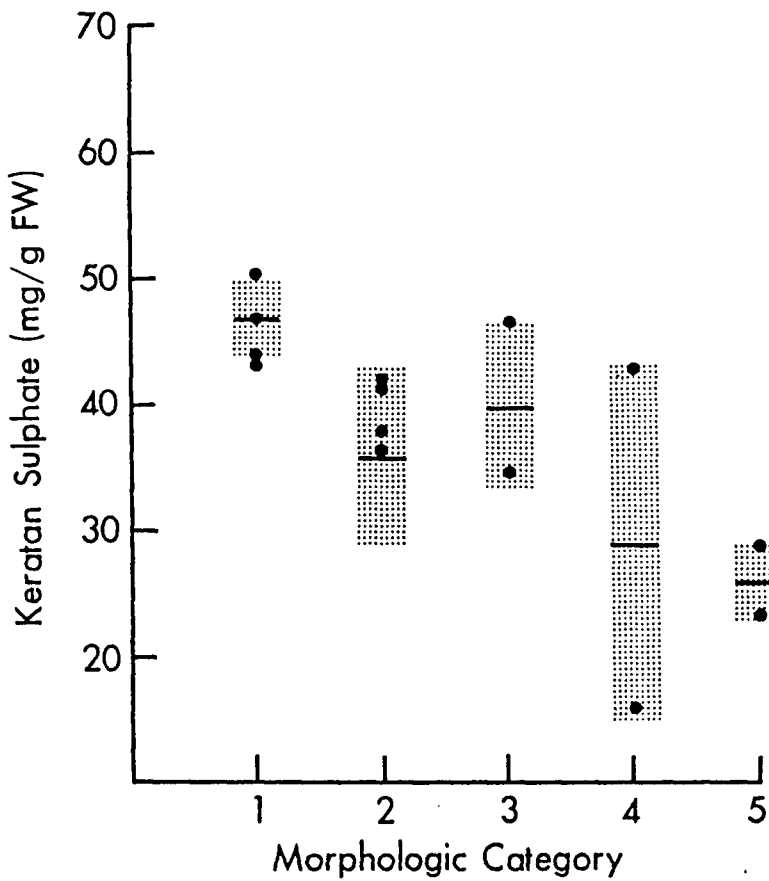


FIGURE 14c: KERATAN SULPHATE CONTENT BY MORPHOLOGIC CATEGORY (cont'd)

14(c). Keratan sulphate content of the posterior anulus. Variation in values for each category existed but a trend for decrease in KS content was apparent.

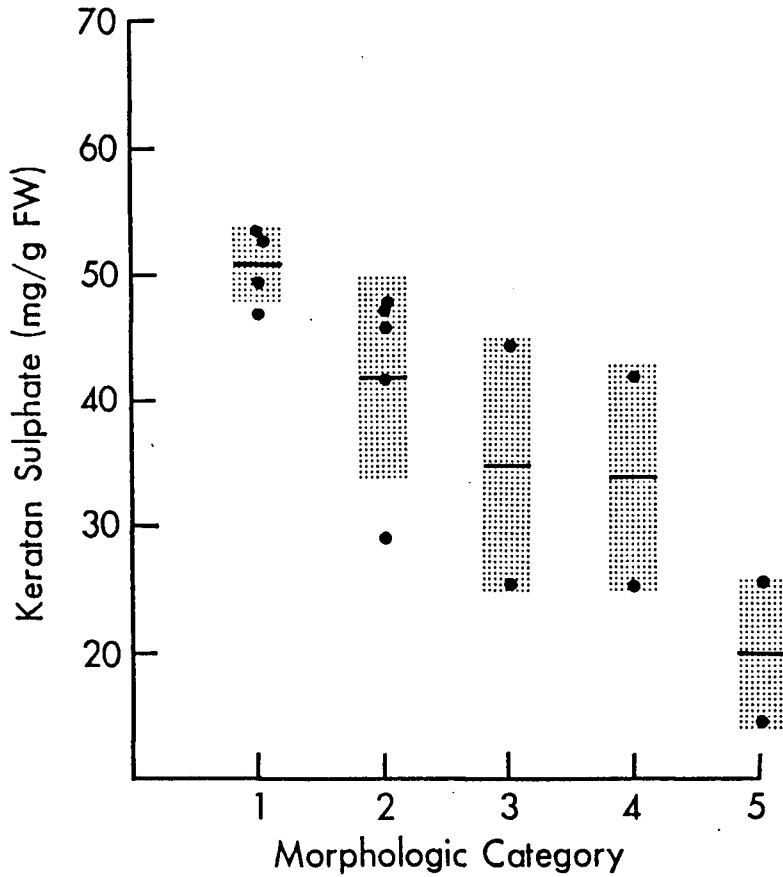
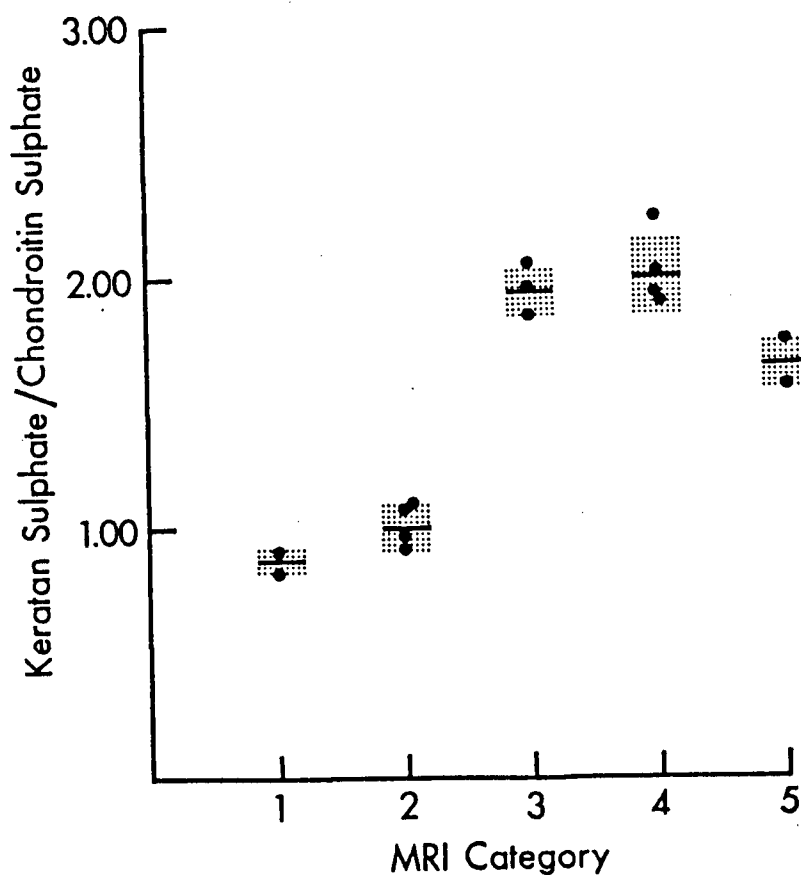


FIGURE 15: THE RATIO OF KERATAN SULPHATE TO CHONDROITIN SULPHATE
BY MRI CATEGORY

The ratio of nuclear keratan sulphate to chondroitin sulphate by MRI category. The clear trend for the ratio to increase with increasing category suggested a differential rate of synthesis and/or degradation for KS with respect to CS.



of the hexose, particularly in the nucleus. The non glycosaminoglycan hexose contents of the nucleus and anulus account for 10-25 per cent and 40-60 per cent of the total hexose, respectively (Mathieson, Bebault and Pearce, unpublished results). The keratan sulphate content of the anterior and posterior anulus was initially greater than the chondroitin sulphate content and decreased less with grade than that of chondroitin sulphate (Figure 13b,c and 14b,c). The ratio of nuclear keratan sulphate to chondroitin sulphate increased with increasing MRI grade (Figure 15). This indicates that an alteration in the relative rates of biosynthesis and/or biodegradation of chondroitin sulphate and keratan sulphate occurs as aging and degeneration proceed. The greater variability in the keratan sulphate data compared to the chondroitin sulphate data and the overestimation of keratan sulphate content reflects the technical pitfalls of the method for estimating hexose and the error in assuming that hexose reflects only keratan sulphate content.

Collagen. Collagen content was greatest in the posterior anulus of an old (grade 5) disc, 305.3 mg/g fresh weight, and least in the nucleus of a young (grade 1) disc, 28.8 mg/g fresh weight. The coefficient of variation was less than 1.5 per cent for duplicate samples. When plotted as a function of MRI and morphologic grade, collagen content increased between grades 2 and 3 in the nucleus and decreased slightly in the anterior and posterior anulus (Figures 16 and 17). The changes and trends were more apparent in the MRI data. The initial collagen concentration of the nucleus was approximately 15 to 20 percent that of the anulus. With increasing grade, the collagen concentrations of the nucleus and anulus converged. The large range of values for morphologic grade 2 discs suggested overlap with MRI grade 1 and 3 discs.

The trends seen were consistent with the literature and tended to be better defined for MRI than for morphologic categories. This was particularly true of the data for the nucleus.

FIGURES 16a-c: COLLAGEN CONTENT BY MRI CATEGORY

16(a).

Collagen content of the nucleus. A change in collagen content occurred between category 2 and 3 discs. This change and the observed changes in CS and KS suggested a distinct change in extracellular matrix composition of the nucleus with increasing category.

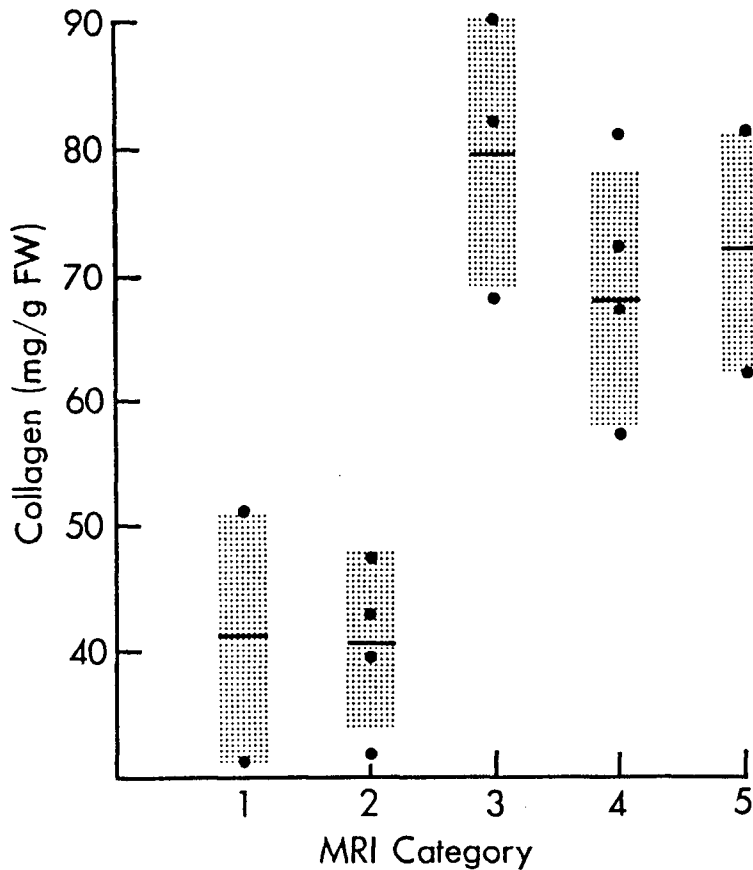


FIGURE 16b: COLLAGEN CONTENT BY MRI CATEGORY (cont'd)

16(b). Collagen content of the anterior anulus. A trend for decreased collagen content in the anulus was apparent. Changes of similar magnitude were seen in the CS and KS plots (Figures 11b,c and 13b,c). This suggested the largest changes in extracellular matrix composition occurred in the nucleus, whereas the anulus changed little.

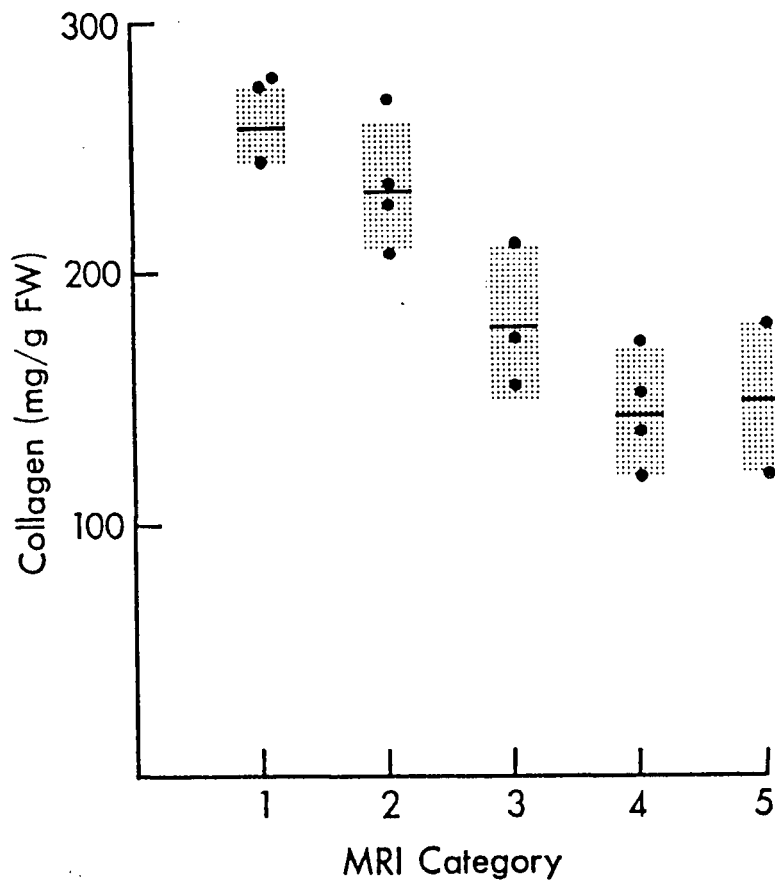


FIGURE 16c: COLLAGEN CONTENT BY MRI CATEGORY (cont'd)

16(c). Collagen content of the posterior anulus. With the exception of the values for category 5, a trend similar to that of the anterior anulus was noted.

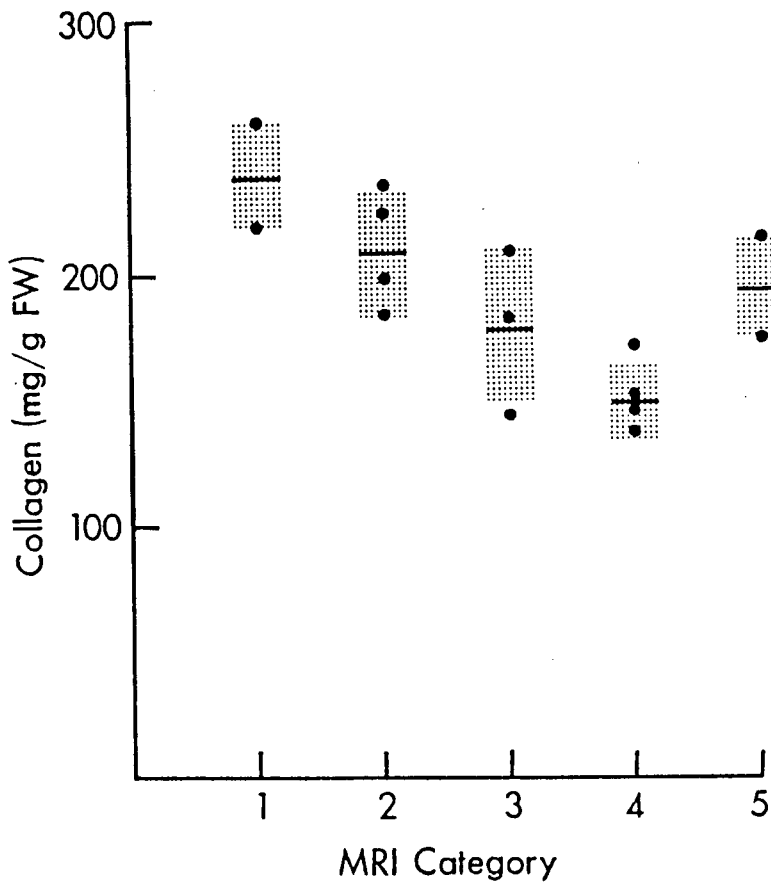


FIGURE 17a-c: COLLAGEN CONTENT BY MORPHOLOGIC CATEGORY

17(a).

Collagen content of the nucleus. Although the trend for increased collagen content was apparent, the imprecision of morphologic category 2 disc assignment obscured an orderly progression.

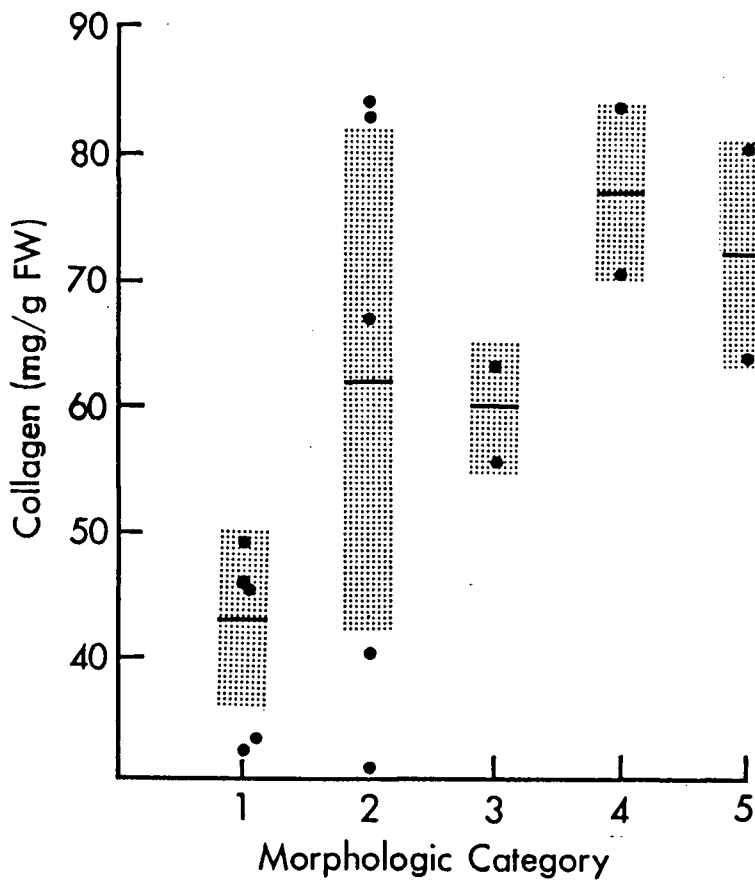


FIGURE 17b: COLLAGEN CONTENT BY MORPHOLOGIC CATEGORY (cont'd)

17(b). Collagen content of the anterior anulus. The variability of category 2 values aside, the trend was for a decrease in collagen content.

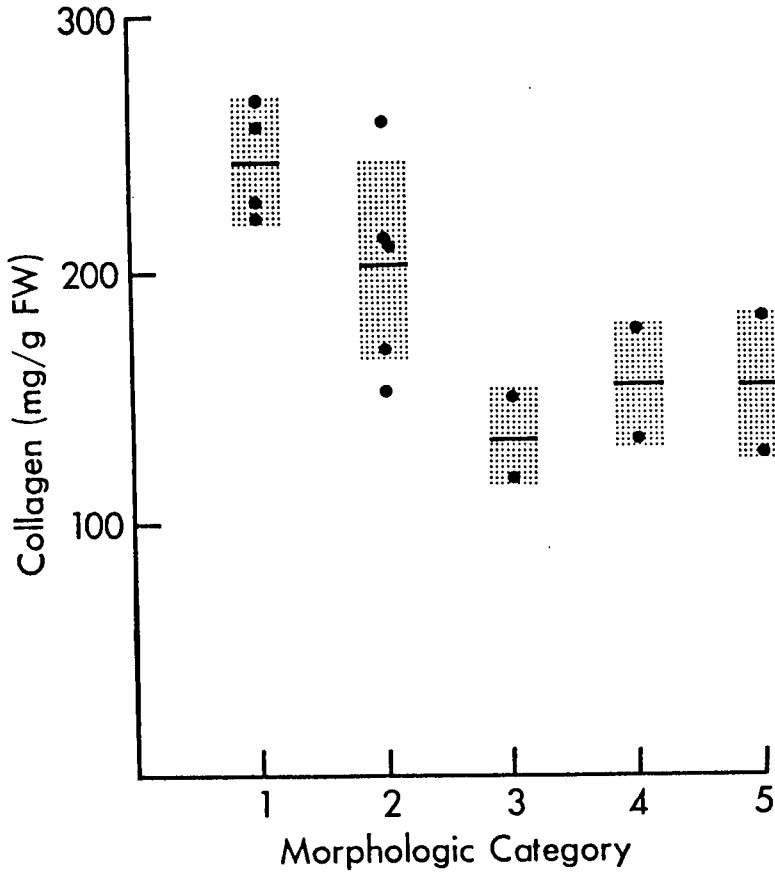
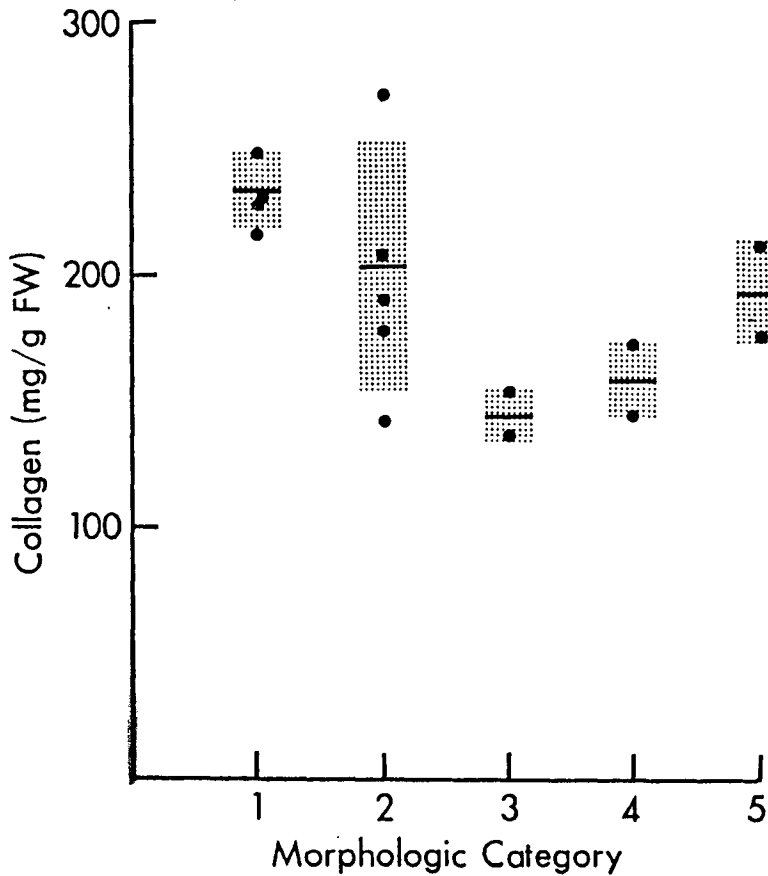


FIGURE 17c: COLLAGEN CONTENT BY MORPHOLOGIC CATEGORY (cont'd)

17(c). Collagen content of the posterior annulus. The findings were similar to those for the anterior annulus (Figure 17b).



3.5 HISTOLOGIC ANALYSIS

Due to the limited number of specimens - 15 - a detailed objective analysis of the data was not justified. However, some clear trends were noted. The distribution of overall category for the morphologic and MRI classifications and the chemical data suggested MRI was more sensitive at detecting early age related or degenerative changes. The histologic examinations supported this. Descriptions of the histologic appearance as a function of MRI category (grade) resulted in consistent findings for each category. For these reasons, the histologic trends were described as a function of MRI category. Observations were made utilizing low and high power bright field objectives in the following manner:

Low Power Examination. Using the naked eye, dissecting microscope and 4x objective, stain distribution and intensity of the anulus and nucleus could be defined according to MRI grade. Because of the difficulty in fixing, embedding and mounting a heterogeneous tissue without damage, the interpretation of macroscopic disruptions was assisted by reference to the photograph of the gross morphology.

High Power Examination. The 4x, 10x and 40x bright field objectives allowed the specific tissue type and distribution to be identified.

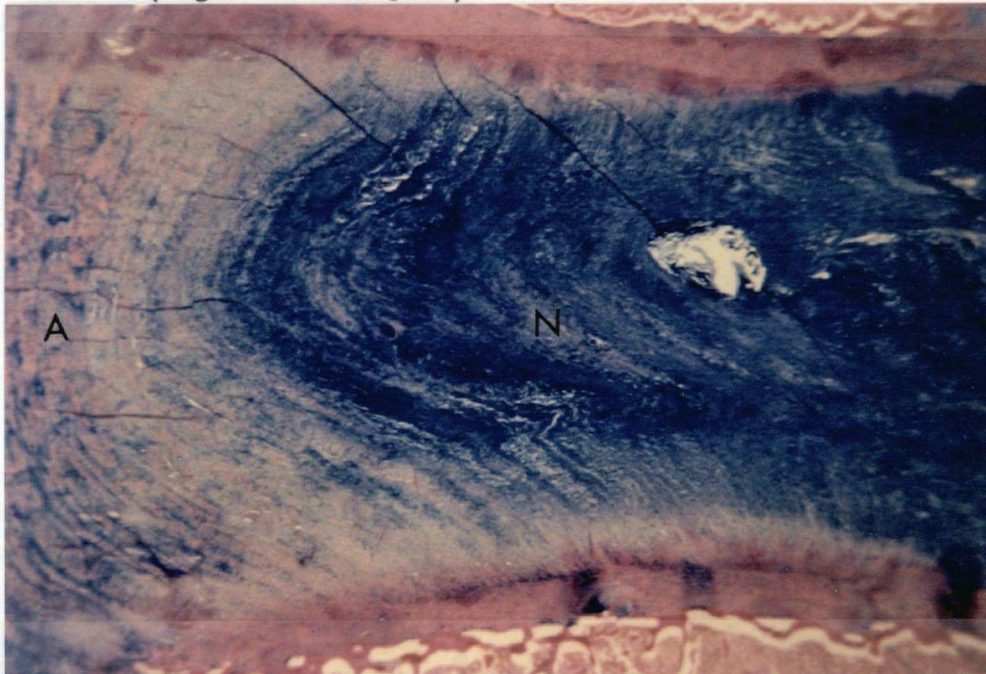
The trends seen, according to MRI grade, were as follows:

MRI Grade 1. Two discs were classified as MRI Grade 1. The staining characteristics of the nucleus and anulus clearly distinguished these two tissues. The nucleus stained intensely and homogeneously with hematoxylin and alcian blue but lightly with aniline blue. Conversely, the anulus stained intensely with Mallory's trichome and lightly with hematoxylin and alcian blue (Figure 18a). The area staining intensely with alcian blue and hematoxylin

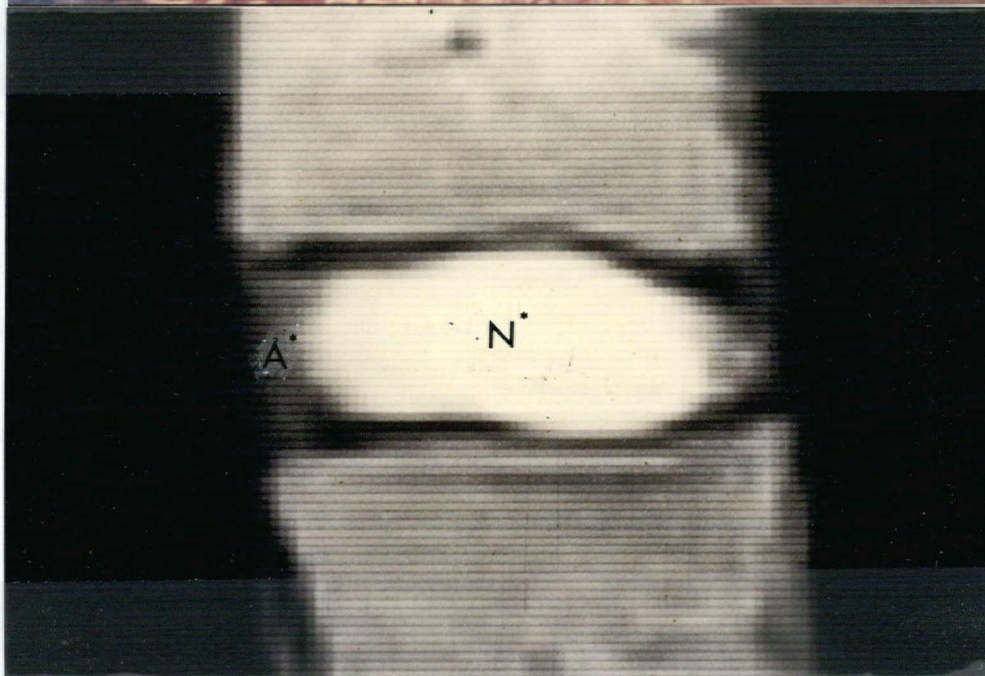
FIGURE 18: ALCIAN BLUE STAINED SECTION AND MRI SCAN OF
AN MRI CATEGORY 1 DISC

The histochemical correlates of the bright and dark MRI signals are represented by this specimen. The intense staining of the nucleus (N) by alcian blue (a) corresponds to the bright homogeneous signal (N*) of the MRI SE 40 image (b). The pink counterstained material (a) of the annulus (A) corresponds to the dark signal (A*) of the MRI (b). The donor was a 21-year-old female. (Magnification 32x.)

(a)



(b)



corresponded to the bright signal in the MRI SE 40 image and the area of the section staining intensely with aniline blue corresponded to the dark signal in the MRI SE 40 image (Figure 18b). The intense staining of the nucleus by alcian blue, which stains sulphated polyanions, compared with that of the anulus was consistent with the chemical assays for chondroitin sulphate and keratan sulphate. The intense staining of anulus relative to the nucleus by Mallory's trichrome, which stains collagen fibers deep blue, was consistent with the assays for collagen.

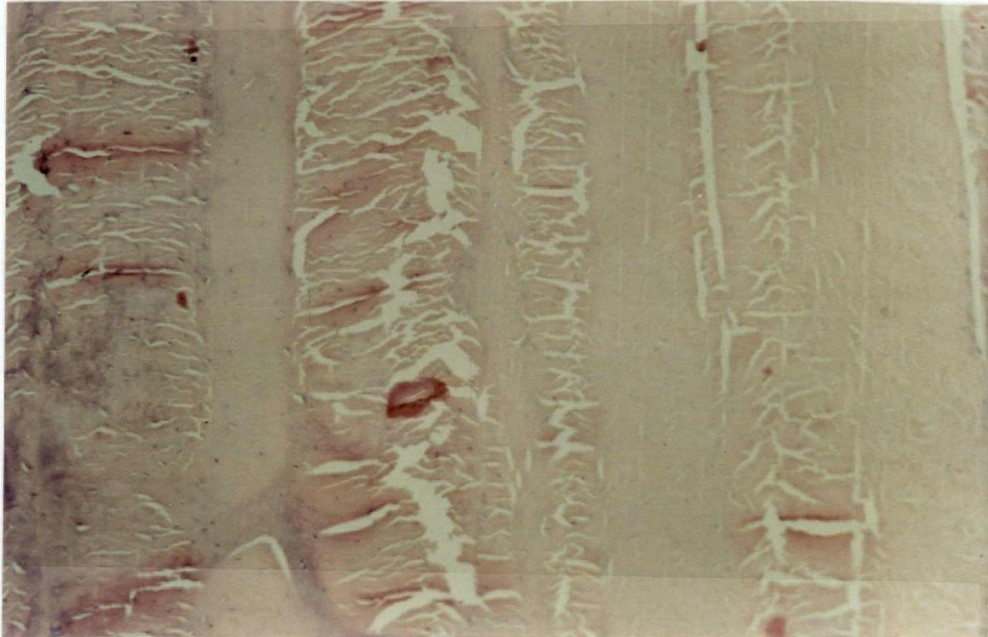
In the outer one-third of the anulus, wide and well-oriented lamellae of tendon-like collagen (Figure 19a) inserted perpendicularly into the vertebral body. The cells resembled fibrocytes having elongate nuclei and poorly defined cytoplasm. Adjacent to the anterior and posterior longitudinal ligaments, neurovascular bundles were seen. There was a gradual change in the histologic appearance of the anulus from tendon-like in the outer one-third to fibrocartilaginous in the juxtannuclear area. As the nucleus was approached, the amount of amorphous interstitial matrix increased, collagen content decreased, became less organized, oriented more horizontally (Figure 19b) and inserted more obliquely into the cartilage endplate. The cells appeared more chondrocytic with round to oval nuclei and territorial matrix production. In general, the posterior anulus was smaller than the anterior anulus and consisted of proportionately more fibrocartilage than the anterior anulus.

The extracellular matrix of the nucleus pulposus was amorphous and contained a sparse network of randomly oriented collagenous fibers (Figure 20). Groups of large chondrocytic cells could be seen per high power field. Cells and collagenous fibers were more apparent adjacent to the anulus.

FIGURE 19: HEMATOXYLIN AND EOSIN STAINED SECTIONS OF THE ANULUS OF
AN MRI CATEGORY 1 DISC

These photomicrographs of paraffin sections from the same disc of a 21-year-old female represent the outer (a) and inner (b) anular morphology. The dense, highly organized alternating collagen lamellae of the outer anulus (a) and the less dense collagenous matrix and more apparent basophilic matrix of the inner anulus (b) are apparent at magnifications of 80x and 320x respectively. The vertebral body margins and endplates would be oriented horizontally inferior to the photomicrographs.

(a)



(b)

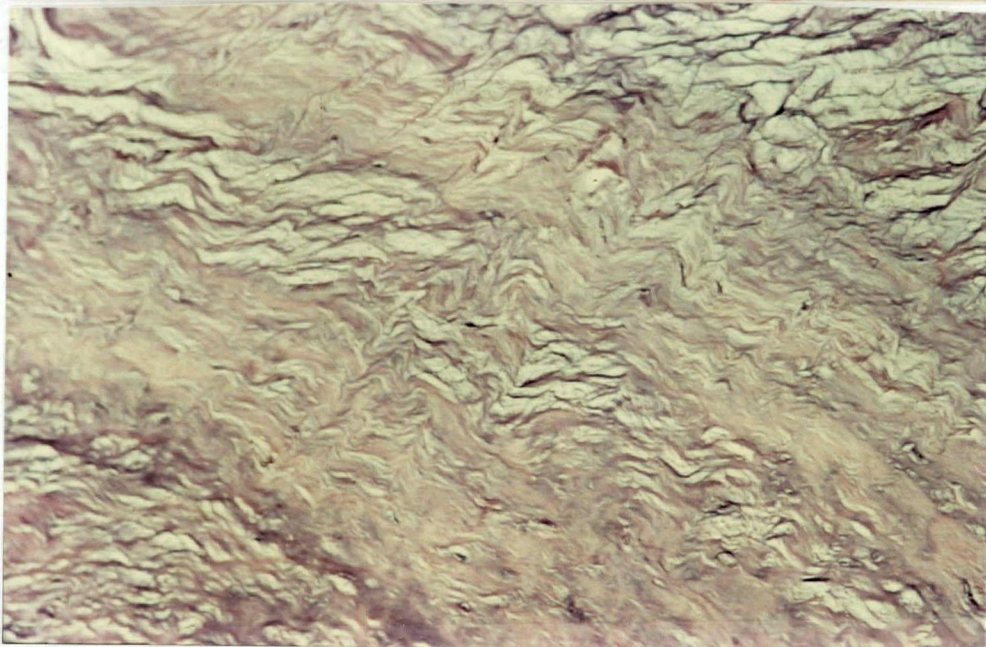
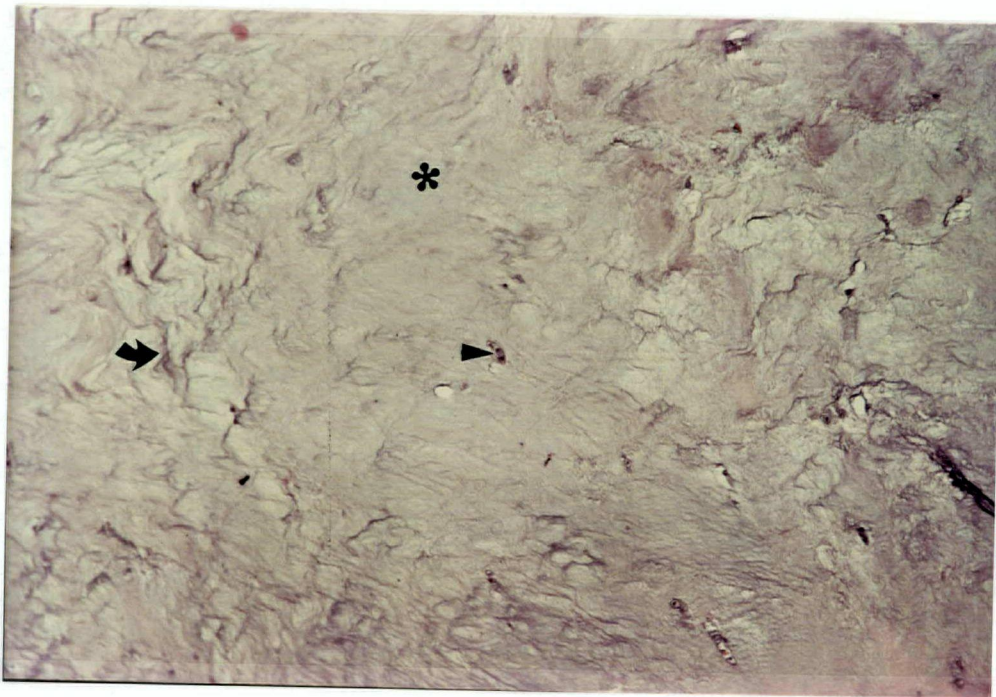


FIGURE 20: HEMATOXYLIN AND EOSIN STAINED SECTIONS OF THE NUCLEUS OF
AN MRI CATEGORY 1 DISC

The nucleus of this disc from a 16-year-old male is characterized by sparse, randomly oriented collagen fibers (↔), chondrocytic cells (▶) and abundant basophilic matrix (*). (Magnification 80x.)



The cartilaginous endplate consists of hyaline cartilage with cells stratified horizontally with respect to the endplate (Figure 21). In one of the discs, small rests of epiphyseal growth plate cartilage were present, reflecting the skeletal immaturity of the donor. The extracellular matrix was ground glass-like and stained deeply with the cationic dyes, particularly the territorial matrix.

MRI Grade 2. Four discs were classified as MRI grade 2. Overall, separate stains of the nucleus by hematoxylin and alcian blue were less homogeneous and intense than that observed in grade 1 discs. More specifically, material counterstained pink (acid fuchsin) extended centrally from the anulus in the sections stained with alcian blue, particularly anteriorly (Figure 22a). This material also stained intensely with aniline blue, suggesting the presence of collagenous fibers (Figure 22b). In the anulus, a general increase in basophilia and discrete basophilic foci were seen between the collagenous lamellae, which stained intensely with alcian blue. In addition, vacuolated areas, consistent with mucin deposition, occurred between lamellae (Figure 23). The decreased homogeneity and intensity of staining of the nucleus corresponded to the decreased nuclear signal intensity in the MRI image and the decrease in chondroitin sulphate and increase in collagen detected by chemical analysis. The counterstained area, which at times extended across the nucleus, corresponded to the dark band or intranuclear cleft seen in the MRI (Figure 24). The decreased homogeneity and intensity of alcian blue staining of grade 2 discs relative to grade 1 discs appeared commensurate with the observed decreases in the chondroitin and keratan sulphate concentrations. Changes in staining of anulus was also reflected in the MRI image and chemical data. The

basophilic foci, if substantially large, corresponded to brighter signals seen in the anular zone (Figure 24). The decrease in collagen concentration seemed appropriate to the change in collagen staining observed.

FIGURE 21: HEMATOXYLIN AND EOSIN STAINED SECTION OF THE ENDPLATE OF
AN MRI CATEGORY 1 DISC

The endplate of this disc from a 16-year-old male consists of hyaline cartilage (H) resting on a network of trabecular bone (T). The cells are stratified horizontally and the territorial matrix of the cells stains deeply with hematoxylin. The nucleus and marrow cavity are at the superior and inferior margins of the photomicrograph respectively. (Magnification factor 320x).

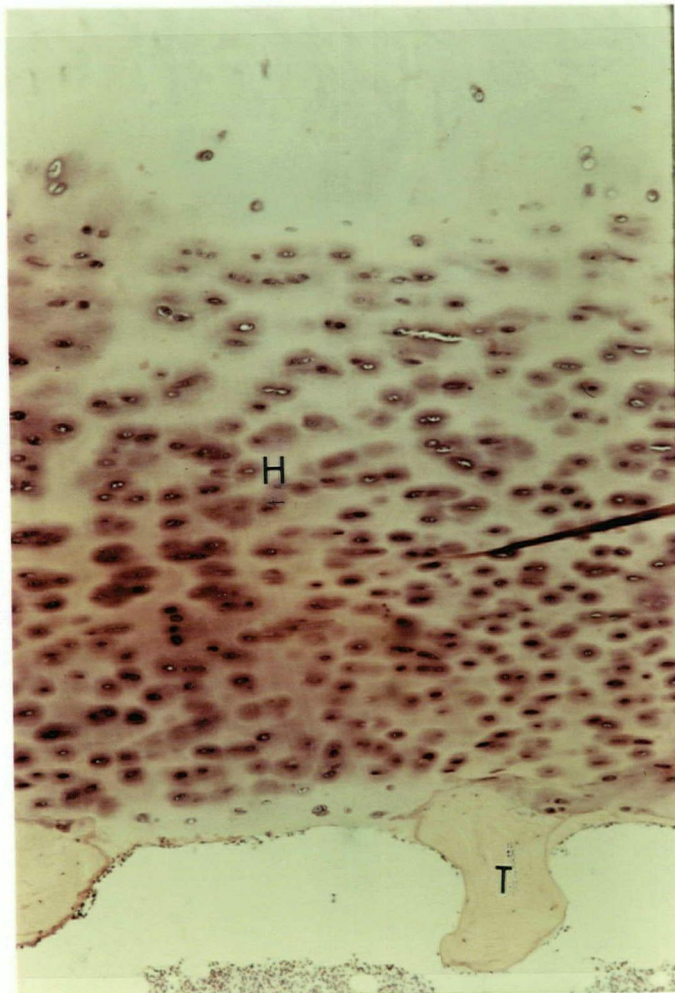
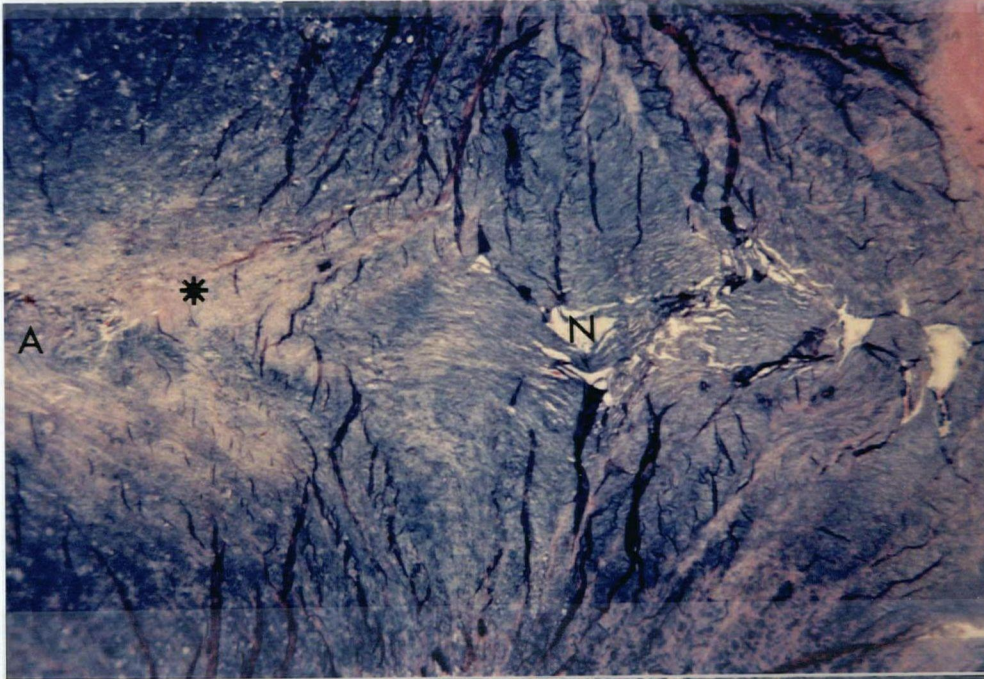


FIGURE 22: ALCIAN BLUE (Figure a) AND MALLORY TRICHROME (Figure b)

STAINED SECTIONS OF AN MRI CATEGORY 2 DISC

These photomicrographs from the same disc of a 39-year-old male at magnification 32x illustrate the early changes in the histochemical appearance of the nucleus. The presence of acid fuchsin counter-stained (a) and aniline blue stained (b) material (*) extending from the annulus (A) into the nucleus (N) suggests the presence of collagen proliferation. This area of collagen proliferation corresponds to the dark band or cleft seen in MRI category 2 discs.

(a)



(b)

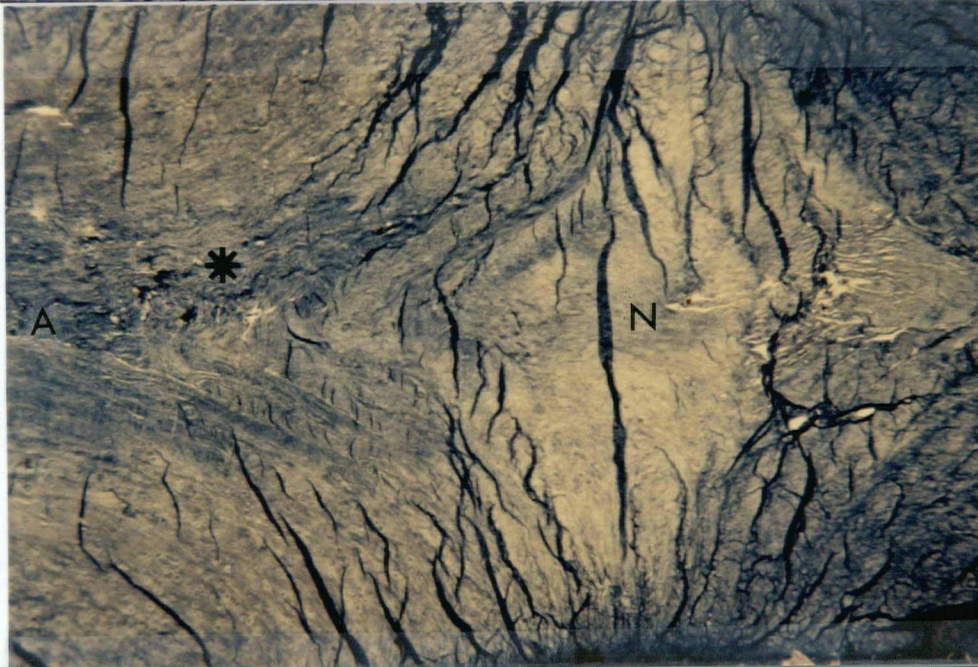


FIGURE 23: HEMATOXYLIN AND EOSIN STAINED SECTION OF THE ANULUS
OF AN MRI CATEGORY 2 DISC

The photomicrographs of a section from a 39-year-old male shown here at magnification 320x indicates the changes seen in the anulus of MRI category 2 discs. The vertebral body and endplate are oriented horizontal to the section. Clear spaces (*) representing areas of mucin deposition, cartilaginous tissue and reduction in collagen density and organization (→) characterize the anulus of MRI category 2 disc. Chondrocytic cells (▲) elaborating cartilaginous matrix are evident in increased numbers with respect to MRI category 1 discs.

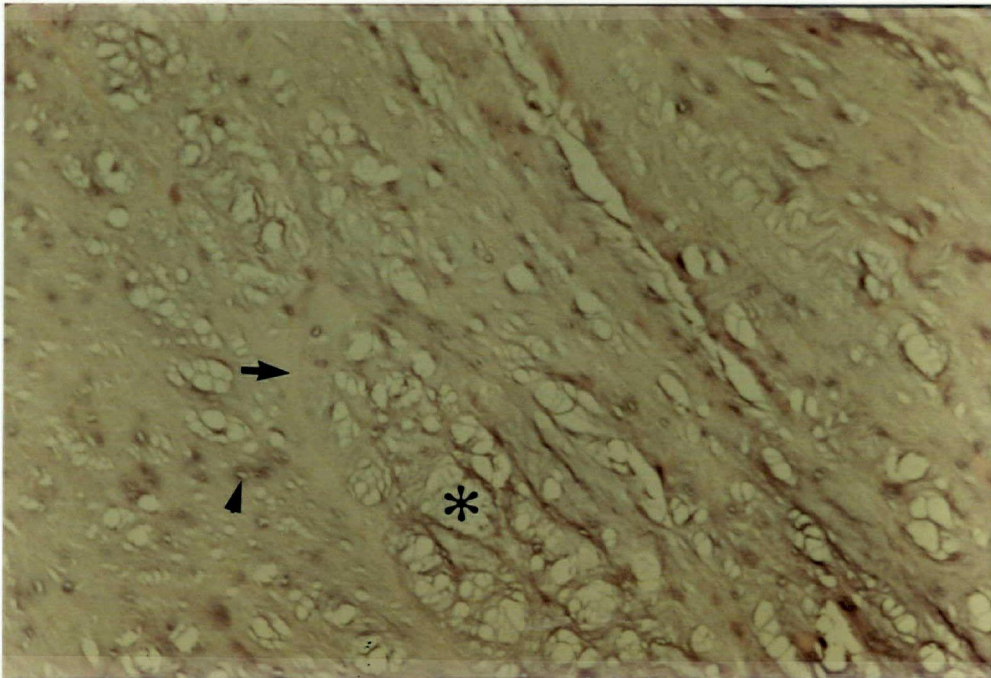
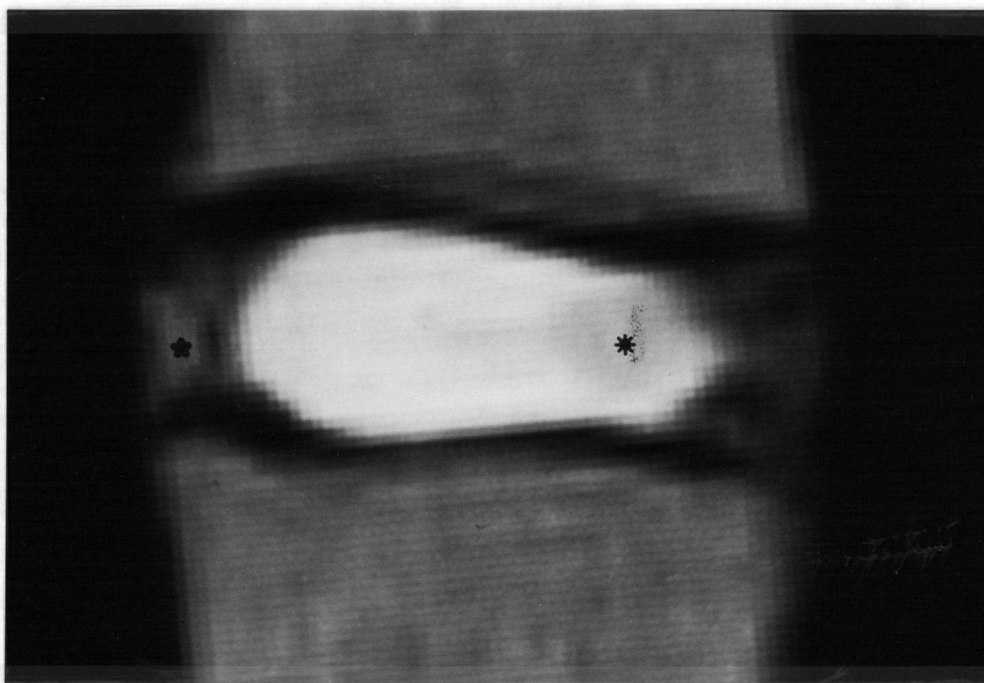


FIGURE 24: MRI SCAN OF AN MRI CATEGORY 2 DISC

The MRI image is from the same disc shown in Figures 22 and 23. The dark signal extending into the nucleus (*) corresponds to the collagen proliferation seen histologically (Figure 22). Bright signals in the annulus (♣) correspond to basophilic regions seen histologically (Figure 23).



With higher objectives, changes in gross tissue morphology corresponded to changes in staining patterns. In the anulus, the collagen lamellae appeared less defined and less regular because of an increase in the amount of inter-lamellar interstitial matrix. The basophilic foci consisted of chondrocytic cells elaborating an unstructured extracellular matrix (Figure 23). In general, the cells in the anulus appeared more chondrocytic, resembling the so-called "giant chondrons", and were more abundant, particularly in the inner anulus. Microscopic disruptions of the collagenous lamellae near their insertion in the endplate were occasionally seen. In the nucleus, collagenous fibers were more abundant and more horizontally oriented near the anulus (Figure 25). The cell density was increased and occasionally clusters of chondrocytic cells - "minichondrons" - were seen. Changes like those of early osteoarthritis, occurred in the cartilaginous endplate including chondrocytic clumping and disorganization of the cellular stratification (Figure 26).

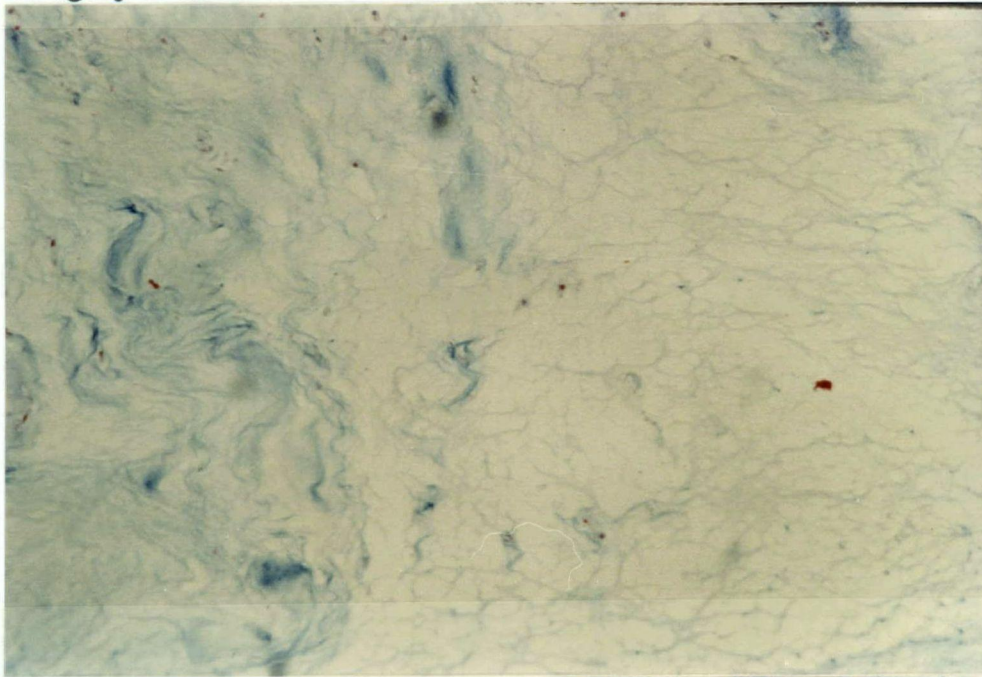
MRI Grade 3. Two discs were classified as MRI Grade 3. With each stain, demarcation of anulus from nucleus was difficult. Overall, the intensity of staining of the disc by aniline blue increased and that by alcian blue decreased. In the anulus, the basophilic foci were larger, more frequent, and corresponded to the bright SE 40 MRI signals seen in the anulus. In the nucleus, there was an increased staining by aniline blue which corresponded with a darker SE 40 MRI signal. Bright signals near the endplates had corresponding areas that stained intensely with alcian blue. The decrease in anular collagen and increase in nuclear collagen observed in the chemical analysis was consistent with the histochemical features.

At higher magnification, the cartilaginous metaplasia seen in grade 2 discs was more extensive in grade 3 discs. At the anterior and posterior margins of

FIGURE 25: MALLORY TRICHROME STAINED SECTIONS OF MRI
CATEGORY 1 AND 2 NUCLEAR ZONES

The 320x magnifications of an MRI category 1 disc from a 16-year-old male (a) and an MRI category 2 disc from a 39-year-old male (b) demonstrate the histochemical changes seen between categories. The density and organization of collagen fibers in an MRI category 2 disc (b) is notably greater than that in an MRI category 1 disc (a). Cells resembling chondrocytes (▶) are more apparent in MRI category 2 discs.

(a)



(b)

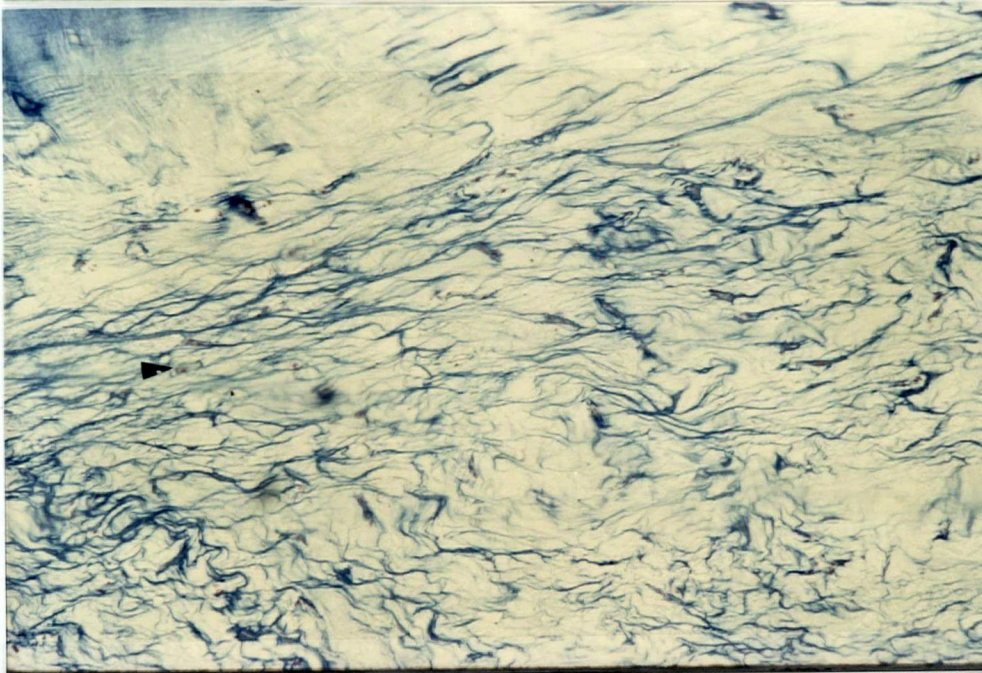
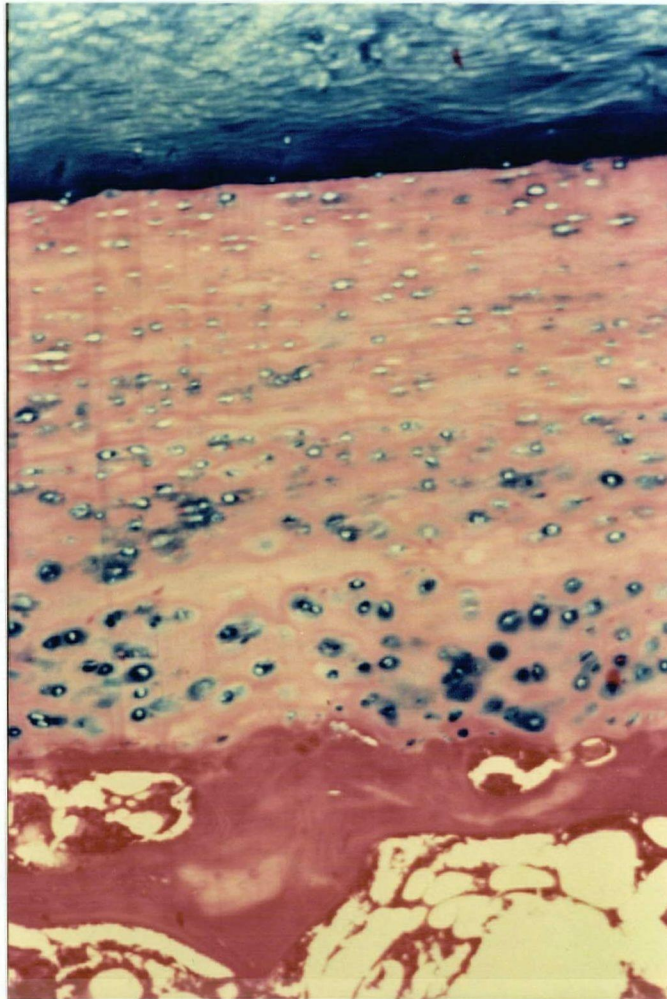


FIGURE 26: ALCIAN BLUE STAINED SECTION OF AN MRI CATEGORY 2 ENDPLATE

In comparison with an MRI category 1 endplate (Figure 21), this photomicrograph from a 39-year-old male demonstrates the distinct changes seen in MRI category 2 endplates. Loss of cellular stratification and the presence of chondrocyte clumping characterize MRI category 2 discs. (Magnification 320x.)



the vertebral body, chondrocyte formation was evident with small areas of endochondral ossification (Figure 27). In the nucleus, increased numbers of "giant chondrons" were seen near the anulus and "mini-chondrons" near the endplate. Alcianophilic areas near the endplate consisted of "mini-chondrons" with abundant territorial matrix. Except for the territorial matrix of the chondrons, the extracellular matrix of the nucleus contained increased amounts of horizontally oriented collagenous fibers, similar to those seen in the inner anulus (Figure 28). The hyaline cartilage endplate was diffusely thinned. Focal defects extending to the marrow cavity and filled with fibrocartilage were observed occasionally (Figure 29). Calcification of the basal layers was apparent in some areas, particularly in the anular region.

MRI Grade 4. Four discs were classified as MRI Grade 4. As in the grade 3 discs, the nucleus and anulus were indistinguishable on the basis of staining. Overall, staining by aniline blue exceeded that of alcian blue except in areas close to the endplate. The staining characteristics were consistent with the observed trends in the chemical data. The alcianophilic areas in the anulus and nucleus corresponded to a bright signal in the MRI image. Macroscopic clefts parallel to the endplate extend through the nucleus, and at times into the anulus, posteriorly more than anteriorly, corresponded to a dark signal in the MRI image (Figure 30). A cellular membrane which stained intensely with aniline blue lined the cleft cavity. The cleft cavity and lining tissue were seen more extensively in MRI category 5 discs.

The tissue in the anulus consisted of poorly defined, disorganized and disrupted fibrocartilaginous lamellae with foci of chondrons surrounded alcianophilic extracellular matrix. The clefts, like those in category 5 discs, in the nucleus were lined by a membrane-like structure which had flattened mesothelial-like cells resting on a loose collagenous network (Figure 31).

FIGURE 27: HEMATOXYLIN AND EOSIN STAINED SECTION OF THE VERTEBRAL BODY
MARGIN OF AN MRI CATEGORY 3 DISC

At 320x magnification, this MRI category 3 disc from a 33-year-old male appears to demonstrate endochondral bone formation (*) in the fibrocartilaginous region interposed between the anulus (a) and vertebral body (v). The less intense pink extracellular matrix (*) seen is suggestive of immature osteoid when compared with the more intense pink of organized lamellar bone (*). Confirmation of this would require a stain such as Masson's trichrome to identify osteoid.

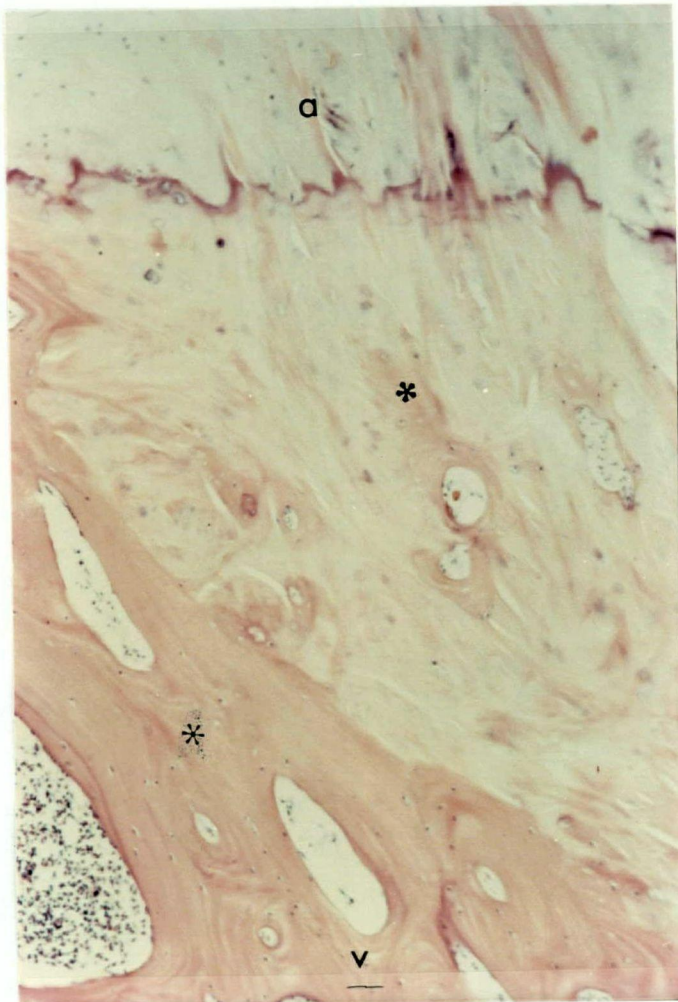


FIGURE 28: ALCIAN BLUE STAINED SECTION OF AN MRI CATEGORY 3 NUCLEUS

This 320x photomicrograph of an MRI category 3 nucleus from a 33-year-old male indicates the progression of changes that were seen in MRI category discs (Figure 25b). An increased number of horizontally oriented collagen fibers and chondrocytic cells characterize an MRI category 3 nucleus.

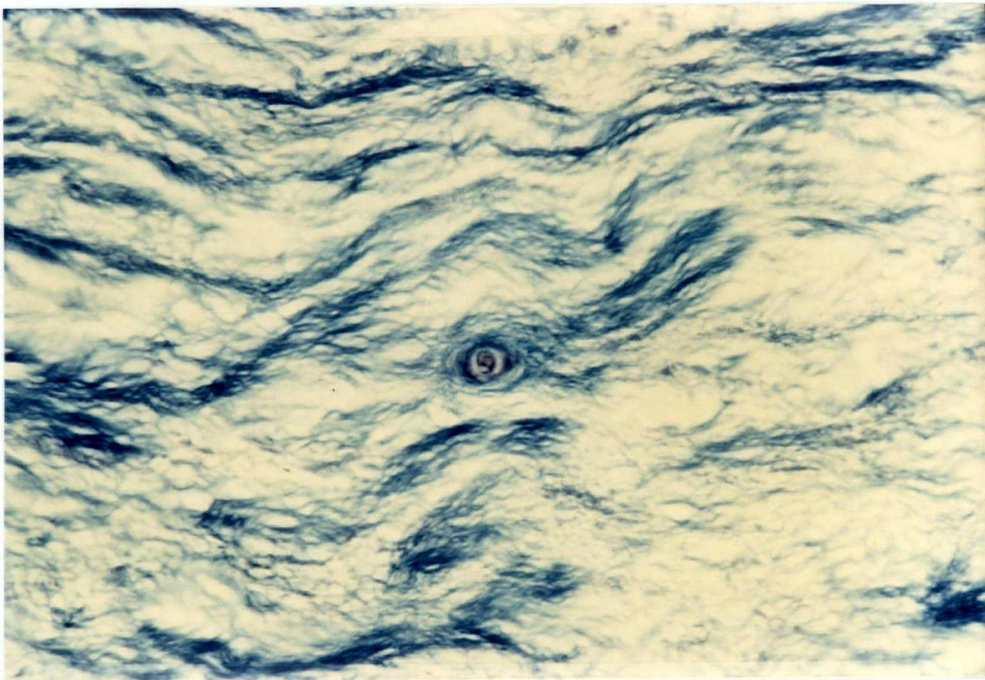


FIGURE 29: HEMATOXYLIN AND EOSIN STAINED SECTION OF AN MRI CATEGORY 3 ENDPLATE

At 320x magnification, thinning, loss of stain intensity (*), and focal defects (*) in this MRI category 3 endplate from a 33-year-old male are apparent.

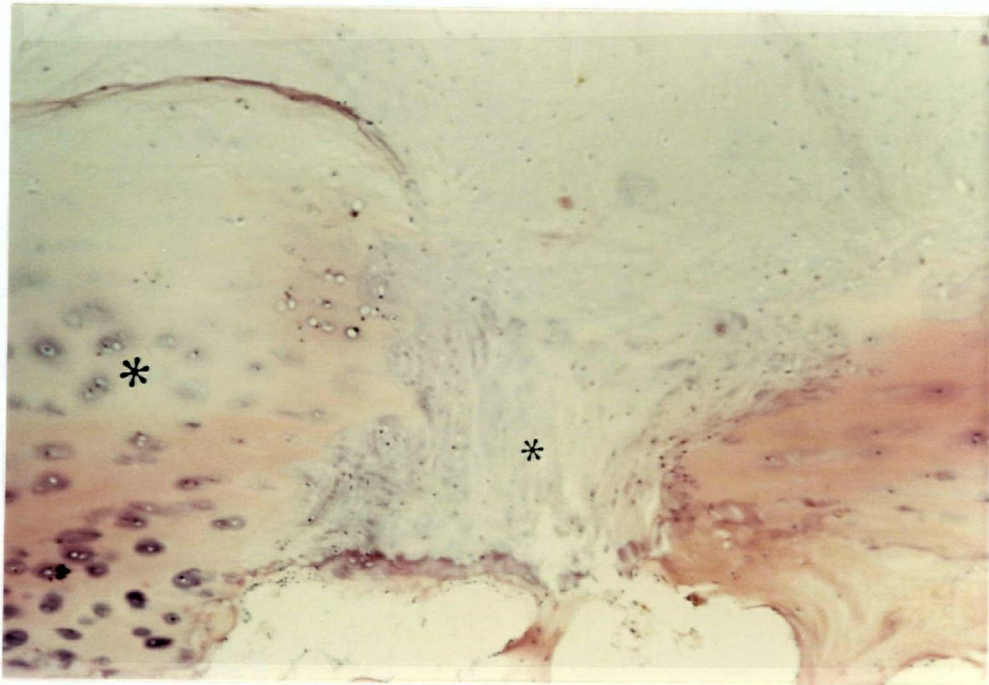
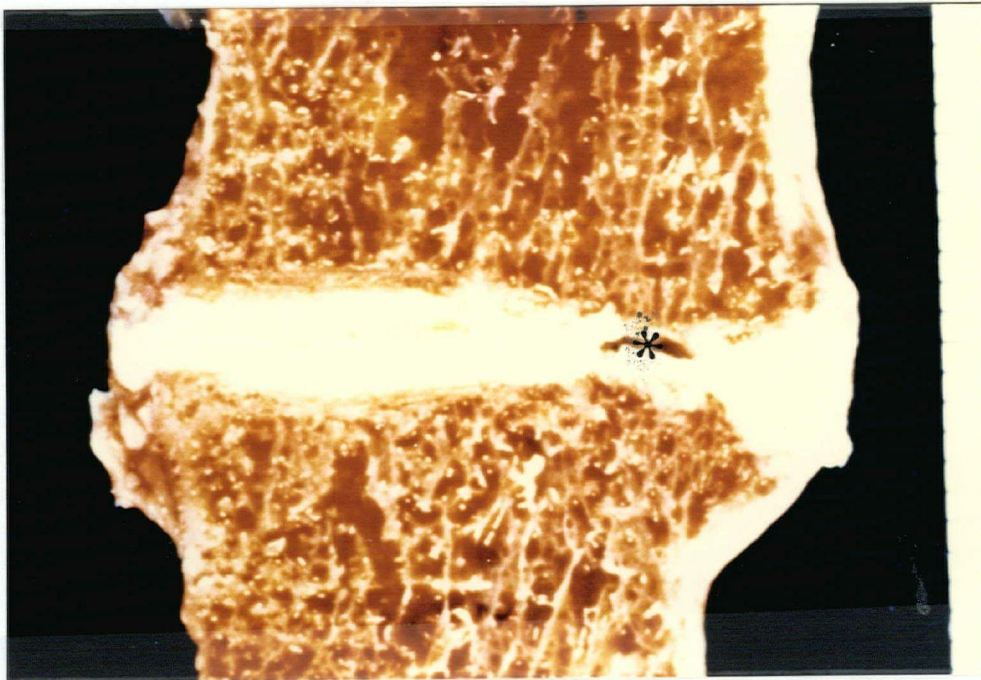


FIGURE 30: GROSS MORPHOLOGY AND MRI SCAN OF
AN MRI CATEGORY 4 DISC

The macroscopic cleft (*) seen in the gross morphology (a) corresponds to the dark signal in the MRI scan (b) in this disc from an 89-year-old female.

(a)



(b)

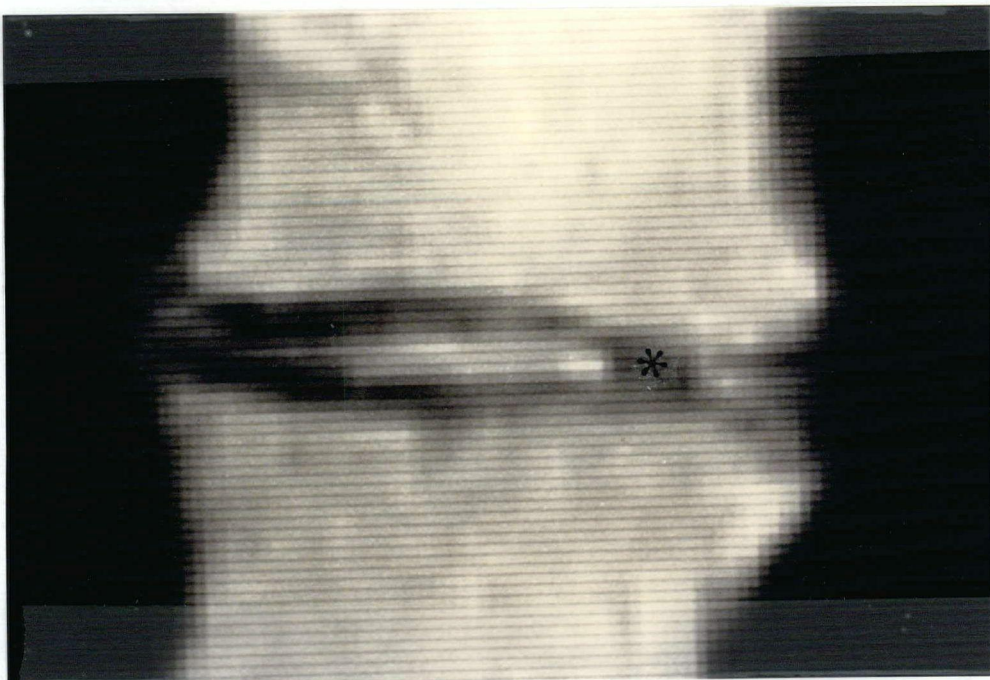


FIGURE 31: HEMATOXYLIN AND EOSIN STAINED SECTION OF A CLEFT IN
AN MRI CATEGORY 4 DISC

In this 320x photomicrograph of tissue lining the cleft cavity seen in Figures 30a and b, the cleft cavity (*) is seen to be lined by a membrane of flattened mesothelial cells (▶) and loose connective tissue (*).



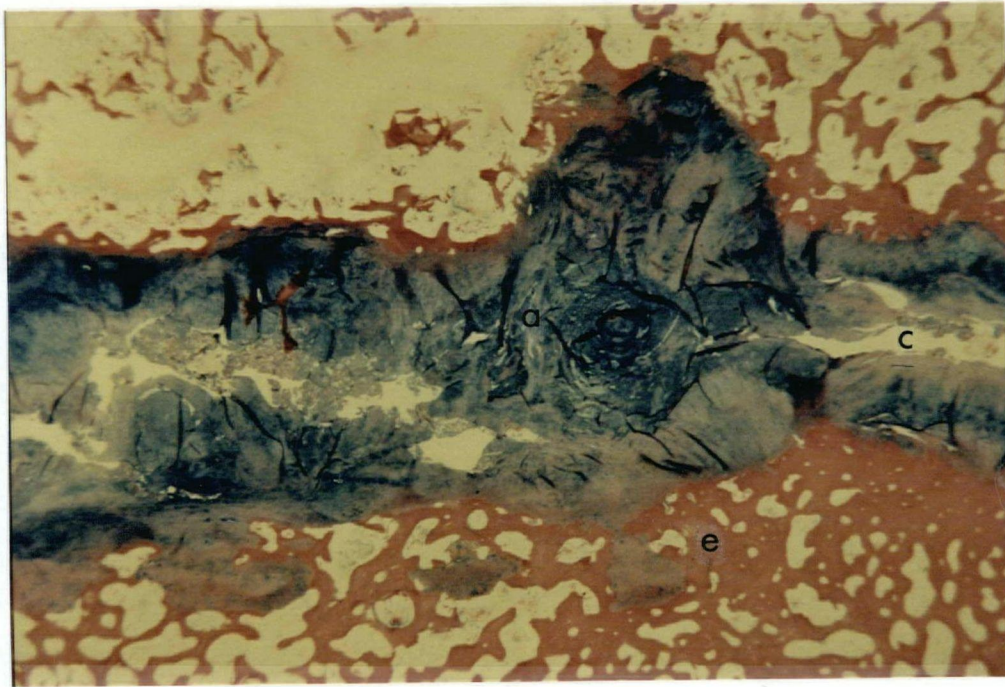
Preservation of this lining during preparation of sections was difficult as evidenced by the fact that fragments were often missing or lying freely in the cavities. When more than one cleft was present, central nuclear tissue was often isolated from the remaining tissue adjacent to the endplate. The tissue immediately below the membranous lining was fibrocartilaginous. The hyaline cartilaginous endplate frequently had defects filled with fibrocartilage. This fibrocartilage extended well into the trabecular network of the vertebral body. The trabeculae of the endplate were thicker and had fewer perforations for vascular communication between the cartilaginous endplate and the marrow cavity. In areas, a second horizontally oriented subchondral plate, or "doubling" of the endplate, was apparent. Foci with distinct thickening of trabeculae, doubling of the endplate or fibrocartilage correspond to a thickening of the dark line representing the endplate in the MRI image. At the margins of the vertebral bodies, osteophytes formed by endochondral ossification of metaplastic cartilage were evident.

MRI Grade 5. Two discs were classified as MRI Grade 5. The uniform staining of nucleus and anulus noted in grade 3 and 4 discs was also seen in grade 5 discs but with the following differences: A single large branching cleft extended through the anulus and loss in disc height had occurred. The alcianophilic staining tissue foci adjacent to the endplate were contiguous and occupied a proportionally larger area (Figure 32b). Thickening of the endplate by cartilaginous metaplasia and bony sclerosis was visible macroscopically and microscopically (Figures 32a and b). The relative increase in the numbers of alcianophilic foci was reflected by the slight increase in chondroitin and keratan sulphate contents of the nucleus and anulus. In the MRI image, clefts corresponded to dark signals and the alcianophilic tissue to bright signals.

FIGURES 32a-c: ALCIAN BLUE STAINED SECTION, GROSS MORPHOLOGY AND MRI SCAN
OF AN MRI CATEGORY 5 DISC

The gross morphology (a) of this category 5 disc from an 89-year-old female orients one to the corresponding areas in the photomicrograph (b) and MRI image (c). The 32x photomicrograph (b) shows alcianophilic staining regions near the endplate (a) and clefts (c) corresponding to the bright (a) and dark (c) signals of the MRI scan. Thickening of the bony endplate (e) was apparent.

(a)



The dark line representing the endplate was diffusely thickened and irregular (Figure 32c).

Few recognizable lamellae remained in the anulus. The tissues in both the anulus and nucleus were similar in appearance (Figure 33). The connective tissue membrane lining the cleft was more apparent than in grade 4 discs (Figure 34). The proportion of tissue consisting of chondrocytic cells and alcianophilic territorial matrix was increased (Figure 35). The endplate region appeared similar to an end stage osteoarthritic joint with diffuse hyaline cartilage loss, trabecular thickening of the subchondral bone, reactive fibrocartilaginous metaplasia and peripheral osteophyte formation.

These observations were consistent with the classifications proposed and contributed to their construct validity. The consistency of the descriptions as a function of MRI category was greater than that for morphologic category for categories 1 and 2. This suggested, as did the frequency matrix and chemical data, that MRI was more sensitive to early age related and degenerative changes.

ALCIAN BLUE STAINED SECTION, GROSS MORPHOLOGY AND MRI SCAN
OF AN MRI CATEGORY 5 DISC (cont'd)

(b)



(c)

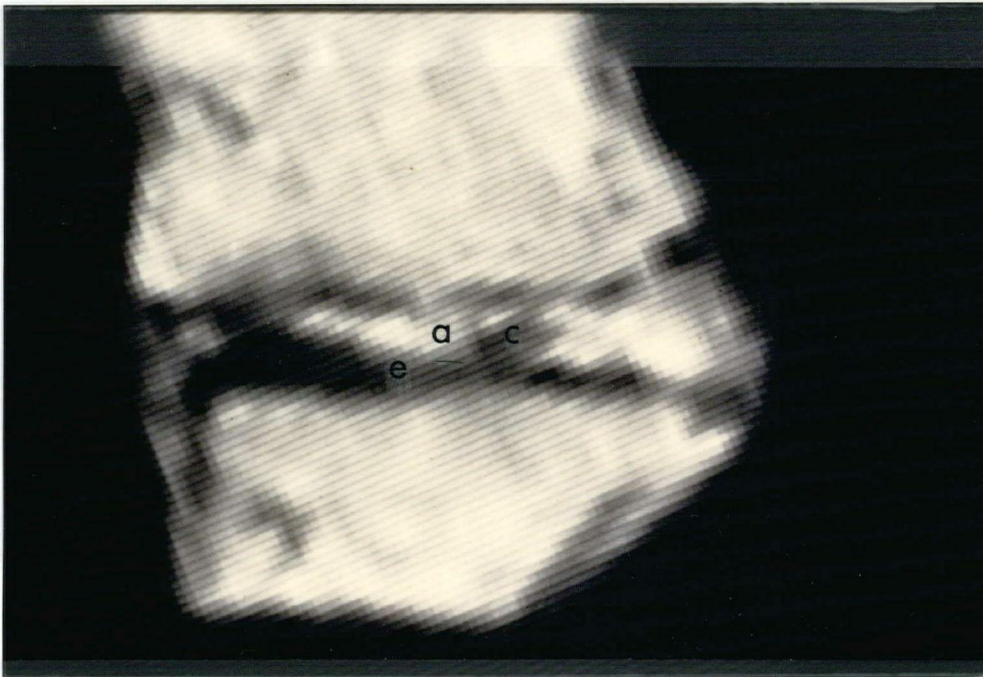


FIGURE 33: MALLORY TRICHROME STAINED SECTION OF AN MRI CATEGORY 5 DISC

In this 320x photomicrograph of a category 5 disc from an 89-year-old female, the annulus is to the left and the nucleus to the right. Poorly organized fibrocartilagenous tissue () with chondrocytic cells () comprise the nucleus and annulus. The nuclear and annular tissue cannot be distinguished.

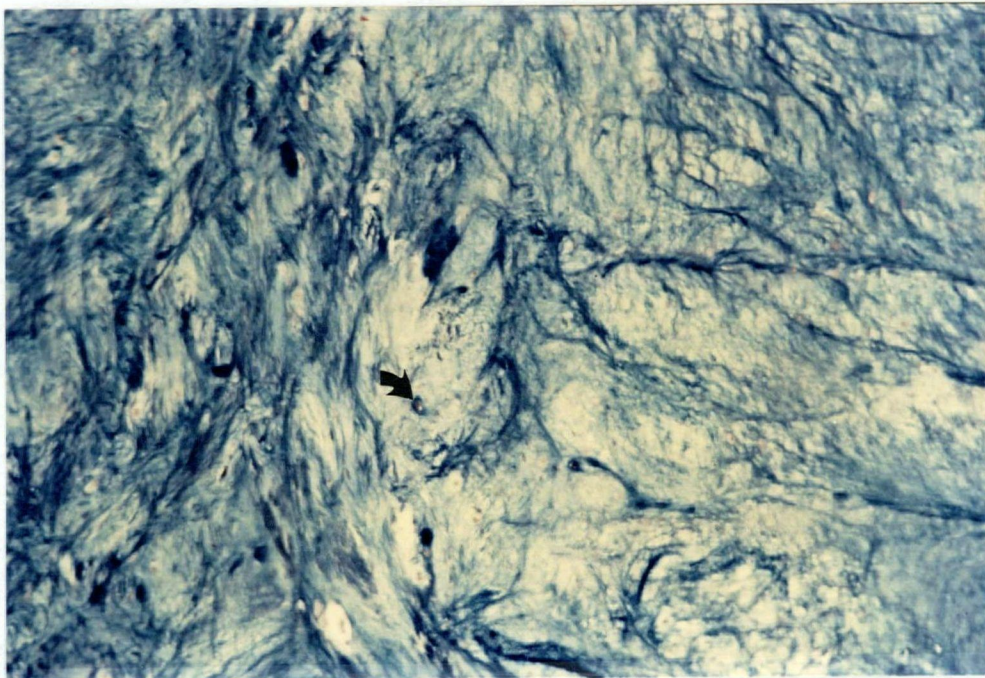


FIGURE 34: MALLORY TRICHROME STAINED SECTION OF A CLEFT IN AN
MRI CATEGORY 5 DISC

The macroscopic cleft (*), associated fibrous membrane (→) and underlying fibrocartilagenous matrix (**) of an MRI category 5 disc. The donor was an 89-year-old female. (Magnification 80x.)

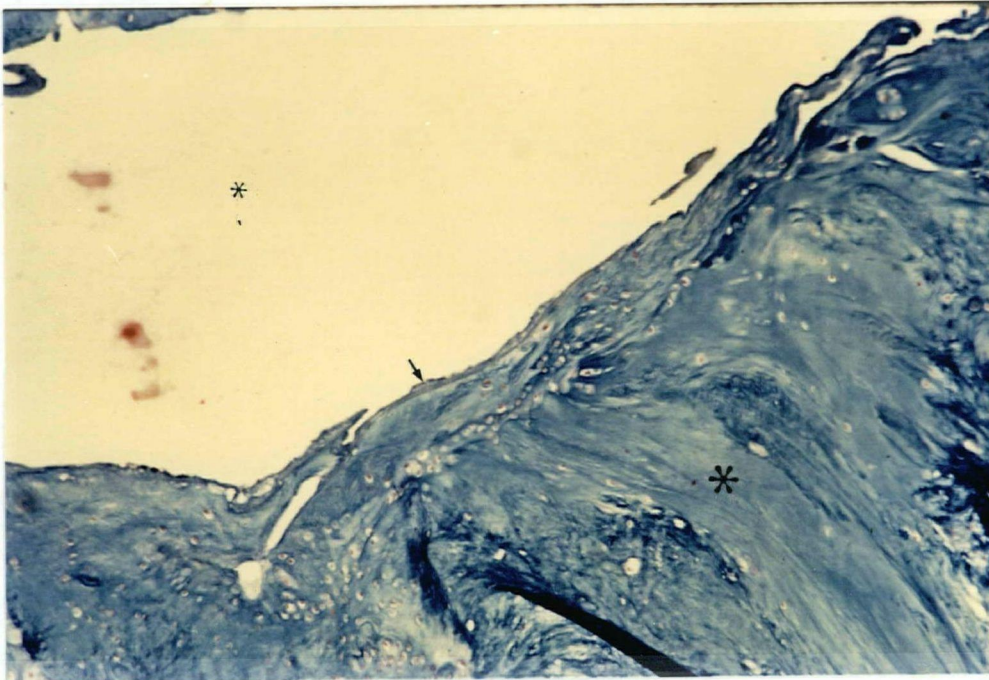
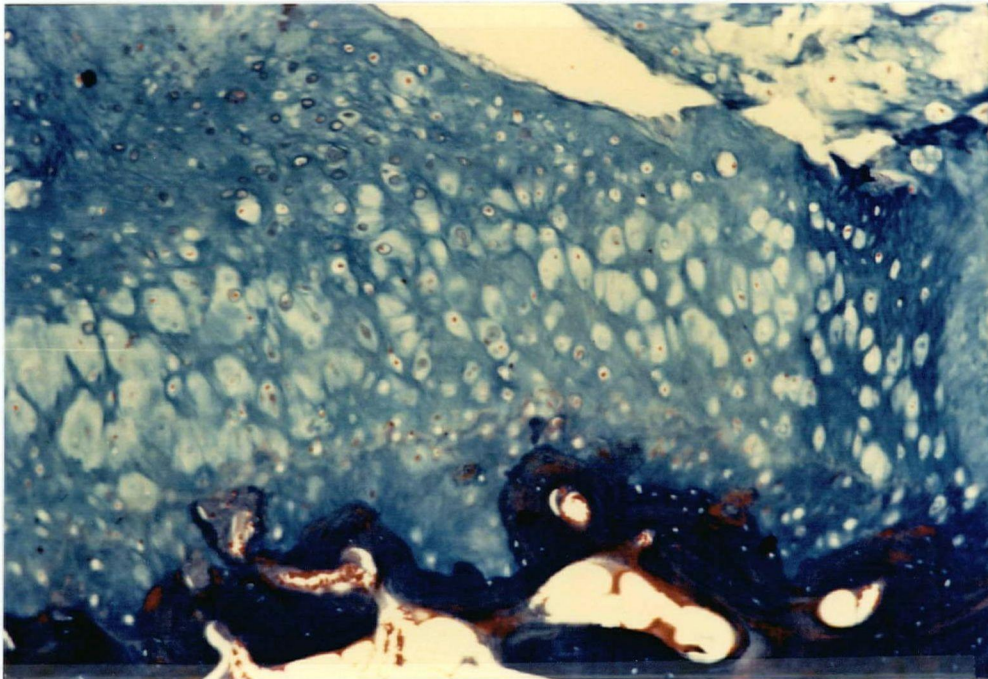


FIGURE 35: MALLORY TRICHROME STAINED SECTION OF AN MRI CATEGORY 5 DISC

In this 320x photomicrograph of a category 5 disc, the area shown corresponds to the area producing a bright signal in the MRI image. High power examination highlights the cellular nature and less fibrous extracellular matrix (*) seen in this region of an MRI category 5 disc. The end plate is inferior and cleft cavity superior.



CHAPTER 4

DISCUSSION

DISCUSSION

4.1 GENERAL

The classifications proposed represent the first formally tested methods of categorizing the morphologic appearance and MRI images of intervertebral discs as they change with aging and degeneration. Previous researchers investigating disc aging and degeneration used arbitrary categories (Lewin, 1964; Pearce, 1986). However, a lack of formal testing of validity has prevented the widespread adoption of these classifications. The results of this experiment indicate that the classifications proposed meet generally accepted criteria for the selection of endpoints in measurement (Tugwell & Bombardier, 1981; Kirshner & Guyatt, 1985; Feinstein, 1985). As a consequence, these classifications should be a universally acceptable and practical means of quantifying disc aging and degeneration.

4.2 METHOD LIMITATIONS

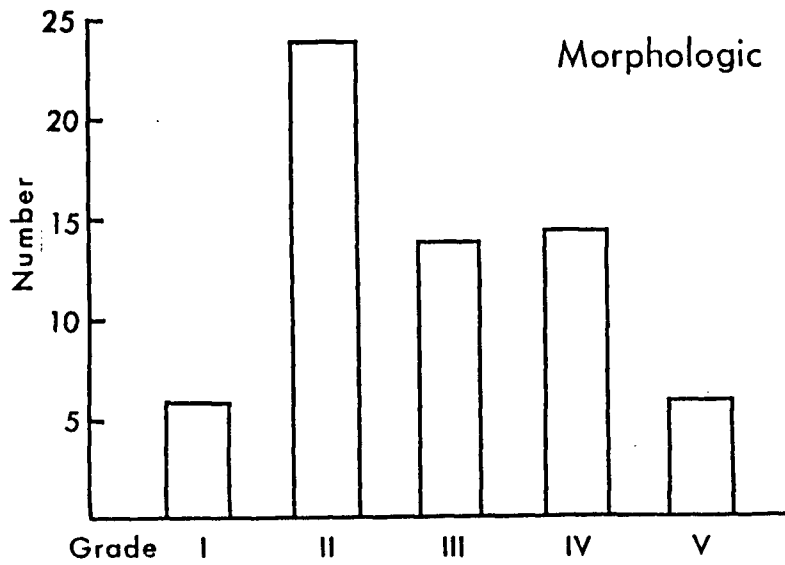
4.2.1 SAMPLE CHARACTERISTICS

The sample size was relatively small when compared to previous reports dealing with disc morphology (Table 1). The number of specimens used in this study represented a compromise. For statistical significance, a minimum sample size of $n = 2k^2 = 50$, where $k = 5$ (the number of categories), is required for kappa calculations (Cicchetti, 1976). The selection of 68 discs from 15 spines exceeded this minimum and, in addition, permitted principal component, discriminant and stepwise regression analysis. Ideally, as many specimens as possible would have been analysed. Time and medical-legal constraints made the collection of more specimens impractical. Moreover, to make the observers' task manageable, restriction of the number of specimens was necessary. The second to eighth decades were evenly represented (Figure 6) and provided a

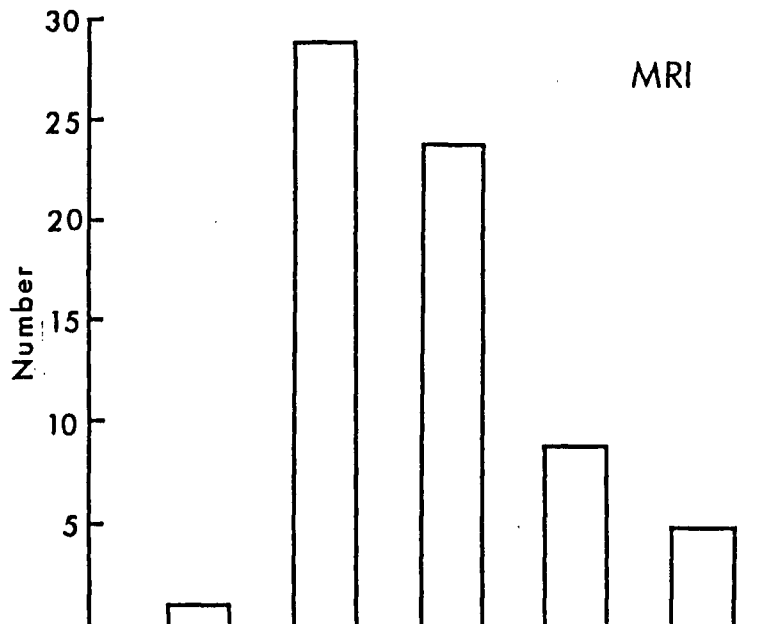
FIGURE 36: DISTRIBUTION OF DISCS ACCORDING TO MORPHOLOGIC AND MRI CATEGORY

The distribution of discs according to overall morphologic (a) and MRI (b) category shows fewer MRI category 1, 4 and 5 discs than the more evenly distributed morphologic categories.

(a)



(b)



challenge spectrum for the morphologic and MRI classifications with a near normal distribution (Figure 36). The relatively few category 1 discs could partly be accounted for by the difficulty in obtaining specimens from the first decade of life. The disproportionately small number of MRI Grade 1 discs likely reflects the sensitivity of MRI to the early changes of aging and degeneration. No attempt was made to control for donor sex since gender is not a major determinant of disc aging and degeneration (Kellgren & Lawrence, 1958). The aims of this research did not include an attempt to correlate clinical findings with disc morphology and MRI appearance. Consequently, no effort was made to select specimens with a history of low back problems. However, when compared with existing reports in the radiology literature, the number of discs examined by MRI, gross and microscopic morphology and biochemistry is unparalleled (Table 2).

4.2.2 IMAGING

The method adopted for imaging may make application of our observations difficult unless a similar protocol is followed. Our sequences differ from those described in other reports. On the basis of personal observation of the preliminary 55 discs, the protocol calling for TE 40 ms and TR 2000 ms appeared to provide images with the greatest morphologic resolution. As a consequence, this sequence was used in defining and testing the MRI classification. Although not always defining the disc well morphologically, the other sequences, particularly inversion recovery, provided additional information about tissue composition (i.e. water content). Our imaging of the anterior elements of dissected spines may have provided a resolution unobtainable clinically where patient movement and surrounding tissues compromise image quality. Although in vivo imaging of lumbar spines has not been done in this

project, images published by other researchers are comparable, suggesting that the resolution of the disc is not compromised significantly by in vivo imaging. Furthermore, the MRI unit used in this experiment operates at a field strength approximately 10 per cent of current units. The newer, more powerful MRI units provide better image resolution and shorter image times so that comparable images in vivo may be possible despite signal attenuation by interposed tissue and increased receiver distance. The imaging of cadaver specimens raises questions about the possibility of postmortem changes secondary to distortion by degradative processes. The avascular nature and low metabolic demands of the relatively small number of cells of mature discs may make disc tissue less susceptible than other tissues to postmortem degradation, particularly if the specimen is kept at 4°C (Nachemson, 1985). The re-examination of three spines after 24 hours showed no detectable differences, supporting this hypothesis (Figure 7).

4.2.3 DEVELOPMENT AND TESTING OF THE CLASSIFICATIONS

The classifications for gross morphologic and magnetic resonance images required many revisions. Categorizing a continuum of changes, such as occurs in disc aging and degeneration, proved to be difficult, perhaps explaining why no classification had been established previously. Because of the multiplicity of terms used to describe disc aging and degeneration, carefully worded descriptions were required to ensure that investigators from a variety of disciplines could understand and apply the classifications. Acceptance of these classifications would reduce the needless duplication of terminology and improve communication.

The methodological framework used to assess these classifications represents a synthesis of work published by several clinical epidemiologists

(Tugwell & Bombardier, 1982; Kirshner & Guyatt, 1985; Feinstein, 1985). This framework addressed the major measurement issues needed to find valid endpoints.

4.2.4 HISTOLOGY AND CHEMISTRY

The chemical and histological methods used to characterize the 15 specimens in greater detail were chosen because of their simplicity and reliability. The chemical results were consistent with trends described previously by other investigators (Sections 1.5 and 3.4). As indicated in Figures 9 to 17, there was overlap between grades. The overlap may reflect inappropriate categorization of discs, heterogeneity of disc composition or limitations inherent in the techniques used.

From the histologic analysis it was apparent that there were regional variations in disc morphology. Because of the mass of tissue required for lyophilization, a given sample could not be histologically homogeneous despite careful dissections. These imprecise methods of sampling resulted in tissue heterogeneity that might obscure subtle differences in composition related to morphology. Estimates of the dry weight by freeze drying are limited by the hydroscopic nature of the tissue. Water regained would be influenced directly by the tissue surface area. However, alternatives such as thermal dessication have greater disadvantages.

The convenience of colorimetric assays makes them attractive, but they do have disadvantages. However, the methods chosen possess refinements which reduce some of the imprecision associated with colorimetric techniques. The micro adaptation of the hexuronate assay described by Bitter and Muir (1962) reduced some of the problems inherent to this assay of chondroitin sulphate. The advantages of this technique include good specificity and sensitivity compared with the earlier method of Dische (1947), immediate and stable colour

development, decreased interference from Cl^- and oxidants, and good reproducibility. Scott and Melvin (1953) improved the anthrone reaction for hexose (keratan sulphate) by controlling the formation of colour by using a water bath at a constant temperature. However, variation in water temperature and acid concentration, colour stability and specificity may result in less satisfactory sensitivity and specificity. In addition, subsequent work in this laboratory demonstrated that the hexose determination not only reflected the keratan sulphate content but also the glycoprotein content. Preliminary work indicates that glycoprotein is a significant component accounting for 40-60 percent of the hexose content of the anulus and 10-25 per cent of that of the nucleus. The technical problems inherent to the hexose assay and the glycoprotein content were likely responsible for the less distinct changes between grades in comparison with those changes observed for chondroitin sulphate. The hydroxyproline assay as described by Woessner (1961) improved the sensitivity, specificity and stability of the hydroxyproline chromogen. However, a large excess of other amino acids, such as glycoprotein, may suppress the reaction and account in part for the less clear trends seen in collagen content.

The limited reproducibility and specificity of the methods employed may account for the variability and consequent overlap in the data collected for each grade. Evaluation of the remaining discs may define more clearly the difference in chemical composition between grades. For statistical significance, analysis of an estimated 15 discs for each grade will be required to provide an acceptable - < 0.20 - Beta error (Schechter, 1986). This work is being undertaken. Should the results not demonstrate clear changes with grade, re-evaluation of the techniques used, particularly those of tissue sampling, will be required.

4.3 RESULTS

The comprehensiveness and credibility of the classifications were evaluated in a subjective manner. Because no 'gold standard' existed, it was necessary to rely on literature review, personal observation and, particularly, expert opinion. Had time permitted, it may have been possible to compare the proposed morphologic classification to that of Lewin (1964). However, such a comparison would have been fraught with problems. The description provided by Lewin was brief and based on the appearance of a horizontal section of the disc. Our classification described changes in a sagittal plane so that comparisons with images provided by MRI and with pathologic descriptions provided by more current authors (Vernon-Roberts, 1977; Milgram, 1982) could be made. Furthermore, Lewin's classification has not been evaluated critically and has not gained widespread acceptance.

The classifications proved to be consistent. The kappa values ranging from 0.5020 to 0.9360 represented an acceptable level of agreement between intra- and interobserver pairs (Kramer and Feinstein, 1981). The number of specimens used to evaluate consistency was sufficient to provide valid estimates of weighted kappa (Cicchetti, 1976). Unfortunately, no consensus on establishing the confidence limits of kappa has developed, so that objective evaluation of the kappa values obtained has not been possible.

In both the morphologic and MRI classifications, one observer pair was more consistent than the other two. This suggested that one observer, Observer 1 in the MRI and Observer 2 in the morphologic, differed in his observation and interpretation of disc parameters from the other two observers. This discrepancy may be ascribable to the differences in experience and expertise of the observers. MRI Observer 1 had not been active in the interpretation of

MRI images. To compound this shortcoming, he received the least preparation before using the classification. Morphologic Observer 2, although interested in the clinical aspects of low back pain, was not familiar with many of the morphologic terms. Improved consistency of application (grading) will require further refinement of the classifications by simplifying terminology, i.e. eliminating jargon, and reducing the complexity of descriptions. Stepwise regression analysis suggested streamlining the classifications should be possible. For the existing classifications, had it been possible to recruit observers with more experience and then familiarize each observer more thoroughly with the terminology used in the description of each parameter and category, better intra- and interobserver agreement might have been obtained.

Intra- and interobserver agreement for the morphologic classification was better overall than that for the MRI. The limited resolution of the MRI unit used in this experiment is a plausible explanation for the reduced consistency in the interpretation of MRI images. The lack of experience with MRI technology would also account for the lower kappa values. Intra-observer agreement was better than interobserver for both classifications, suggesting that the descriptions and instructions for using the classifications were understandable and workable on an individual basis. It also suggested that systematic differences in interpretation by observers occurred. The latter hypothesis will be more fully discussed below.

Although agreement between observer pairs was 'moderate' in one pair and 'substantial' in the remaining five, the classifications were not flawless. Scrutiny of the data suggested that both random error and bias contributed to observer variability. The discrepancies between intra-observer and interobserver values indicated observer bias occurred. Examination of the

frequency matrices support this hypothesis. For example, in Table 7 Observer 1 consistently recorded a higher MRI grade than Observers 2 and 3. Similarly, in Table 6 Observer 2 consistently recorded a lower morphologic grade. To substantiate this impression, principal component analysis was done for each MRI observer. Differences in factor loadings for each observer were apparent (Table 13). This indicated that each observer emphasized different parameters when assigning an overall grade.

Random error also contributed to observer disagreement. In the frequency matrices, although systematic differences occurred, scatter along either side of the diagonal was apparent (Tables 6 and 7). Comparisons of the variance accounted for by stepwise regression and principal components suggested that using all parameters to assign grade instead of emphasizing important individual elements identified by regression may have contributed to observer variability. For example, in the MRI data, stepwise discriminant analysis for nuclear zone (NZ) alone had multiple correlation coefficient of 0.8841 whereas the first principal component accounted for 0.5889 of the total variance (Tables 9 and 11). This data suggested that attempts to use all parameters to assign overall grade impedes the decision making process and thereby increases variability. In essence, observers were not able to see the 'forest' (grade) for the 'trees' (parameters). In both the MRI and morphologic stepwise discriminant analyses, the nuclear zone parameters - NZ, TINZ, TMNZ - accounted for 0.8841 and 0.8606 of the variance in the MRI and morphologic models respectively (Tables 8 and 9). This indicated that grade was largely a function of changes in the nuclear zone. The apparent chemical and histologic changes in the nucleus support this (Sections 3.4 and 3.5). For the MRI data, a frequency matrix of nuclear zone (NZ) by grade was created (Table 14). The

TABLES 13a-c: MRI PRINCIPAL COMPONENT ANALYSIS BY OBSERVER

Summary of principal component analysis excluding correlations. The eigen values and weightings of each eigen vector were different for each observer suggesting individual biases in evaluating discs.

13(a). OBSERVER 1

	EIGEN VALUE	DIFFERENCE	PROPORTION	CUMULATIVE
PRIN. 1	2.94681	1.02302	0.267892	0.26789
PRIN. 2	1.92378	0.47087	0.174889	0.44278
PRIN. 3	1.45291	0.22688	0.132083	0.57486
PRIN. 4	1.22603	0.26607	0.111458	0.68632
PRIN. 5	0.95996	0.11624	0.087269	0.77359
PRIN. 6	0.84372	0.34105	0.07601	0.85029
PRIN. 7	0.50266	0.08091	0.045697	0.89599
PRIN. 8	0.42176	0.10769	0.038342	0.93433
PRIN. 9	0.31406	0.01172	0.028551	0.96288
PRIN. 10	0.30234	0.19639	0.027486	0.99037
PRIN. 11	0.10595		0.009632	1.00000

EIGENVECTORS

	PRIN. 1	PRIN. 2	PRIN. 3	PRIN. 4	PRIN. 5	PRIN. 6	PRIN. 7	PRIN. 8	PRIN. 9	PRIN. 10	PRIN. 11
EPS	0.313659	0.026006	-0.459174	-0.31423	0.461640	0.067264	-0.487280	0.020690	-0.481256	-0.042801	0.012972
EPI	0.282612	-0.039717	-0.507355	0.244104	0.320722	-0.213149	0.421220	-0.149217	0.485609	0.122791	0.051739
NZ	-0.156885	0.065114	0.272081	0.393337	0.487215	0.648232	0.264874	-0.022710	-0.100884	0.053715	-0.032955
AZAS	0.353468	-0.105184	0.225598	-0.464421	0.057273	0.210936	0.035380	-0.737775	0.058777	-0.024803	-0.002772
AZAI	0.314412	-0.198713	0.077910	-0.531152	0.150336	0.256090	0.154243	0.641775	0.197886	0.098707	0.026725
AZPS	0.355872	-0.443454	0.167940	0.330647	-0.106001	-0.058482	-0.083367	0.051619	-0.011446	-0.055162	-0.715352
AZPI	0.321188	-0.455605	0.197586	0.359217	-0.181281	0.003807	-0.080937	0.030135	-0.076758	-0.030819	0.693440
VBAS	0.196870	0.404531	0.413784	0.134257	0.278664	-0.167667	-0.482998	0.072859	0.495336	-0.129759	0.042404
VBAI	0.289113	0.289698	0.355775	-0.019101	0.182467	-0.490810	0.441087	0.072831	-0.476693	0.064727	0.008510
VBPS	0.329987	0.388232	-0.068792	0.145403	-0.397394	0.254317	-0.090313	0.002529	-0.024474	0.694450	-0.029806
VBPI	0.335110	0.374745	-0.176035	0.094903	-0.338599	0.287480	0.201069	0.080072	-0.023886	-0.680122	-0.001216

13(b). OBSERVER 2

	EIGEN VALUE	DIFFERENCE	PROPORTION	CUMULATIVE
PRIN. 1	2.86983	1.23477	0.260893	0.26089
PRIN. 2	1.63506	0.11579	0.148642	0.40954
PRIN. 3	1.51928	0.31032	0.138116	0.54765
PRIN. 4	1.20896	0.18615	0.109906	0.65756
PRIN. 5	1.02281	0.20072	0.092983	0.75054
PRIN. 6	0.82209	0.22223	0.074735	0.82528
PRIN. 7	0.59986	0.12505	0.054533	0.87981
PRIN. 8	0.47481	0.10378	0.043165	0.92297
PRIN. 9	0.37103	0.04554	0.033730	0.95670
PRIN. 10	0.32549	0.17471	0.029590	0.98629
PRIN. 11	0.15078		0.013707	1.00000

EIGENVECTORS

	PRIN. 1	PRIN. 2	PRIN. 3	PRIN. 4	PRIN. 5	PRIN. 6	PRIN. 7	PRIN. 8	PRIN. 9	PRIN. 10	PRIN. 11
EPS	0.196646	-0.042327	0.386905	0.571939	-0.117035	0.282716	-0.428844	0.041036	-0.387321	-0.222320	-0.063794
EPI	0.196395	0.031487	0.458872	0.435319	-0.119255	-0.446092	0.380492	-0.190992	0.310458	0.240830	0.107316
NZ	0.102850	0.343441	-0.191239	0.374888	0.498450	0.518632	0.206536	0.138567	0.311122	0.124132	0.053498
AZAS	0.294777	-0.290166	0.342636	-0.261542	0.395918	-0.073226	-0.250927	0.176949	0.489731	-0.365966	-0.113799
AZAI	0.273739	-0.355458	0.274020	-0.266620	0.322035	0.256167	0.422702	-0.129968	-0.478670	0.230580	0.073177
AZPS	0.325362	-0.399759	-0.425419	0.184044	0.012956	-0.153268	-0.190076	0.128732	0.004916	0.088859	0.659202
AZPI	0.354263	-0.350923	-0.433141	0.205971	-0.100981	-0.022990	0.080473	-0.171271	0.067759	0.070979	-0.682019
VBAS	0.368472	0.212696	0.064496	-0.293878	-0.298641	0.345183	-0.309940	-0.523913	0.252090	0.261866	0.132121
VBAI	0.357622	0.100965	0.025367	-0.146909	-0.547256	0.220945	0.382762	0.534969	0.063966	-0.230173	0.040133
VBPS	0.354135	0.413240	-0.192573	-0.028225	0.187325	-0.266102	0.160141	-0.354874	-0.244919	-0.583525	0.089285
VBPI	0.359531	0.399454	0.014187	-0.135326	0.170411	-0.343967	-0.276046	0.402389	-0.235793	0.463766	-0.191077

13(c). OBSERVER 3

	EIGEN VALUE	DIFFERENCE	PROPORTION	CUMULATIVE
PRIN. 1	2.27303	0.578044	0.206639	0.20664
PRIN. 2	1.69498	0.094066	0.154089	0.36073
PRIN. 3	1.60092	0.216209	0.145538	0.50627
PRIN. 4	1.38471	0.354611	0.125883	0.63215
PRIN. 5	1.03010	0.182571	0.093645	0.72579
PRIN. 6	0.84753	0.237237	0.077048	0.80284
PRIN. 7	0.61029	0.096928	0.055481	0.85832
PRIN. 8	0.51336	0.055490	0.046669	0.90499
PRIN. 9	0.45787	0.143995	0.041625	0.94662
PRIN. 10	0.31388	0.040550	0.028534	0.97515
PRIN. 11	0.27333		0.024848	1.00000

EIGENVECTORS

	PRIN. 1	PRIN. 2	PRIN. 3	PRIN. 4	PRIN. 5	PRIN. 6	PRIN. 7	PRIN. 8	PRIN. 9	PRIN. 10	PRIN. 11
EPS	-0.062067	0.003497	0.517575	0.268555	0.323728	-0.417638	0.441282	0.356669	-0.193350	-0.125839	-0.041783
EPI	-0.021658	0.074648	0.468160	0.442054	0.260865	0.217493	-0.563652	-0.087679	0.342065	0.111951	-0.095317
NZ	-0.133471	0.451356	0.250267	-0.175857	0.003297	0.580887	0.488945	0.009129	0.215044	0.159569	0.191329
AZAS	0.455145	-0.033036	0.076457	-0.297066	0.367601	-0.117736	0.206084	-0.481715	0.341558	-0.283886	-0.277295
AZAI	0.450462	-0.164300	-0.017389	-0.255154	0.474118	0.091015	-0.142136	0.242618	-0.192526	0.419064	0.424106
AZPS	0.218024	0.477043	-0.302334	0.382266	0.094038	-0.126764	-0.036016	-0.060167	0.046747	-0.406775	0.538406
AZPI	0.346853	0.307350	-0.338619	0.394763	0.043452	0.067254	0.180046	0.076448	-0.133817	0.407128	-0.535160
VBAS	0.271021	-0.331533	0.253624	0.358982	-0.372315	0.021751	0.248951	-0.506636	-0.165726	0.231436	0.290972
VBAI	0.338997	-0.426363	-0.071493	0.189905	-0.197290	0.340257	0.138456	0.506152	0.356514	-0.322690	-0.028839
VBPS	0.363146	0.259967	0.351851	-0.190064	-0.251695	0.237066	-0.245545	0.059977	-0.550662	-0.352139	-0.173052
VBPI	0.282319	0.285117	0.211792	-0.212525	-0.464324	-0.475037	-0.103307	0.219479	0.409568	0.277582	0.063903

TABLE 14: EVALUATION OF AGREEMENT BETWEEN
NUCLEAR ZONE AND OVERALL MRI CATEGORY

The frequency matrix comparing grade and nuclear zone. The diagonal represents perfect agreement. When differences occurred, grade was usually assigned a higher value than nuclear zone.

		GRADE					
		1	2	3	4	5	
NZ	1	20	7	0	0	0	27
	2	1	153	18	3	0	175
	3	0	2	113	5	0	120
	4	0	0	6	39	0	45
	5	0	0	0	5	36	41
		21	162	137	52	36	408

OBSERVED AGREEMENT 0.9694
 EXPECTED AGREEMENT 0.7208
 KAPPA STATISTIC 0.8903

clustering along the diagonal indicated a high level of agreement which was confirmed by a Kappa statistic of 0.8903. The dependence of grade on nuclear zone suggested the other parameters may contribute to random error by interfering with the assignment of overall grade. The pattern of disagreement noted in Table 14 indicated that the other parameters frequently result in a higher grade being assigned to a disc. Recalculating kappa for nuclear zone showed improvement in interobserver agreement when compared to values obtained for grade (Table 15). These differences could not be evaluated statistically but suggest a revised classification scheme emphasizing the nuclear zone changes would help reduce observer variability. The stepwise discriminant analysis for the MRI indicated that grade be weighted by nuclear zone according to the equation

$$\text{Grade} = 0.90 \text{ NZ} + 0.33$$

Although no method for setting confidence limits on kappa has been established to indicate their significance, interobserver kappa values for grade assigned on this basis showed further improvement (Table 15). The improvement in kappa for Observers 3 versus 1 was the greatest, suggesting these observers were influenced to a greater degree by other parameters when deciding about overall grade.

Plots of grade against nuclear zone for individual observers produced linear relationships with differing slopes (Figure 37). These data suggest individual observers systematically interpret nuclear zone changes differently. The convergence of the lines at category 2 indicates that unanimity is likely for discs with this characteristic. However, the plots diverge, particularly for the higher grades, implying that observers are less likely to agree about category for older or more degenerate discs. Therefore,

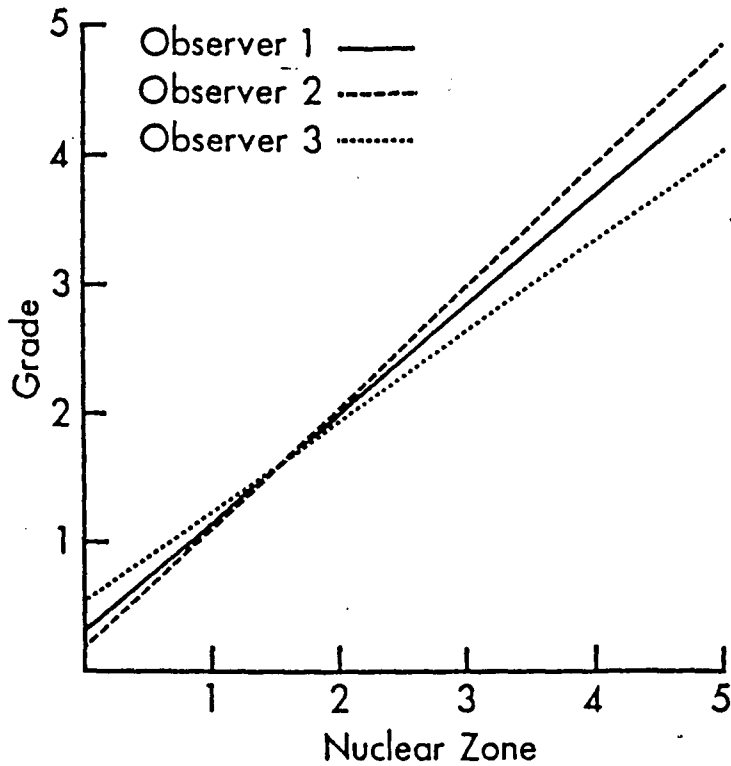
TABLE 15: INTEROBSERVER AGREEMENT FOR OVERALL MRI CATEGORY
NUCLEAR ZONE AND REGRESSION EQUATION

A comparison of kappa values for MRI observer pairs based on grade; nuclear zone and the equation derived by stepwise regression. Improvement in kappa values occur from left to right. For observer pairs 3 vs 1 this improvement was greatest.

OBSERVER PAIR	GRADE	NZ	$0.90NZ + 0.33$
1 vs 2	0.5020	0.5283	0.5480
2 vs 3	0.6970	0.7232	0.7322
3 vs 1	0.6146	0.6635	0.71805

FIGURE 37: PLOTS OF OVERALL MRI CATEGORY AND NUCLEAR ZONE BY OBSERVER

The intercepts and slopes of the first equation obtained by stepwise regression by observer. For each observer, nuclear was the first variable picked and accounted for more than 85 per cent of the variance. The differences between each observer emphasize the variation between observers except with MRI category 2 discs.



although redevelopment of the classification with increased emphasis on nuclear zone changes will reduce observer variability, education of observers by simple and succinct descriptions will be necessary to reduce systematic error.

Stepwise discriminant analysis indicated the classifications could distinguish five stages in the process of disc aging and degeneration. Nuclear zone parameters contributed the most to discriminatory function as expressed by Wilk's lambda (Tables 8 and 9). Because of concerns about using regression analysis on categorical data and data that is not necessarily normally distributed, the MRI data was further analyzed using CATMOD, a SAS procedure for analyzing categorical data. This test of homogeneity was used to evaluate the probability that nuclear zone grade selected at random would correspond to the same overall grade. This hypothesis, tested by the Pearson chi-square statistic, was significant to a probability level of 0.0001. On this basis, it was felt that the results obtained by regression analysis were not misleading. Further verification of this was provided by the MRANK procedure which tested non-parametrically the hypothesis about the relation between grade and nuclear zone. Spearman's rank correlation coefficient was significant to a level of 0.0001.

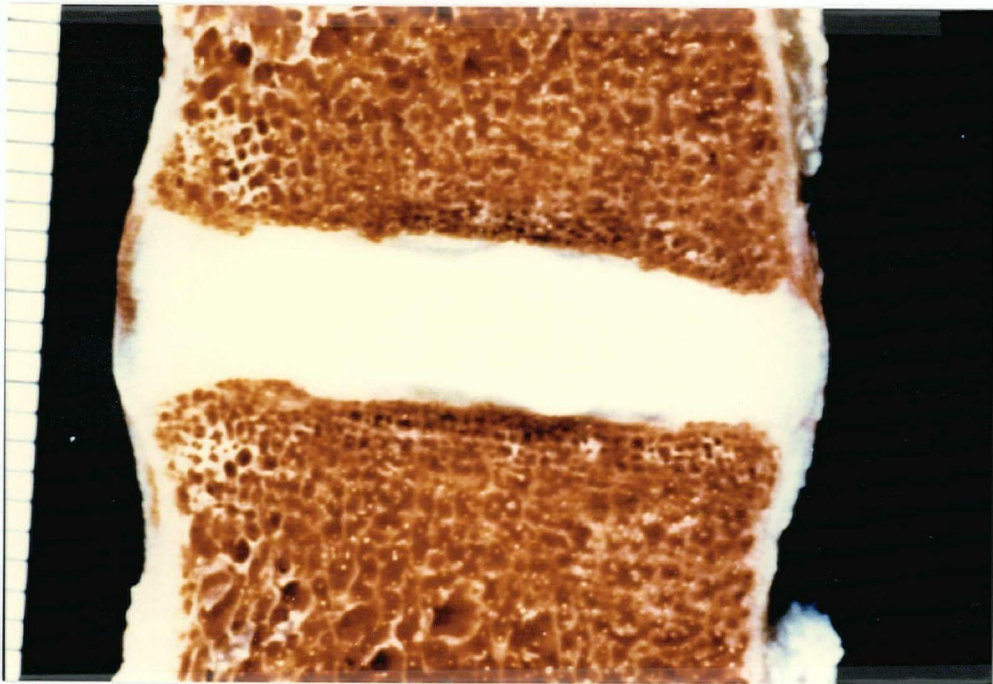
Although no 'gold standard' existed, the conformity of the two classifications with each other and with the chemical and histologic data indicated that the classifications were valid assessments of disc aging and degeneration. The kappa value of 0.6176 for comparison of the morphologic and MRI classifications represented a 'substantial' level of agreement (Table 12) and disagreements were usually within one category. This level of agreement provides MRI with a firm morphologic basis for interpretation. Examination of the frequency matrix suggests a possible explanation for the disagreements that occurred

between the two classifications (Table 12). At the lower end of the scale, MRI grades were consistently higher than morphologic grade, whereas at the upper end of the scale the opposite was seen. For example, MRI frequently portrayed a gross morphologic grade 1 disc as grade 2. This accounts for the skewing of grade distribution when one compares MRI and morphologic grades (Figure 36) and could be interpreted as a greater sensitivity of MRI for the detection of early degenerative changes. At the other end of the scale, the inability of MRI to recognize category 4 and 5 discs probably reflects its limited resolution. The changes observed in category 4 and 5 discs are principally structural and not chemical. Alternatively, the gross morphologic classification may not have sufficient sensitivity to detect subtle changes in morphology. The chemical and histologic data support the former hypothesis. When the chemical parameters, particularly chondroitin sulphate, were plotted as a function of MRI grade, there was a distinction between grades 1 and 2 not seen when these parameters were plotted as a function of morphologic grade (Figures 9-17). The nuclei of MRI grade 1 discs stained homogeneously and intensely with alcian blue (Figure 18) while the nuclei of some morphologic grade 1 discs - MRI grade 2 - had collagenous counterstained material extending centrally from the anulus (Figure 22). On gross inspection of the disc in Figure 24, these histochemical and light microscopic changes could not be anticipated (Figure 38). Because of the small number of specimens available for histologic and chemical examination, these trends could not be tested for statistical significance. However, the remaining discs are being analyzed to substantiate these trends.

The trends seen in the comparison of histologic and MRI appearances suggested that MRI is sensitive to changes in extracellular matrix composition. With increasing grade, there was an apparent reversal in the MRI image. For

FIGURE 38: GROSS MORPHOLOGY OF AN MRI CATEGORY 2
AND MORPHOLOGIC CATEGORY 1 DISC

By MRI and morphologic criteria, this disc was assigned an overall category of 2 (Figure 24) and 1 respectively. The histochemical preparation (Figure 22) confirms the presence of changes (i.e. collagen) within the nucleus not apparent in the gross morphology.

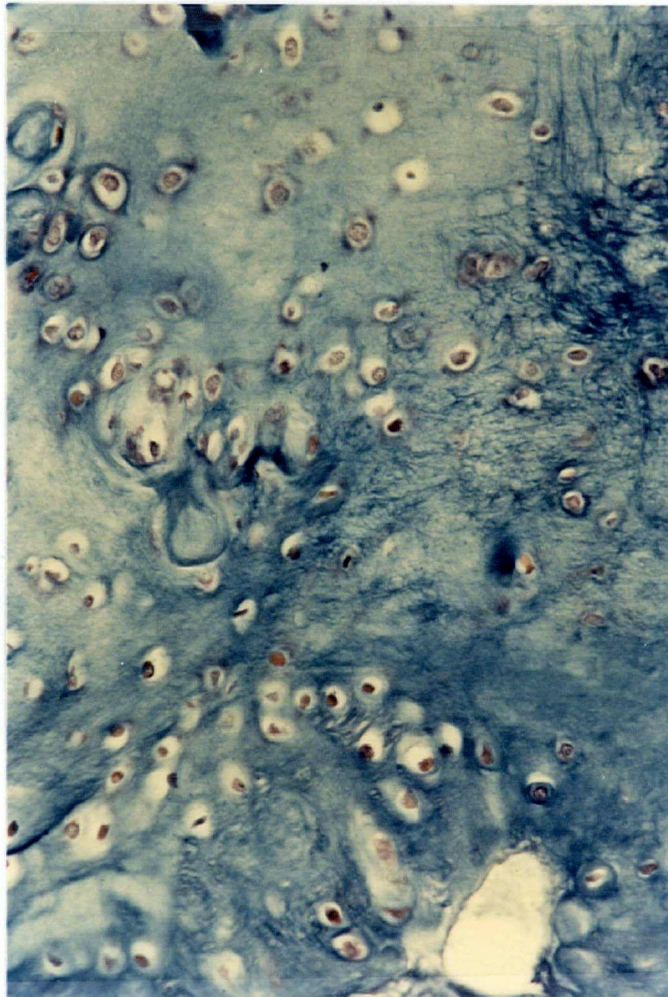


grades 1 to 3, the brightness of the nuclear signal progressively decreased. In grades 4 and 5, the brightness increased particularly near the endplate. This phenomenon, a loss and then subsequent gain in bright signal, has not been described previously in the literature. Direct comparison with the histology indicated that in the higher grade discs, bright signals corresponded to cellular regions with alcianophilic staining matrix (Figures 32, 35 and 39). Dark signals corresponded either to areas rich in collagenous fibers or to macroscopic clefts (Figure 39). Although sensitive to extracellular matrix composition, the in-plane resolution of 1 mm and volume averaging approximately 8 mm limited the morphologic detail provided by MRI. This may account for the apparent lack of MRI sensitivity to structural changes in morphologic grade 4 and 5 discs.

This research suggests MRI is sensitive to extracellular matrix composition. Until recently, the radiographic technique of choice for obtaining clinical information about disc degeneration is contrast discography (Adams, Dolan, & Hutton, 1986). Comparison of this 'gold standard' with MRI suggested that MRI was more accurate (Gibson et al, 1986). This research demonstrating the agreement between gross morphology and MRI as well as the histologic and chemical trends observed support this suggestion. However, as a potential diagnostic technology, further clinical evaluation is required (Guyatt et al, 1986). This work and that outlined previously have established technologic capability of MRI, the possible uses and accuracy of MRI such as the detection of clinically important changes in the disc. However, impact on health care providers, therapeutic impact and impact on patient outcome require evaluation. These criteria are unlikely to be assessed here until a clinical MRI unit is established in one of the U.B.C. teaching hospitals.

FIGURE 39 ALCIAN BLUE STAINED SECTION OF AN MRI CATEGORY 5 DISC

High power (320x) examination of the alcian blue stained section of a disc from an 89-year-old female (Figure 32) showing the tissue features of the bright signal seen in the MRI image (a). The cellular nature and alcianophilic territorial matrix is distinct from regions generating dark signals.



The overlap between grades seen in the chemical data may, as previously described, represent limitations of the techniques used. Alternatively, the overlap may reflect heterogeneity of disc composition or inappropriate categorizations with respect to number and separation. The heterogeneity of disc tissue, particularly in grades 3 to 5, was apparent from the histochemical, histologic and MRI evaluations. This is the more likely explanation for the overlap. Since chemical analyses are a volume average, localized differences in composition will necessarily be obscured. Despite this, the trends seen indicate a relationship presently poorly understood. For most parameters either trends or sharp breaks occurred despite the range of values. Thus, the grading schemes appear to distinguish meaningful categories of composition.

The histologic data presented represents untested personal observation. The trends described were consistent with those described in Section 1.4.1. Although this supports these observations, statistical evaluation would require a research plan like that used to evaluate the morphologic classification. Histologic preparation of the remaining specimens will be undertaken. Cooperation of individuals interested in the histologic examination of the disc would permit statistical evaluation of the histologic changes with grade and the correlation of histology to the MRI.

4.4 SUMMARY

In the classifications proposed, consistency, ability to distinguish stages in the process of disc aging and degeneration and conformity with other methods of assessment make them an acceptable and workable means of quantifying disc aging and degeneration. Establishing these classifications will improve reporting, communication and cooperation between investigators. An improved

understanding of disc degeneration and its role in low back pain would undoubtedly result. Refinement of these classifications with emphasis on nuclear zone changes and improved education should reduce observer variability. MRI appears sensitive to changes in extracellular matrix composition and should provide investigators with a reliable and accurate means of assessing the disc in vivo.

4.4.1 CONCLUSIONS

- 1) Valid morphologic and MRI classifications of intervertebral disc aging and degeneration are presented.
- 2) MRI is a sensitive method of detecting early changes in disc composition.
- 3) Dark signals in the MRI image correspond to collagen-rich regions of the disc or macroscopic clefts. For example, the 'intranuclear cleft' reported in the literature represents a localized collection of collagen-rich matrix in the nucleus pulposus.
- 4) Bright signals correspond to areas with alcianophilic extracellular matrix.
- 5) In terms of spatial resolving power histology > MRI= gross morphology > chemistry.

REFERENCES

- Adam, M., Deyl, Z. (1984) Degenerated annulus fibrosus of the intervertebral disc contains collagen type II. *Ann. Rheum. Dis.* 43:258-263.
- Adams, M.A., Hutton, W.C. (1983) The effect of fatigue on the lumbar intervertebral disc. *J. Bone Joint Surg. [Br]* Mar; 65(2):199.
- Adams, M.A., Muir, H. (1976) Qualitative changes with age of proteoglycans of human lumbar discs. *Ann. Rheum.* 35:289.
- Adams, P. (1976) Age related changes in Proteoglycan of the intervertebral disc. *Ann. Rheum. Dis.* Apr. 35(2):289.
- Adams, P., Muir, H. (1976) Qualitative changes with age of proteoglycans of human lumbar discs. *Ann. Rheum. Dis.* 35:289-296.
- Adams, P., Eyre, D.R., Muir, A. (1977) Collagen of the human annulus fibrosus. *Rheumatol. Rehabil.* 35:289.
- Aguila, L.A., Pirdino, D.W., Modic, M.T., Dudley, A.W., Weinstein, M.A. (1985) The intranuclear cleft of the intervertebral disk. *Radiology* 155:155-158.
- B.C. Hospital Services Commission, D.A. Bolton, Research Officer Hospital Programmes, Victoria, B.C.
- Berk, R.A. (1979) Generalizability of behavioural observations:
A. Clarification of interobserver agreement and interobserver reliability. *Am. J. Mental Def.* 83:460-472.
- Bitter, T., Muir, H. (1962) A modified uronic acid carbazole reaction. *Anal. Biochem.* 4:330-334.
- Bogduk, N. (1983) The innervation of the lumbar spine. *Spine* 8(3):286.
- Bombardier, C., Tugwell, P. (1982) A methodological framework to develop and select indices for clinical trials. *J. Rheum.* 9:753-757.
- Broom, A. (1955) Paths of nutrition in intervertebral disc. *Acta. Orthop. Scand.* 24:177-180.
- Brown, M.D. (1977) The pathophysiology of disc disease. *Orthop. Clin. N. Am.* 2(2):359.
- Brown, M. (1982) Pathology of lumbar disc disease. *The Spine Vol. 2.*
Edited by R. Rothman, Philadelphia J.B. Lippincott. p.510.

- Brown, M.A., Tsaltas, T.T. (1976) Spine 1:240-244.
- Bywaters, E.G.L. (1980) Aging and degenerative disease in the spine. The Joints and Synovial Fluid. Edited by Gardner, D.C. New York Academic Press.
- Buckwalter, J.A. (1980) Fine structure of the human intravertebral disc. American Academy of Orthopaedic Surgeons Symposium on Low Back Pain. Edited by J. Kelsey, A. White. C.V. Mosby Philadelphia.
- Budinger, T.F., Lauterbur, P.C. (1984) Nuclear magnetic resonance technology for medical studies. Science 426:288-298.
- Bywaters, E.G.L. (1980) Disc degeneration. American Academy of Orthopaedic Surgeons Symposium on Low Back Pain. Edited by J. Kelsey, A. White C.V. Mosby Philadelphia.
- Chaffetz, N.I., Genant, H.K., Moon, K.L., Helms, C.A., Morris, J.M. (1983) Recognition of lumbar disc herniation with NMR. Am. J. Radiol. 141.
- Cicchetti, D.V. (1976) Assessing inter-rater reliability for rating scales. Br. J. Psychiatr. 129:452-456.
- Cicchetti, D.V., Fleiss, J.L. (1977) Comparison of the null distributions of weighted kappa and the C ordinal statistic. Applied Psych. Meas. 1: 195-201.
- Cicchetti, D.V., Fleiss, J.L. (1978) Inference about weighted kappa in the non-null case. Applied Psych. Meas. 2:113-117.
- Copius Peereboom, J.W. (1970) Gerontologie 16:352.
- Copius Peereboom, J.W. (1973) Histochemie 37:119.
- Coventry, M.B. (1945) The intervertebral disc: Its micro anatomy. J. Bone Joint Surg. 27:105-112.
- Culling, C.F.A. (1963) Handbook of histopathologic techniques. Butterworths, London.
- Difabio, J., Pearce, R.H., Caterson, B. (1987) Three non-aggregating proteoglycans of the human intervertebral. Trans. Ortho. Res. Soc. 12:296.
- Dickson, I.R. et al. (1967) Nature 215:50.
- Eyre, D.R., Muir, A. (1977) Quantitative analysis of types I and II collagens in human intervertebral discs at various ages. Biochim. Biophys. Acta 492:29-42.

- Eyre, D.R., Muir, A. (1976) Types I and II collagens in intervertebral disc. *Biochem. J.* 157:267-270.
- Eyre, D.R. (1980) Biochemistry of the intervertebral disc. *International Review Connective Tissue Research*. Vol.8. D.A. Hall, D.S. Jackson (Eds). New York Academic Press: 227-291.
- Farfan, A.F. (1972) Tear pattern and geometry in the annulus fibrosus. *J. Bone Joint Surg.* [AM] 54A:492.
- Feder, N., Sidman, R.L. (1958) Methods and principles of fixation by freeze substitution. *J. Biophysic. Biochem. Cytol.* 4:593-599.
- Feinstein, A.R. (1985) *Clinical epidemiology*. W.B. Saunders, Philadelphia, PA.
- Friberg, S., Hirsch, C. (1949) Anatomical and clinical studies on lumbar disc degeneration. *Acta Orthop. Scand.* 19:222.
- Gardner, D.C. (1965) Disorders of the connective tissue of the intervertebral disc. *Pathology of the connective tissues*. Arnold Press, London.
- Gower, W.E., Pedrini, V. (1969) Age related variations in protein-polysaccharides from human nucleus purposus, annulus fibrosus and costal cartilage. *J. Bone Joint Surg.* 51A:1154.
- Han, J.S, Kaufman, B., El Yousef, S.J., Benson, J.E., Bonstelle, C.T., Alfidí, R.J., Haaga, J.R., Yeung, H., Huss, R.G. (1983) NMR imaging of the spine. *Am. J. Radiol.* 141: 1137-1145.
- Hardingham, T.E., Ewins, R.J.F., Muir, A. (1976) Proteoglycan of the intervertebral disc. *Biochem. J.* 157:127.
- Hardingham, T.E., Adams, P. (1976) A method for determination of hyaluronate in the presence of other glycosaminoglycans and its application to human intervertebral disc. *Biochem. J.* 159:143-147.
- Harris, R.I., MacNab, I. (1954) Structural changes in lumbar intervertebral discs. *J. Bone Joint Surg.* [Br] 36B:304.
- Hassler, O. (1970) *Acta Orthop. Scand.* 40:765.
- Higuchi, M., Kaneda, K. (1983) Changes in the intervertebral disc in bipedal mice. *Clin. Orthop.* 175:251.
- Hilton, R.C., Ball, J. (1984) Vertebral rim lesions in the dorsolumbar spine. *Ann. Rheum. Disease* 43:302-307.
- Hirsch, C. (1952) Structural changes in the annulus fibrosus. *Acta Orthop. Scand.* 22:184.

- Hirsch, C. (1953) Studies in the mechanics of low back pain. Acta Orthop. Scand. 22:184.
- Hirsch, C. (1963) The anatomical basis for low back pain. Acta Orthop. Scand. 33:1-17.
- Jackson, H.C. (1966) Nerve endings in the human lumbar spinal column and related structures. J. Bone Joint Surg. [AM] 48A:1272.
- Keiffer, S.A. (1969) Discographic anatomical correlations of developmental changes with age in the intravertebral disc. Acta Rad. 9:733-739.
- Keith, D.A., Paz, M.A, Glimcher, M.J. (1977) J. Histochem. Cytochem. 25:1154.
- Kellgran, J.H. (1977) The anatomical source of back pain. Rheum. Rehab. 16:3.
- Kelsey, J.L. (1980) Epidemiology of low back pain. American Academy of Orthopaedic Surgeons Symposium on Low Back Pain. C.V. Mosby, Philadelphia.
- Kelsey, J.L., White, A.A. (1980) Epidemiology and impact of low back pain. Spine, 5(2):133.
- Kiernan, J.A. (1981) Histological and histochemical methods. Pergamon Press, Toronto.
- Kirkaldy-Willis, W.H. (1983) Managing low back pain. Churchill Livingstone, New York.
- Kirkaldy-Willis, W.H. (1984) The spine integrated function and pathophysiology. Adult Orthopaedics. Edited by R.L. Cruess and W.J. Rennie. Churchill Livingstone, New York.
- Kirshner, B., Guyatt, G. (1985) A methodologic framework for assessing health indices. J. Chron. Dis. 38:27-36.
- Kleinbaum, D.G., Kupper, L.L. (1978) Applied regression analysis and other multivariable methods. Duxbury Press, Boston, Mass.
- Knutson, F. (1944) The instability associated with disc degeneration in the lumbar spine. Acta Radiologica Vol. XXV.
- Koran, L.M. (1975) N. Eng. J. Med. 293:642 and 293:695.
- Kramer, M.S., Feinstein, A.R. (1981) Clinical biostatistics LIV. The Biostatistics of Concordance. Clin. Pharmacol. Ther. 29:111-123.
- Landis, J.R., Koch, G.B. (1977) The measurement of observer agreement for categorical data. Biometrics 33:159-174.

- Langman, J. (1975) Medical Embryology. Williams and Wilkins, Baltimore, Md.
- Last, J. (1966) Anatomy. Lea and Febiger, Toronto.
- Levin, T. (1964) Osteoarthritis in lumbar synovial joints. Acta Orthop. Scand. (Suppl.) 73.
- Liche, R.D. (1965) Histopathologic technique and practical histochemistry. McGraw-Hill, New York.
- Lipson, S.J., Muir, H. (1980) Vertebral osteophyte formation in experimental disc degeneration. Morphologic and proteoglycon changes over time. Arthr. Rheum. 23(3):319.
- Lipson, S.J., Muir, H. (1981) Proteoglycans in experimental intervertebral disc degeneration. Spine 6:194-210.
- Lipson, S.J., Muir, H. (1981) Experimental intervertebral disc degeneration: morphologic and proteoglycan changes over time. Arthr. Rheum. 24:12.
- MacNab, I. (1977) Backache. Williams and Wilkins, Baltimore, Md.
- MacNab, I. (1956) Vertebral lipping in the lumbar spine. J. Bone Joint Surg. 38A 927-928.
- Maravilla, K.R., Lesh, P., Weinreb, J.C., Selby, D.K., Mooney, V. (1985) Magnetic resonance imaging of the lumbar spine with CT correlation. Am. J. Neuroradiol. 6:237-245.
- McGill, C.M. (1968) Industrial back problems. J. Occup. Med. 10:174-178.
- Mikhael, M.A., Ciric, I.S., Kudrna, J.C., Hindo, W.A. (1985) Recognition of lumbar disc disease with magnetic resonance imaging. Computerized Radiol. 9(4):213-222.
- Milgram, J.W. (1982) Osteoarthritic changes at the severely degenerated disc in humans. Spine 7(5):498.
- Mixter, W.T., Barr, J.S. (1934) Rupture of the intervertebral disc with involvement of the spinal cord. N. Eng. J. Med. 211:210-215.
- Modic, M.T., Weinstein, M.A., Pavlicek, W., Boumpfrey, F., Starnes, D. (1983) Magnetic resonance imaging of the cervical spine. Am. J. Radiol. 141:1129-1136.
- Modic, M.T., Paulicek, W., Weinstein, M.A., Boumpfrey, F., Ngo, F., Hardy, R. (1984) Magnetic resonance imaging of intervertebral disk disease. Radiology 152:103-111.
- Mooney, V. (1983) The syndromes of low back disease. Ortho. Clin. North Am. 14(3):491.

- Moses, L.E., Emerson, J.D., Hossein, H. (1984) Analyzing data from ordered categories. N. Eng. J. Med. 311:442-448.
- Nachemson, A. (1965) Loading of the lumbar spine. Acta Orthop. Scand. 33:104.
- Nachemson, A. (1966) The load on lumbar discs in different positions of the body. Clin. Orthop. 45:107.
- Nachemson, A., Elfstrom, G. (1970) Intravital dynamic pressure measurements in lumbar discs. Scand. J. Rehabil. Med. Supp. 1.
- Nachemson, A. (1975) The role of degenerative disc disease in low back pain. Spine 1(1):59.
- Nachemson, A. (1976) The lumbar spine, an orthopaedic challenge. Spine 1:59-71.
- Nachemson, A. (1984) Variation in the nutrition of canine intervertebral disc induced by motion. Spine 8(8):866.
- National Center for Health Statistics (1973) Limitation of activity due to chronic conditions, United States 1969 and 1970. Series 10, No. 80.
- Naylor, A. (1977) The biochemical changes in the human intervertebral disc in degeneration and nuclear prolapse. Orthop. Clin. N. Am. 2(2):343.
- Norman, D. et al. (1983) Magnetic resonance imaging of the spinal cord and canal. Am. J. Radiol. 141:1147-1152.
- Park, W.M. (1980) The place of radiology in the investigation of low back pain. Clin. Rheum. Dis. 6(1):93-132.
- Park, W. (1980) The role of radiography in low back pain. Clin. Rheum. Dis. 6:93.
- Parke, W., Schiff, D. (1977) The applied anatomy of the intervertebral disc. Orthop. Clin. N. Am. 2(2):309.
- Peacock, J. (1952) Nerve supply to the lumbar spine. J. Anat. 86:162.
- Pearce, R.H., Grimmer, B.J. (1986) Degeneration and the chemical composition of the human intervertebral disc. Proc. Orthop. Res. Soc. 32:211.
- Pearce, R.H., Grimmer, B.J. (1976) Biochem. J. 157:753.
- Pearse, A.G.E. (1968) Histochemistry. Little, Brown and Co., Boston.
- Pech, P., Haughton, V.M. (1985) Lumbar intervertebral disc: correlative MR and anatomic study. Radiol. 156:699-701.

- Pedrini, V.A., Ponseti, I.V. (1973) Glycosaminoglycans of the intervertebral disc. *J. Lab. Clin. Med* 82:938-950.
- Pedrini, V.A., Pedrini-Mille, V. (1979) Proteoglycans of the intervertebral disc. *Trans. Orthop. Res. Soc.* 2:18.
- Pritzker, K.P.H. (1977) Aging and degeneration in lumbar intervertebral discs. *Orthop. Clin. N. Am.* 8(1):65.
- Rothman, R., Simeone, L. (1982) *Spine*. J.B. Lippincott, Philadelphia, PA
- Rothman, R. (1970) *The intervertebral disc*. W.B. Saunders Co., Philadelphia, PA
- Rowe, M.R. (1969) Low back pain in industry. A position paper. *J. Occup. Med.* 11:161-169.
- Schmorl, G., Yunghanns, H. (1971) *Pathologic anatomy of the intervertebral disc in the human spine in health and disease*. Grune and Stratton, New York.
- Scott, T.A., Melvin, E.A. (1953) Anthrone method for hexoses. *Anal. Chem.* 25:1656-1661.
- Senneck, C.D. (1985) The anatomy of lumbar spondylosis. *Clin. Orthop.* 193:20.
- Snedecor, G.W., Cochran, W.G. (1980) *Statistical methods*. Iowa State University Press. Ames, Iowa.
- Sorce, D. (1984) Non-collagenous protein of the intervertebral disc. *Trans. Orthop. Res. Soc.*
- Spengler, D.M. (1982) *Low back pain*. Grune and Stratton, New York.
- Stevens, R.L., Muir, H. (1979) Proteoglycans of the intervertebral disc. *Biochem. J.* 179:561-578.
- Sweeny, P.R., Pearce, R.H., Vance, H.G. (1963) The chemical anatomy of rat skin. *Can. J. Biochem.* 41:2307-2326.
- Thompson, S.W. (1966) *Selected histochemical and histopathologic techniques*. Charles C. Thomas, Springfield.
- Tugwell, P., Bombardier, C. (1982) A methodologic framework for developing and selecting endpoints in clinical trials. *J. Rheum.* 9:758-762.

- Urban, J., Maroudas, A. (1979) Measurement of fixed charge density in the intervertebral disc. *Biochem. Biophys. Acta* 586:166-178.
- Urban, J., Maroudas, A. (1980) The chemistry of the intervertebral disc in relation to its physiological function and requirements. *Clin. Rheum. Dis.* 6:51-76.
- Vernon-Roberts, B. (1977) Degenerative changes in intervertebral discs. *Rheum. Rehab.* 16:13.
- Vernon-Roberts, B. (1981) Pathology of intervertebral disc disease. Low back pain. Edited by M.I.V. Jayson.
- Vernon-Roberts, B. (1984) Vertebral rim lesions in the dorsolumbar spine (letter). *Ann. Rheum. Dis.* 43(4):662.
- Vernon-Roberts, B. (1986) Personal communication.
- Wiberg, G. (1949) Back pain in relation to the nerve supply of the intervertebral disc. *Acta Orthop. Scand.* 19:211.
- Woessner, J.F. (1961) The determination of hydroxyproline in tissue and protein samples containing small proportions of this imino acid. *Arch. Biochem. Biophys.* 93:440-447.
- Wu, A.C., Yao, R.F. (1976) Mechanical properties of intervertebral disc annulus fibrosus. *J. Biomech.* 9:1.

APPENDIX 1

A. DESCRIPTION OF MORPHOLOGIC CLASSIFICATION SCHEDULE

GRADE I

- NUCLEAR ZONE The tissue is gel-like and bulging. It is bluish-white in colour. The demarcation from anulus is distinct.
- ANULAR ZONE The tissue is organized into discrete lamellae. It is white in colour. The demarcation from nucleus is distinct.
- ENDPLATE The cartilaginous portion is smooth, 1mm thick and hyaline in appearance. The subchondral plate is smooth with a slightly concave contour. Schmorl's nodes (vertical herniations) may be seen.
- VERTEBRAL BODY The margins of the vertebral body are smooth and rounded.

GRADE II

- NUCLEAR ZONE The tissue appears to be semi-gelatinous. Yellow pigmentation can be seen. The demarcation from anulus is less distinct.
- ANULAR ZONE Chondroid or mucinous material can be seen between the inner lamellae. The remaining lamellae are white. Tears, running perpendicular to the lamellae, may be seen between the junction of the anulus and vertebral body. The demarcation from nucleus is less distinct.
- ENDPLATE Focal and diffuse thinning of the cartilage is apparent. The subchondral plate is smooth and may have a more pronounced concave contour.
- VERTEBRAL BODY The margins of the body are slightly pointed.

GRADE III

- NUCLEAR ZONE The tissue is consolidated. Yellow to brownish pigmentation can be seen. The demarcation from anulus is indistinct. Focal gaps and defects are present within the tissue.

ANULAR ZONE Chondroid or mucinous material can be seen between the inner and outer lamellae. Uninvolved lamellae are white. A relative widening of the anular zone is apparent. The demarcation from nucleus is indistinct. Focal gaps and defects, particularly between lamellae, may be seen.

ENDPLATE Thinning of the cartilage is apparent and focal defects extending to the subchondral plate are present. The contour of the subchondral plate is undulating. Steps, defects and doubling of the subchondral plate may be seen.

VERTEBRAL BODY Cartilaginous or compact bony lipping of the margins of the body can be seen.

GRADE IV

NUCLEAR ZONE The tissue is consolidated and brown. Clefts extend through the tissue parallel to the endplate and may extend into the anular zone. Traces of glistening white tissue can be seen lining the clefts.

ANULAR ZONE The lamellar structure is less distinct. Yellow to brown pigmentation can be seen. Focal gaps and defects are more apparent. Clefts from the nucleus may extend into the inner anular zone.

ENDPLATE White tissue extending from the subchondral bone through cartilage defects may be seen. The contour of the subchondral plate is irregular. Focal sclerosis may be seen.

VERTEBRAL BODY Marrow filled osteophytes project less than 2mm from the vertebral body margin.

GRADE V

NUCLEAR ZONE Tissue loss with loss of disc space height is apparent. Clefts extending through the nuclear and anular zone are present. Glistening white tissue lining the clefts is more prominent. The remaining tissue is deeply pigmented.

ANULAR ZONE Lamellae are indistinct. Clefts may extend through the entire anular zone. The remaining tissue bulges outwards.

ENDPLATE White tissue extending from the subchondral bone is more apparent. The subchondral plate is thickened and sclerotic.

VERTEBRAL BODY Marrow filled osteophytes extend 2mm or more beyond the margin of the vertebral body.

B. DESCRIPTION OF MRI CLASSIFICATION SCHEDULE

GRADE I

NUCLEAR ZONE The signal from the nuclear tissue is homogeneous and bright. The demarcation between anulus and nucleus is distinct.

ANULAR ZONE The anular tissue generates a homogeneous dark gray signal distinct from that of the nucleus.

ENDPLATE The region of the cartilaginous and bony endplate appears as a single dark line which clearly demarcates the marrow cavity from nucleus tissue except where Schmorl's nodes exist.

VERTEBRAL BODY The contour of the vertebral body margin is smooth and rounded with no projections.

GRADE II

NUCLEAR ZONE Overall the signal intensity remains bright but a distinct gray tone within the nuclear tissue is seen. This gray tone often appears as a horizontal band or cleft within the nuclear zone. This gray tone may also be seen in the anular zone thereby making the demarcation of anulus and nucleus less distinct.

ANULAR ZONE The signal intensity from anular tissue may be increased by the presence of a lighter gray tone. This gray tone is contiguous with that in the nuclear zone. Areas of relatively dark signal intensity may be seen in the anulus where the inner anulus meets the endplate.

ENDPLATE The contour of the dark line is smooth and distinct with a slight concavity.

VERTEBRAL BODY No distinct projections from the vertebral body can be seen but the margins of the body are tapered and slightly pointed.

GRADE III

NUCLEAR ZONE The overall signal intensity is diminished to a light gray tone. A stippling of brighter and darker signals can be seen on this gray background. The demarcation of anular and nuclear tissue is indistinct.

ANULAR ZONE The gray anular signal intensity is indistinguishable from that of the nucleus. Areas of dark signal intensity within the anulus can be seen where it meets the endplate. These areas are readily identified anteriorly.

ENDPLATE The dark line is less distinct in focal areas. The line has a more concave contour.

VERTEBRAL BODY Projections from the margins of the body may be seen. The signal intensity of the projections may be gray or dark and is distinct from that of the marrow.

GRADE IV

NUCLEAR ZONE The quantity of gray signal is diminished. Areas of bright and dark signal intensity are larger and more apparent.

ANULAR ZONE The quantity of gray signal is decreased. The bright and dark signals may be contiguous with those seen in the nuclear zone.

ENDPLATE Focal defects of variable size can be seen in the dark line.

VERTEBRAL BODY Projections from the body exhibit a signal intensity similar to marrow. These projections extend less than 2 mm beyond the margins of the body.

GRADE V

NUCLEAR ZONE Bright and dark signal intensities dominate. Gross loss of disc space height is apparent.

ANULAR ZONE The bright and dark signal intensities seen are contiguous with those seen in the nuclear zone. Loss of disc space height and anular bulging is apparent.

ENDPLATE Defects in the line are readily seen. Diminished signal intensity of the marrow adjacent to the line makes the line appear thicker.

VERTEBRAL BODY Projections from the body exhibit a signal intensity similar to marrow. These projections extend more than 2 mm beyond the margins of the body.

APPENDIX 2

OUTLINE OF PARAMETERS AND INSTRUCTIONS TO OBSERVERS

A. MORPHOLOGIC

1. Assign each disc a grade based on overall impression.
2. Examine each zone indicated in Figure 1. Assign a number to that zone for each parameter (as indicated below).
3. Use the examples derived from discs I-V as a guide.
4. Because the parameter items are attempting to categorize a spectrum of findings, the items (numbers) will not always perfectly match with what you see.
5. Choose the item which most closely approximates what you see.
6. When the choice between two items is equivocal, choose the item with the highest numerical value.

PARAMETERS

Zone Parameter

Annular	Tissue integrity	
	Intact	1
	Tearing at the junction of the anulus and the vertebral body.....	2
	Cleft(s), parallel to the endplate, extending from the nucleus to the inner anulus	3
	Cleft(s), parallel to the endplate, extending from the nucleus to the outer anulus	4
	Gross disruption	5
	Tissue morphology	
	Discrete lamellae	1
	Chondroid or mucinous material between lamellae	2
	White glistening tissue lining clefts, remainder of tissue as in (1) (Red=r)	3
	White glistening tissue lining clefts, remainder of tissue as in (2) (Red=r).....	4
	Amorphous tissue lining clefts only	5

Osteophytes		
	Margin of vertebral body smooth and rounded	1
	Margin of vertebral body pointed	2
	Cartilaginous or compact bony lipping	3
	Marrow filled osteophytes \leq 2 mm.	4
	Marrow filled osteophytes \geq 2 mm.	5
Endplate	Cartilage	
	Smooth, thickness 1 mm.	1
	Focal or diffuse thinning	2
	Focal defects extending to subchondral plate	3
	Diffuse cartilage loss	4
	Total cartilage loss	5
	Subchondral	
	Smooth contour with slight concavity	1
	Smooth contour with distinct concavity	2
	Irregular contour	3
	Focal sclerosis or doubling of the endplate	4
	Diffuse sclerosis	5
Nuclear	Tissue Integrity	
	Intact	1
	Focal gaps and defects	2
	Clefts parallel to endplate (confined to nuclear zone) ...	3
	Diffuse clefting (extending to anular zone)	4
	Gross disruption with disc space collapse	5
	Tissue morphology	
	Gel-like, bulging	1
	Semi-gelatinous	2
	Consolidated	3
	Consolidated with amorphous tissue lining clefts (color varies from white - red)	4
	Amorphous tissue only	5

B. MRI

1. Assign each disc a grade based on overall impression.
2. Examine each zone indicated in Figure 1. Assign a number to that zone for each parameter (as indicated below). Choose the item (number) which best describes each parameter.

PARAMETERS

ENDPLATE	a distinct dark line with a smooth and slightly concave contour	1
	a distinct dark line with a more concave contour ..	2
	the dark line is irregular in contour and less distinct in focal areas	3
	focal defects in the dark line make the demarcation of marrow and nucleus indistinct in the areas where defects occur	4
	diminished signal intensity from the marrow adjacent to the dark line makes the line appear thicker	5
NUCLEAR ZONE	a bright, homogeneous signal	1
	the bright signal is interrupted by a gray signal in the form of a horizontal band or cleft	2
	the background signal is gray with a stippling of focal bright and dark signals	3
	the gray background signal is diminished in quantity, the bright and dark signals are larger ..	4
	bright and dark signals dominate, loss of disc space height is apparent	5
ANULAR ZONE	a homogeneous, dark gray signal	1
	a zone of dark signal intensity may be seen where the inner anulus meets the endplate	2
	the gray signal of the nucleus and anulus is indistinct, the zone of dark signal intensity at the junction of anulus and endplate is more apparent	3
	bright and dark signals extend between anulus and nucleus	4
	bright and dark signals extend between anulus and nucleus, loss of disc space height and anular bulging are seen	5

VERTEBRAL BODY	margins of the body are smooth and rounded	1
	margins of the body are tapered and slightly pointed	2
	projections from the body margins of gray to dark signal intensity are seen	3
	projections with signals of intensity similar to marrow are seen and measure less than 2 mm	4
	as in 4 but measure more than 2 mm	5

MORPHOLOGY RECORDING FORM

Disc _____ Grade _____

<u>Zone</u>	<u>Parameter</u>				
Anular	Tissue integrity	ASAZ _____	AIAZ _____	PSAZ _____	PIAZ _____
	Tissue morphology	ASAZ _____	AIAZ _____	PSAZ _____	PIAZ _____
	Osteophytes	ASAZ _____	AIAZ _____	PSAZ _____	PIAZ _____
Endplate	Cartilage	SEP _____	IEP _____		
	Subchondral	SEP _____	IEP _____		
Nuclear	Tissue integrity	NZ _____			
	Tissue morphology	NZ _____			

MRI RECORDING FORM

DISC

GRADE

PARAMETER

ZONE

ENDPLATE

SEP _____

IEP _____

NUCLEAR ZONE

NZ _____

ANULAR ZONE

ASAZ _____

A1AZ _____

PSAZ _____

PlAZ _____

VERTEBRAL BODY

ASAZ _____

A1AZ _____

DSAZ _____

D1AZ _____

APPENDIX 3

Hematoxylin and Eosin (Culling, 1963)

- 1) Deparaffinization by 5 minutes each in xylene I, xylene II, abs. ethanol, 95% (v/v) ethanol, 70% ethanol and tap water, gently agitating (dipping) with each solution,
- 2) 8 minutes in hematoxylin (Edward Gurr).
- 3) 6 dips (approximately 10 seconds) in 0.1% (v/v) HCl in abs. ethanol.
- 4) 5 min. in tap water.
- 5) 30 sec., constantly dipping, in LiCO_3 .
- 6) 5 min. in tap water.
- 7) 8 min. in 2% (w/v) eosin (Fisher) in 70% (v/v) ethanol.
- 8) 2 dips each in 95% (v/v) ethanol I, 95% (v/v) ethanol II, absolute ethanol I, absolute ethanol II, xylol I and xylol II.
- 9) 5 min. in xylene

Alcian Blue (Keirnan, 1981)

- 1) Deparaffinization as in Step (1) for H. and E.
- 2) 30 min. in Alcian Blue 8GX [1.0g in 100ml 0.1 M HCl] (N.A. Scientific).
- 3) 3 min. in tap water.
- 4) 6 min. in acid fuchsin (Edward Gurr).
- 5) dist. water rinse and then dehydrate as in steps 8) and 9) of H. & E.

Mallory's Trichrome (Lillie, 1965)

- 1) Deparaffinization as in step (1) of H & E.
- 2) 5 min. in distilled water.
- 3) 6 min. in acid fuchsin.
- 4) 4 min. in aniline blue (Edward Gurr).
- 5) dist. water rinse, dehydrate as in steps (8) and (9) of H. & E.